10-31-2007

Thermochemical Treatment of TiO2 Nanoparticles for Photocatalytic Applications

Mark Schmidt
University of South Florida

Thermochemical Treatment of TiO_2 Nanoparticles for Photocatalytic Applications

by

Mark Schmidt

A thesis submitted in partial fulfillment
of the requirements for the degree of
Master of Science in Electrical Engineering
Department of Electrical Engineering
College of Engineering
University of South Florida

Major Professor: Elias Stefanakos, Ph.D.
D. Yogi Goswami, Ph.D.
Nikolai Kislov, Ph.D.

Date of Approval
October 31, 2007

Keywords: photocatalysis, methyl orange, doping, calcination, thermal treatment

DEDICATION

I dedicate this thesis to my wife. Without her, this journey would not have been possible. I will be forever grateful for her support, encouragement and trust. I hope to honor her selflessness in the work that lies ahead.

ACKNOWLEDGEMENTS

I would like to thank my advisor, Dr. Elias Stefanakos, for the opportunity to work with him and the members of the Clean Energy Research Center. I greatly appreciate the trust and confidence he placed in me. I would like to especially thank Dr. Nikolai Kislov. His wisdom, guidance, patience and enthusiasm will never be forgotten. I would also like to thank Dr. Yogi Goswami for his guidance during our time together. His insights and leadership are greatly appreciated.

I would also like to thank the staff and faculty of the CERC. I would especially like to recognize the guidance and assistance given to me by Dr. Nikhil Kothurkar, Mr. Chuck Garretson, Dr. Sesha Srinivasan and Dr. Burton Krakow. Finally, I would like to thank my fellow students of the CERC for their help and support, especially Ms. Paula Algarin.

NOTE TO READER

Note to Reader: The original of this document contains color that is necessary for understanding the data. The original thesis is on file with the USF library in Tampa, Florida.

TABLE OF CONTENTS

LIST OF TABLES

LIST OF FIGURES

Thermochemical Treatment of TiO_2 Nanoparticles for Photocatalytic Applications

Mark Schmidt

ABSTRACT

Titanium Dioxide (TiO_2) has been considered an ideal photocatalyst due to factors such as its photocatalytic properties, chemical stability, impact on the environment and cost. However, its application has been primarily limited to ultraviolet (UV) environments due to its high band gap (3.2 eV). This high band gap limits the harvesting of photons to approximately 4% of sunlight radiation. Research today is focused on lowering this gap by doping or coupling TiO_2 with other semiconductors, transition metals and non-metal anions, thereby expanding its effectiveness well into the visible range.

This thesis explores the effects of thermal and thermochemical ammonia treatment of nano-particulated TiO_2. The objective is to synthesize a photocatalyst with a lower band gap energy that demonstrates photocatalytic activity in the visible range while at the same time retaining its photocatalytic properties in the UV range. Specifically, this study utilizes pure commercial nano-particulated TiO_2 powder (Degussa P-25), and uses this untreated TiO_2 as a baseline to investigate the effects of thermal and thermochemical treatments.

Nitrogen-doping is carried out by gas phase impregnation using anhydrous ammonia as the nitrogen source and a tube furnace reactor. The effects of temperature, time duration and gas flow rate on the effectiveness of thermally and thermochemically treated TiO_2 are examined. Thermally treated TiO_2 was calcinated in a dry inert nitrogen (N_2) atmosphere and the effects of temperature and treatment duration are investigated.

The band gap of the thermally treated and thermochemically ammonia treated TiO_2 have been measured and calculated using an optical spectrometer. The photocatalytic properties of all materials have been investigated by the degradation of methyl orange (MO) in an aqueous solution using both visible simulated solar spectrum (VSSS) and simulated solar spectrum (SSS) halogen light sources. Methyl orange degradation has been measured and calculated using an optical spectrometer. The phase structure and particle size of the materials is determined using x-ray diffraction (XRD). The BET surface area of the samples has been obtained using an Autosorb. Surface or microstructure characterization has also been obtained by scanning electron microscopy (SEM) and transmission electron microscopy (TEM).

CHAPTER 1: THE NEED FOR A VISIBLE-LIGHT PHOTOCATALYST

Today, one of the greatest health threats to our planet is the lack of potable water. According to United Nations Children's Fund (UNICEF), more than one billion people lack safe drinking water. Further, nearly 6,000 people die from water related illness each day. Of these two million deaths annually, the majority are children [2]. A substantial problem exists in remote areas that lack clean water and other basic essentials such as proper sanitation. These places also tend to lack the electrical power necessary for water treatment. Today, there is hope that polluted water sources can be disinfected by utilizing the energy of the sun and using a class of materials referred to as photocatalysts.

Titanium dioxide (TiO_2) has been considered an ideal photocatalyst due to factors such as its photocatalytic properties, chemical stability, impact on the environment and cost. Decomposing organic pollutants using TiO_2 is currently considered a possible decontamination process that could relieve much of the world's problems with potable water [3]. However, TiO_2 is a wide band gap (3.2 eV) semiconductor and as such its application has been primarily limited to ultraviolet (UV) environments. This high band gap limits the harvesting of photons to approximately 4% of the sun's available radiation, which is far too small for practical use. Research today is focused on lowering the band gap of TiO_2 by doping or coupling TiO_2 with other semiconductors, transition metals and

non-metal anions, and thereby expanding its effectiveness well into the visible range.

This thesis explores the effects of thermal and thermochemical ammonia treatments on nano-particulated TiO_2. The objective is to synthesize a photocatalyst with a lower band gap energy that demonstrates photocatalytic activity in the visible range while at the same time retaining its photocatalytic properties in the UV range. Specifically, this study will utilize pure commercial nano-particulated TiO_2 powder (Degussa P-25), using this untreated TiO_2 as a baseline to investigate the effects of thermal and thermochemical ammonia treatments.

CHAPTER 2: PHOTOCATALYSIS

2.1 Photocatalysis Defined

The term catalysis can be thought of as a chemical reaction that results from the action of a catalyst. Simply defined, a catalyst is a substance that increases the rate of reaction without being consumed during the reaction. Photocatalysis is a specialized catalytic process. Over the years, the exact definition of photocatalysis has grown and evolved along with this area of research. One of the early definitions of what is now known today as photocatalysis was “a catalytic reaction involving light absorption by a catalyst or a substrate” [4]. Another definition for photocatalysis, which was described as a complimentary definition, was a “catalytic reaction involving the production of a catalyst by absorption of light”. This was commonly referred to as photo-assisted catalysis [4].

Today, catalysis is defined by Serpone et al. as “a process in which a substance (the catalyst) accelerates, through intimate interaction(s) with the reactant(s) and concomitantly providing a lower energy pathway, an otherwise thermodynamically favored but kinetically slow reaction with the catalyst fully regenerated quantitatively at the conclusion of the catalytic cycle” [4]. More simply put, the catalytic process allows us to increase the rate of a reaction by

the addition of a substance, the catalyst, which itself remains unaltered after the reaction has completed.

From its early beginnings, photocatalysis has now grown to become an extension of catalysis. Photocatalysis can simply be thought of as a catalytic chemical reaction where photons are involved. This photoreaction only takes place in the presence of both the catalyst and photons of sufficient energy. Ultimately, simpler more inclusive definitions were sought. The term photocatalysis now can be thought of simply as a reaction where “light and a substance (the catalyst or initiator) are necessary entities to influence a reaction” [4].

2.2 Photogenerated Catalysis Versus Catalyzed Photolysis

Under this very broad definition of photocatalysis is a number of differing reaction mechanisms. As a result, photocatalysis has been further refined into two main groups by Salomon et al., photogenerated catalysis, and catalyzed photolysis, as is shown in Table 1. In photogenerated catalysis, the ground states of the catalyst and substrate are involved in a thermodynamically spontaneous catalytic step [4]. By contrast, in catalyzed photolysis the catalyst, the substrate or both are in an excited state during the catalytic step [4].

Table 1 Salomon's Classification of Photocatalysis [1]

Catalytic in Photons	Non-Catalytic in Photons
Photogenerated catalysis	Catalyzed photolysis
photoinduced catalytic reactions (stoichiometric photogenerated catalysis)	catalyzed photochemistry catalyzed photoreaction sensitized photoreaction photosensitized reactions photo-assisted catalysis (stoichiometric photogenerated catalysis) substance-assisted photoreactions substance-catalyzed photoreactions

2.3 Principles of Photocatalysis

Serpone et al. [4], Carp et al. [5], and Linsebigler et al. [6] provide excellent overviews of photocatalysis with specific reference to TiO_2. Many of the ideas expressed in this section come from these and other authors that have written on this thoroughly examined subject. The reader is encouraged to see the complete writings for detailed analysis.

The concept of photocatalysis can be thought of as an extension of a catalytic reaction where some compound A is converted to some compound(s) B:

$$A \leftrightarrow B$$

The use of a catalyst in this reaction changes the rate of the reaction, but the catalyst itself, by definition, must be preserved in both quantity and state, and

is completely separable from the other reactants at the completion of the catalytic cycle. This reaction which is now a catalytic process is given by:

$$A + Catalyst \leftrightarrow B + Catalyst$$

Although the reaction mechanics for these two processes are different, the end result is the same with a resultant species (compound B). However, in the catalytic process the catalyst in its original state is also one of the final products. Regarding the actual rate of reaction of these two processes, the reaction rate will be increased using a catalyst only if the total activation energy is lower than that of the reactants alone.

If this reaction occurs as the result of the absorption of photons by the catalyst, then the process is photocatalytic. In this case, the reaction is give by the equation:

$$A + h\nu + Catalyst \rightarrow B + Catalyst$$

where $h\nu$ is a quantum of energy from the incident photons sufficient to cause the reaction.

In regards to this thesis, the photocatalyst is a nano-particulated TiO_2 powder, Degussa P-25. For solid material photocatalysts, the pollutant is first adsorbed onto the surface of the catalyst. Here the pollutant undergoes a chemical transformation as it comes into contact with the reactive surface sites of TiO_2. Finally, the intermediate or final product is desorbed from the catalyst.

The adsorption mechanism of the pollutant onto the surface of the catalyst can be accomplished by either chemisorption or physisorption. Chemisorption is adsorption of the pollutant due to a strong chemical bond at the interface of the catalyst and pollutant. Alternatively, physisorption is a non-chemical bond between the pollutant and catalyst that is due to weaker forces such as van der Waals forces. In the event that the adsorption is an unusually strong chemisorption bond, the photocatalytic effect can be degraded or even eliminated, and is instead considered stoichiometric catalysis. At the other extreme, if the bond is too weak, the pollutant is poorly adsorbed, not allowing for bond rupturing or bond making, which also degrades or eliminates the reaction. The bond between the catalyst and pollutant must be strong enough to allow for this bond braking and making within the residence time of the intermediates, while allowing for both adsorption and desorption to occur.

From the reactions given above, the process of photocatalysis can be seen from two distinct positions. First, progressing from a chemical reaction to catalysis and then to photocatalysis. In this case, the photocatalysis is caused by catalysis of a thermal reaction. When light is absorbed by the catalyst it creates an excited state producing active surface sites. The second possible cycle is from a chemical reaction to a photochemical reaction to photocatalysis. After the catalyst absorbs photons, surface photochemical processes are said to be catalysis of a photoreaction as light is here considered as one of the reagents. This photochemical reaction is a function of the absorbed photons creating

intermediate species, the excited state of the catalyst, which in turn reacts with another reagent forming the final reaction species.

As it relates to this paper, photogenerated catalysis will be the focus, and specifically the Langmuir-Hinshelwood process. This process occurs at photochemically active sites at the surface of the catalyst when the necessary quantum of energy is absorbed by the catalyst. This in turn causes the creation of electron-hole pairs enabling electrons and holes to migrate to the surface. At the surface electrons and holes are reactive species capable of reducing and or oxidizing a pollutant. The mechanism of the Langmuir-Hinshelwood process is given by [4]:

1. $M + S \rightarrow M_{ads}$
2. $M_{ads} \rightarrow M + S$
3. $Catalyst + h\nu \rightarrow e^{-} + h^{+}$
4. $M_{ads} + h^{+} \rightarrow M_{ads}^{+}$
5. $M_{ads}^{+} + e^{-} \rightarrow M_{ads}$
6. $M_{ads}^{+} \rightarrow S + products$

where M is a reagent and S is a surface site. This mechanism starts with the adsorption of the reagent onto the catalyst surface site. The second step shows desorption of the reagent. This adsorption-desorption process creates what is

referred to as a Langmuir equilibrium, which was a topic of considerable study for this thesis. The third step shows the absorption of some necessary quantum of energy from a photon by the catalyst creating an electron-hole pair. Step four shows the creation of a reactive species due to hole trapping. Step five shows the decay of this species through the recombination of this species with an electron. Ultimately, step six shows that the photocatalytic process concluded with the formation of some products and the surface of the catalyst returning to its original state [4].

In contrast to photogenerated catalysis, if the photocatalytic reaction was categorized as catalytic photolysis it could be considered a catalytic photoreaction if the initial photoexcitation occurred in the adsorbed molecule that interacted with the ground state of the catalyst. Alternatively, it is categorized as a sensitized photoreaction if the photoexcitation occurred initially in the catalyst substrate, which in turn transferred an electron into the ground state of the reagent molecule. Regardless of the process in which the initial excitation of the system occurred, the transfer of the electron or energy transfer, it is the de-excitation that causes the chemical reaction as shown in steps three and four above [6]. The results of this study suggest that more than one possible process occurs, and it was possible to speculate that sensitized photoreactions took place during this investigation under certain conditions.

The transfer of an electron that causes the initial excitation in either the donor or acceptor molecule is a one electron reaction where the electron jumps

from the donor reactant to the empty orbital of the acceptor reactant. For this to be possible, the orbitals of the acceptor and donor must overlap with either an empty or half-filled state available resulting in an ion pair.

When the initial excitation is due to an energy transfer, the process is caused by electron exchange or dipole-dipole resonant coupling. In either case, here the orbitals must again overlap for this excitation. Further, if electron exchange is the mechanism, two independent one-electron transfer steps, one in each direction, is required. In contrast, the dipole-dipole resonant coupling is an interaction between the "oscillating dipole of an excited state molecule coupled with the induced dipole in a ground state quencher molecule" [6].

2.4 Electronic Excitation

The first step in photocatalysis is the absorption of a photon with sufficient energy by the reagent or substrate. This photon absorption creates highly reactive species with electronically excited states. The absorption rate of energy is on the order of 10^{-15}s, and occurs considerably quicker that the de-excitation event. The rate of de-excitation is determined by the pathway that will minimize the lifetime of the reactive species. This pathway can be by emission of radiation, or radiation-less decay, and if it is emitted as radiation, as in fluorescence, the carrier lifetime of the excited state is on the order of 10^{-9} to 10^{-5}s [6].

2.5 Band Gap Excitation

Semiconductors are identified as solids whose electrical conductivity is determined by the amount of energy that is required to move electrons from the valence band to the conduction band, whereas metals have a “sea of electrons” available for conduction. In traditional semiconductors, such as silicon, hybrid orbital (sp^3 orbital) of silicon can overlap with other atoms to form two different molecular orbitals as seen in Figure 1. These orbitals are said to be in phase if both are negative or positive (also commonly referred to as up or down), which forms a bonding molecular orbital with energy E_b. The orbital can be out of phase if one is positive and one negative, which forms an anti-bonding orbital with energy E_a. The bonding orbital of the solid will interact splitting the E_b energy level into discrete energy levels forming a valence band V_b by virtue of the valence electrons that are contained in this band. The energy level E_b is full, and therefore the valance band of the semiconductor is full of electrons. Similarly, the anti-bonding orbital overlap and also split into discrete energy levels E_a, which forms the energy band that is completely emptied. The energy band formed by the anti-bonding orbital is referred to as the conduction band C_b. This conduction energy band is separated from the valence band by the defined energy gap E_g, which in the ideal sense has no energy states. The stateless energy gap E_g is said to extend from the top of the valence band to the bottom of the conduction band. Again, in the idealized sense, electrons cannot be present in the energy gap E_g, and therefore there is no recombination of electrons and holes that may be photo-activated in the solid [6].

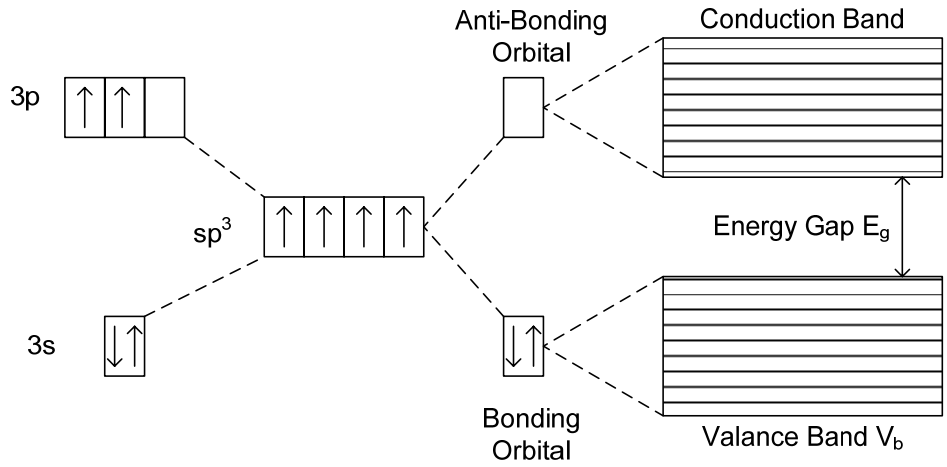

Figure 1 Formation of Energy Bands Involving Hybridization [7]

For photoexcitation of an electron from the valence band to the conduction band, a photon of sufficient energy must be absorbed by the electron. This excitation causes the creation of the electron-hole pair (e^-, h^+) and is shown in Figure 2. The lifetime of this electron-hole pair is on the order of nanoseconds, which is sufficient time to undergo a charge transfer with the adsorbed species on the surface of the semiconductor catalyst. This can be done in solution or in the gas phase. The term heterogeneous photocatalysis is used to describe the charge transfer to the adsorbed species if the semiconductor catalyst remains intact during a continuous exothermic process [6].

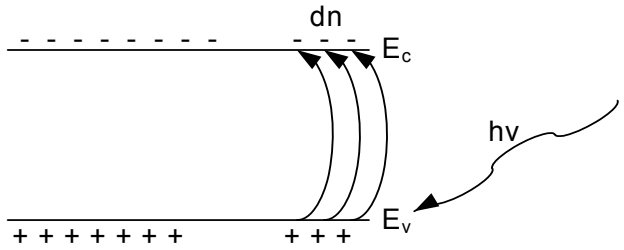

Figure 2 Formation of an Electron-Hole Pair Due to the Absorption of a Photon

The breakout of Figure 3 shows the photoexcitation of an electron and the creation of an electron-hole pair. Photocatalysis of either organic or inorganic compounds begins with the absorption of a quantum of energy greater than, or equal to, the energy gap of the semiconductor photocatalyst. Once created, this electron-hole pair has several de-excitation pathways which the electrons and holes can follow [6].

For photocatalysis to occur, these photogenerated electrons and holes must migrate to the surface of the catalyst where they can be transferred to the adsorbed organic or inorganic pollutant as shown in Figure 3. However, in competing de-excitation pathways, both surface and volume recombination can occur, as denoted by pathways A and B. The electron-hole recombination rate, if too high can degrade, or even halt photocatalysis [6]. The concept of charge separation, by any number of means, is an important idea as it relates to doped semiconductor catalysts, and is explored further in this study.

Pathway C depicts the transfer of an electron that has migrated to the surface of the catalyst to an acceptor, which in turn reduces the acceptor. In the aqueous batch reactor used in this study, this acceptor is oxygen. Pathway D

shows the migration of a hole to the catalyst surface that is then used to oxidize a donor species by the transfer of an electron from the donor. The occurrence and rate of these two mechanisms are functions of probability. This is determined by their band edges relative to the valence and conduction bands in relation to the redox potentials of the adsorbed pollutant [6].

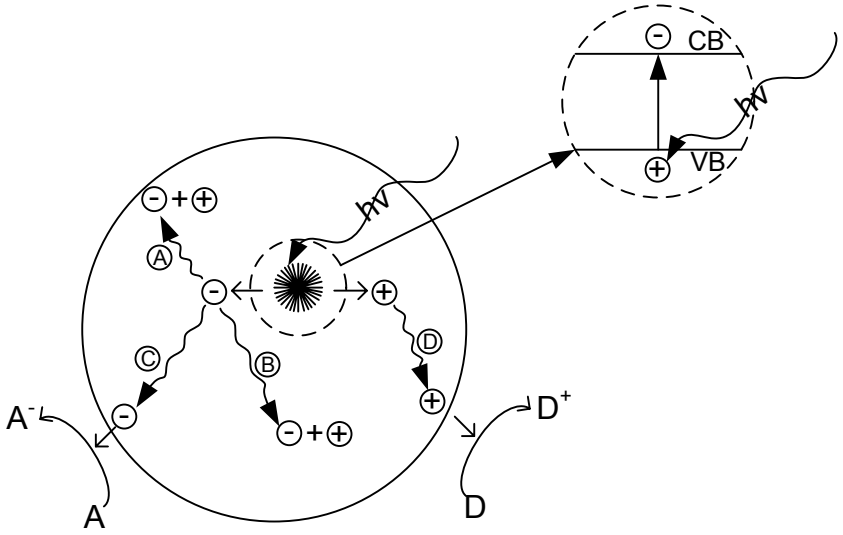

Figure 3 Photoexcitation and De-Excitation Pathways

The efficiency of the photocatalyst in degrading the pollutant is therefore dependent upon the diffusion of the electron-hole pair to the surface. Additionally, in a non-idealized semiconductor catalyst, surface traps exist and the concentration of holes and electrons at the surface are not equal [6]. Methods are employed for surface trapping of these charge carriers at the surface, which will be discussed below.

2.6 Band Edge Position

As noted, the mechanism for a photo-induced electron to transfer to an adsorbed pollutant on a semiconductor catalyst is controlled by the band energy position and the redox potential of the adsorbed species. Referring to the Normal Hydrogen Electrode (NHE) scale on Figure 4, for an oxidation reaction to occur the potential level of the donor species must be above (more negative) then the valence band position of the semiconductor catalyst. Likewise, for a reduction reaction to take place the potential level of the acceptor species must be below (more positive) that the conduction band position of the semiconductor catalyst. It should be noted that the band edge position of the semiconductors catalysts shown in Figure 4 are given for a pH=1, and that the pH of the solution influences the band edge position of the semiconductor [6].

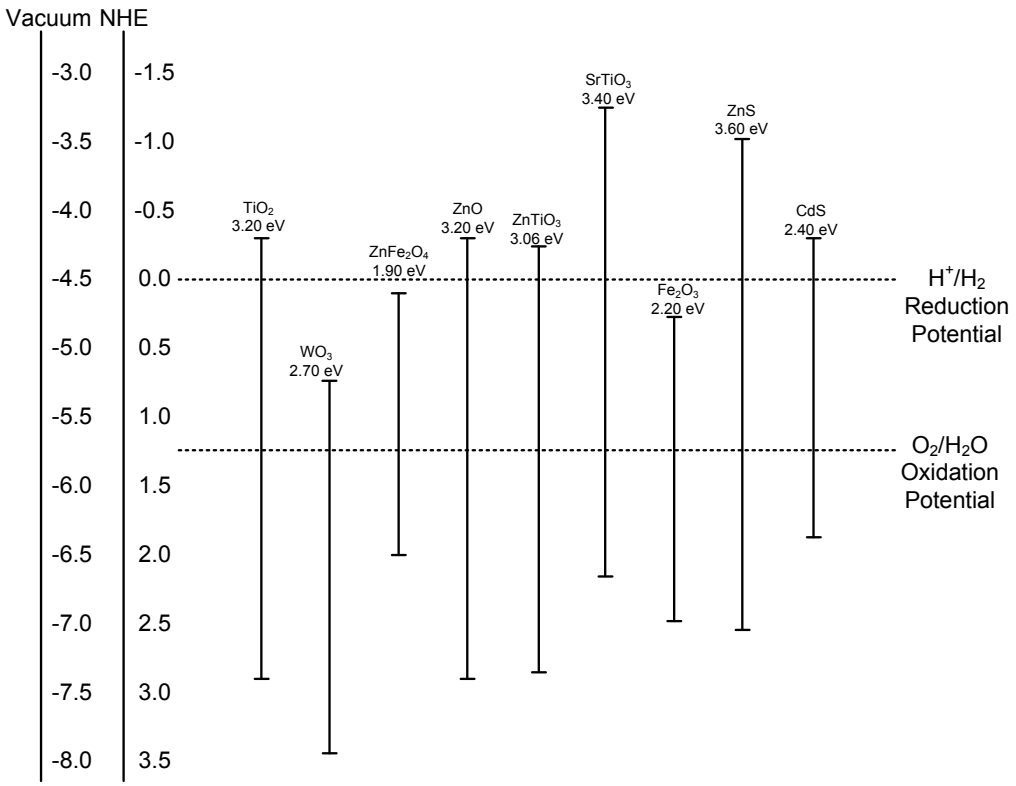

Figure 4 Band Edge Positions of Common Semiconductor Photocatalyst

2.7 Charge Separation, Trapping and Recombination

Given that two of the pathways outlined above lead to surface or volume recombination, charge separation or charge trapping is needed to reduce the probability of recombination and increase the photocatalytic effect. Since the crystal structure of the photocatalyst is not pure, but instead has both surface and bulk defects, it is expected that surface states (or charges) exist across the surface. These surface states, which differ in energy from the bulk, serve as charge carrier traps. The carrier lifetimes of the electrons and holes are therefore increased since these traps stifle the recombination of electrons and holes [6].

The problem of recombination is especially acute for doped materials, one of the topics of this study. For doped semiconductor catalysts both lattice defects and additional electronic states greatly increase the probability of recombination. Figure 5 shows a simplified view of electron trapping in the bulk and at the surface of the semiconductor. Both the localized bulk and surface traps in this diagram are located in the band gap. When an electron is trapped at one of these sites it becomes localized at that site on the surface or in the bulk. It is the energy difference between the traps and the bottom of the conduction band and the decrease in entropy due to electron trapping that determines the population of the charge carriers in the traps [6]. Similarly, valence band holes can also be trapped. Oxygen is commonly considered to scavenge electrons and is a process that is investigated and reported on in this study.

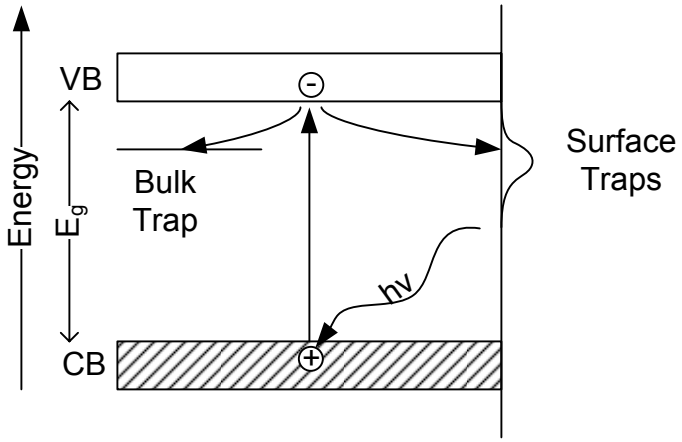

Figure 5 Surface and Bulk Traps [6]

2.8 Quantum Size Effects

Quantum size effects are considered for particles that range in size from 1 to 10 nm. The average particle size for pure Degussa P-25 TiO_2, which is used in this study, is on the order of 10 to 30 nm, and should not experience these effects. However, this is an important aspect as many studies suggest an optimum particle size between 10 and 20 nm, and will therefore be considered here. When the particle size becomes comparable to the de Broglie wavelength of the charge carriers in the photocatalyst, certain phenomena occur. The effective mass of the quantum particles of the photocatalyst is the determining factor on what size of particles experience quantum effects. Unlike particles larger than 10 nm, the electrons and holes of quantum sized particles do not experience the electronic delocalization present in a bulk semiconductor possessing a conduction band and valence band. This is due to the fact that the electrons and holes are confined in a potential well that has small geometrical dimensions. It is this confinement that creates the quantization of discrete

electronic states. The result is an increase in the effective band gap of the semiconductor [6].

It has been shown through modeling and experiment that the effective band gap can be significantly increased through quantization. This increase is most pronounced in semiconductors with small band gaps and can be quite significant, increasing by a factor of six for materials such as lead sulfide (PbS). Therefore, considerations of quantum size effects are important in photocatalytic materials [6, 8].

CHAPTER 3: TITANIUM DIOXIDE AS A MODEL PHOTOCATALYST

3.1 The Importance of Titanium Dioxide

Titanium dioxide (TiO_2) is an indirect gap, n-type semiconductor with electrons as the majority carriers [9]. TiO_2 has been considered an ideal photocatalyst due to its photocatalytic properties, chemical stability, impact on the environment and cost. However, its application has been primarily limited to ultraviolet (UV) environments due to its high band gap (anatase = 3.2 eV). This high band gap limits the harvesting of photons to approximately 4% of the solar radiation.

The importance of TiO_2 as a photocatalyst lies in its ability to oxidize a large number of organic compounds into harmless compounds such as carbon dioxide and water using ultraviolet light, and potentially, visible-light. TiO_2 is highly photoactive as the H^+/H_2 reduction potential and O_2/H_2O oxidation potential lie within its band gap [8]. This is accomplished by the redox energy of electron-hole pairs on the adsorbed pollutant. The important point is that the conduction and valence bands of TiO_2 lie in energetically favorable positions to both reduce and oxidize the adsorbed species. This means that TiO_2 not only has the oxidation potential to degrade pollutants, but also the reduction potential

necessary for splitting water molecules to create hydrogen gas, a topic of great importance today.

3.2 The Lattice Structure of Anatase and Rutile TiO_2

Of the numerous forms of TiO_2, only rutile, anatase and brookite occur in nature. Of the three, only anatase and rutile can be utilized as photocatalysts. The lattice structure for anatase and rutile is described in terms of distorted TiO_6 octahedra [10]. As seen in Figure 6, this configuration consists of Ti^{4+} ions surrounded by six O^{2-} ions. The crystal structure of rutile has each octahedron in contact with 10 neighboring octahedrons. The rutile structure has two octahedrons sharing the edge oxygen pairs and eight octahedrons sharing the corner oxygen atoms. In contrast, the anatase crystal structure, shown in Figure 7, has each octahedron in contact with eight neighboring octahedrons. The anatase structure has four octahedron sharing the edge oxygen pairs and four octahedron sharing a corner oxygen pair [6]. The structural differences of the anatase and rutile structures are small, but electronically significant. The crystal structures differ by the amount of distortion of each octahedron, and by the pattern of the octahedra chains [6].

The structure of anatase, as seen in Figure 7, is significantly distorted compared with rutile which results in a greater Ti–Ti distances than rutile, 3.79 and 3.04 angstrom versus 3.57 and 2.96 angstrom, but a shorter Ti–O distance, 1.934 and 1.980 angstrom versus 1.949 and 1.980 angstrom [6].

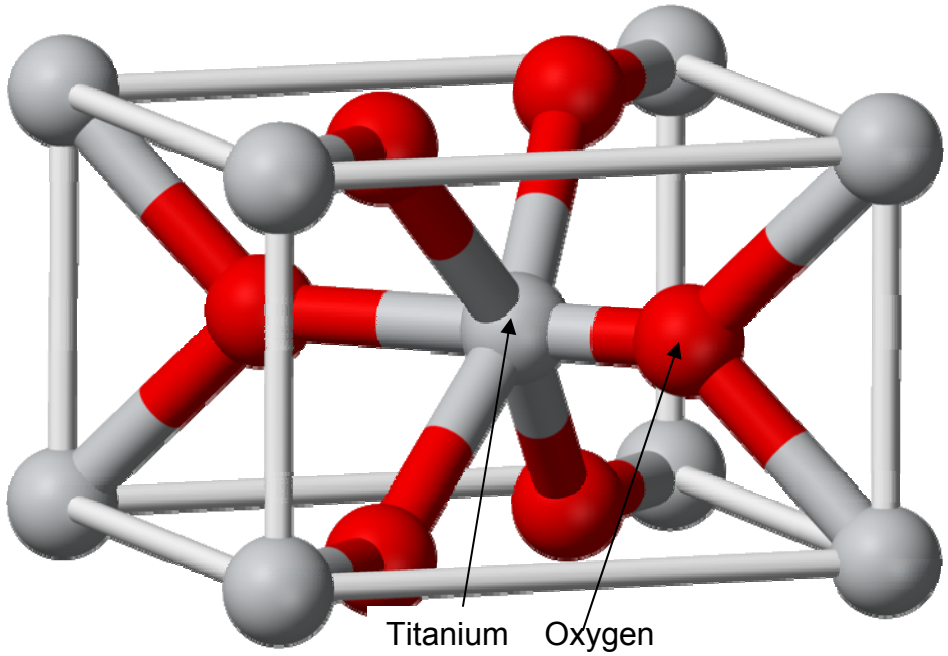

Figure 6 Stick and Ball Model of Anatase Titanium Dioxide

The structure of rutile, depicted in Figure 7, is described as having a slight orthorhombic distortion [6]. It is these small structural differences that are responsible for the differences in electronic band properties. As mentioned, the band gap of anatase is 3.2 eV whereas the band gap of rutile is 3.0 eV. Despite the lower energy required for electron-hole pair creation, anatase is reported to be more active than rutile [11].

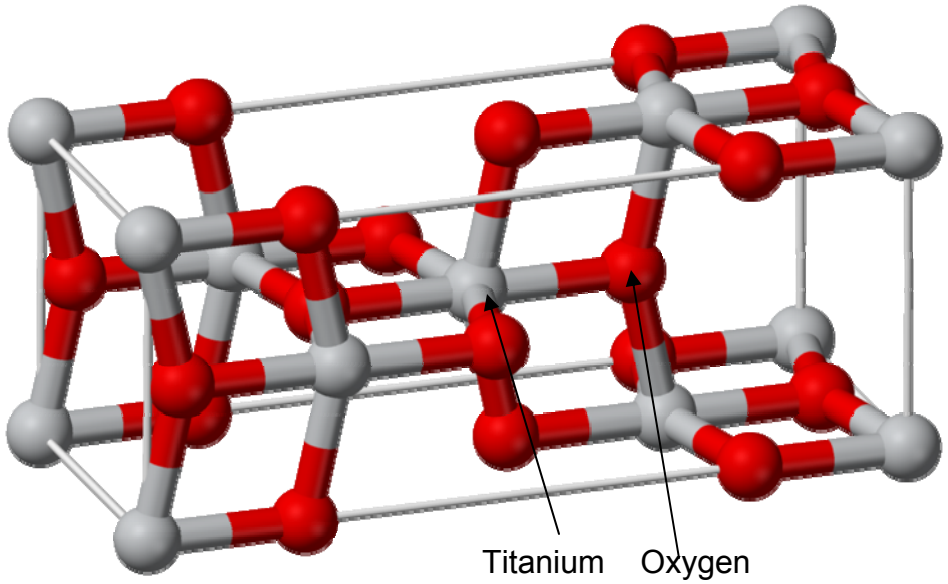

Figure 7 Stick and Ball Model of Rutile Titanium Dioxide

One of the most important features of the crystal structure is the three types of oxygen vacancy sites shown in Figure 8 [6, 10]. These oxygen vacancies play an important role in photocatalysis and their effects are explored in detail below.

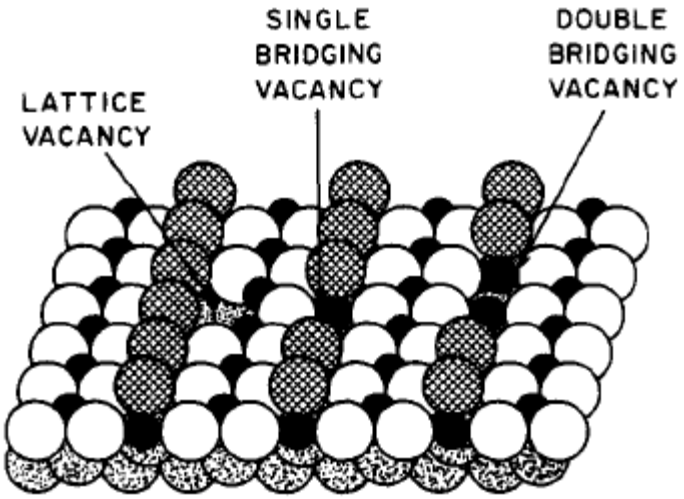

Figure 8 Oxygen Vacancies in TiO_2 Lattice Structure [6]

3.3 Electronic Structure of TiO_2

The filled valence band is composed of the O2p orbital and the empty conduction band is composed of the Ti3d, Ti4s, and Ti4p orbital. The Ti3d orbitals dominate the lower portion of the conduction band [6].

3.4 Photoadsorption and Photodesorption of Oxygen on $Ti0_2$

The photoadsorption and photodesorption of O_2 on TiO_2 is an important mechanism of TiO_2 photocatalysis. Adsorbed oxygen participates in electron charge transfer from the substrate, and electron scavenging during photooxidation of organics. In separate studies by Bickley et al. [12] and Nakamura et al. [13] it was concluded that adsorbed water enhances the photoadsorption of oxygen on rutile TiO_2 surfaces. This is believed to be done by trapping the photogenerated holes at OH^- sites. The formation of surface

HO_2^- by electron trapping and O_3^- by hole trapping reactions is the primary route for oxygen photoadsorption [6].

3.5 Photooxidation at the Liquid-Solid Interface of TiO_2

When a photon with the energy required to excite an electron from the valence to conduction band is absorbed, an electron-hole pair is created and potentially can participate in a redox reaction. The reduction potential and oxidation potential is equivalent to the band energy, which can be estimated. It is also possible that the electron-hole pair may recombine by several mechanisms as described above. For a photocatalytic reaction to take place however, the electrons and holes must migrate to the surface of the catalyst and react with adsorbed species. In a steady state photocatalytic reaction, the rate of oxidation by the holes has to be balanced by the rate of reduction by the electrons [6].

After the initial creation of the electron-hole pair the actual process of oxidation taking place at the interface of the catalyst and solution is an area of significant debate. There are two generally accepted oxidation mechanisms. One is the direct oxidation of the adsorbed pollutant by the hole. The other is oxidation by the adsorbed hydroxyl radical attacking the adsorbed organic species. While research has found hydroxyl radicals and hydroxylated oxidation intermediates in support of that mechanism, it is not possible to distinguish this from the direct hole oxidation mechanism given that the reaction intermediates are similar [5].

The study by Draper et al. concluded that the primary mechanism of oxidation was by the direct hole oxidation route [14]. In the study they hypothesized that trapped electrons react with pre-adsorbed molecular oxygen and produce O_2^- and O_2^{2-} anions. The study itself does not reach a conclusion regarding the actual role these species play. It is possible that these anion directly oxidize the pollutant, create hydroperoxide radicals and hydroxyl radicals, or continue reacting with other trapped electrons which may produce water [6]. In addition to scavenging electrons during photooxidation, oxygen may play a larger role in photocatalysis. Other electron scavengers achieve only a fraction of the oxidation and photomineralization effect as oxygen. This has led researchers such as Linsebigler et al. to speculate on a larger role for oxygen in photocatalysis [6].

3.6 Trapping, Recombination, and Interfacial Electron Transfer

Carrier lifetime is an important limiting factor in the photocatalytic rate and illustrates the importance of the electron or hole trapping species to be pre-adsorbed on the surface of the catalyst. Conduction band electrons may be trapped within 30 ps [6]. This is compared with the trapping of the valence band holes that require an average time of 250 ns is very fast. The recombination rate of trapped electrons with free or trapped holes occurs between 10^{-11} to 10^{-6} s [6].

The mean lifetime of a single electron-hole pair is approximately 30 ns for a low charge carrier concentration, and hole trapping can compete with the recombination process [6]. Trapped holes are relatively un-reactive with

electrons. For high charge carrier concentrations, the electron-hole pairs recombine within a fraction of one nanosecond [6]. This illustrates that charge carrier trapping must happen very fast to achieve an effective photochemical conversion [6].

The rate of photooxidation was found by Gerischer et al. to be equal to, and limited by, the reduction rate of dissolved oxygen in the solution [15]. Their study theoretically predicted that if O_2 is not reduced at a sufficiently high rate, electrons will accumulate on the surface of the catalyst. This was later confirmed in the study by Wang et al. who determined that the rate of radiation-less recombination of electrons and holes is “enhanced until the sum of the electron-hole recombination and the electron transfer to O_2 is equal to the rate of the hole photogeneration” [16]. This is the basis for using metals such as palladium or platinum for scavenging to eliminate electron accumulation on the $Ti0_2$ [6]. Although not reported in this study, the effect of copper ions from fresh copper surfaces may have played a role in the photocatalytic rate of the initial experiments. What was found was an increase in the photocatalytic rate for fresh copper surfaces, which degraded with time. These copper ions could potentially have come from the copper cooling coils originally designed for the photocatalytic reactors. Stainless steel replaced these copper coils and no variations in the photocatalytic rate were recorded subsequently.

3.7 Photomineralization Reactions in Aqueous Photocatalytic Suspensions

As possibly the most heavily researched photocatalyst, TiO_2 has been tested with virtually every class of organic compound [5]. It has been concluded that valence band holes can oxidize any organic compound to CO_2, H_2O and some form of mineral acid. The photooxidation and photomineralization process are non-selective. The "photogenerated holes in the semiconductor particles, the hole-trapping radical species, and the activated oxygen species (by electron trapping) are all strong oxidation agents for organic compounds" [6].

3.8 Modifications of TiO_2 for Improved Photocatalytic Performance

The premise of this study is the use of TiO_2 as a visible-light photocatalyst. To achieve this goal it is necessary to modify TiO_2 to improve the visible-light absorption, prevent or delay charge carrier recombination and improve its surface properties. To achieve these goals, it is necessary to modify TiO_2 to achieve each particular goal.

3.8.1 Surface Modification Using Metals

Modifying TiO_2 using a metal to change the surface properties can improve the photocatalytic reaction rate, and also change the intermediate products [6, 10]. Figure 9 illustrates a Schottky barrier that is created at the interface of the catalyst and metal. Platinum has been studied extensively and found to form particle clusters on the catalyst surface covering approximately 6%

of the surface area allowing for a large TiO_2 surface area for adsorption of the pollutant to the catalyst surface.

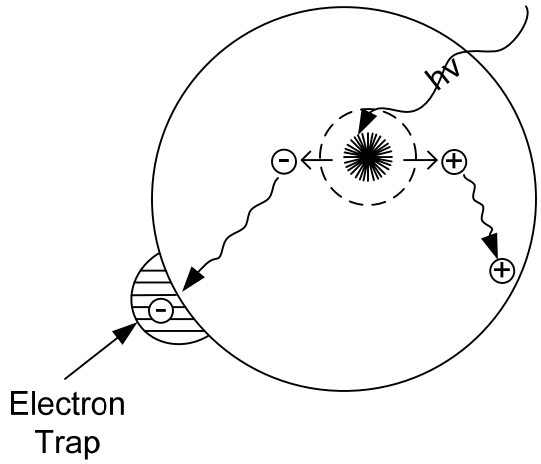

Figure 9 Metal as an Electron Trap

The required quantum of energy creates an electron-hole pair and the metal acts as an electron trap for the electron migrating to the surface. This suppresses the recombination of the electron-hole pair. The hole is then able to migrate to the surface of the catalyst and oxidize the adsorbed organic compound [6]. Further, metals such as platinum and silver have their own catalytic effect.

Metals change the photocatalytic properties of TiO_2 by changing its electrical properties due to the distribution of electrons that occurs. At the heterojunction, the Fermi levels of the metal and semiconductor align resulting in a flow of electrons from the catalyst to the metal. This leads to an increase in hydroxyl groups that play an important role in the photocatalytic reaction as described above [6].

3.8.2 Transition Metal Doping

Doping TiO_2 using transition metals ions has also been widely studied. Similar to metal doping, the use of transition metal ions allows for electron traps that suppress electron-hole recombination. Preliminary work using iron (Fe^{3+}) was done during this study. As was noted above, the original photocatalytic reactor used copper cooling coils in the solution. The effect of copper ions from the experimental setup on the photocatalytic rate was found to be a rate determining factor.

Doping TiO_2 using Fe_3^+ results in an increase in Ti^{3+} intensity by trapping electrons thereby suppressing electron-hole recombination [10]. It was concluded that a doping threshold exists where only small concentrations produce a positive effect on the photocatalytic rate. It should be noted that not all transition metals produce a positive result. Some transition metals actually decrease the photocatalytic rate due to an increase in electron-hole recombination by creating recombination centers [10].

3.8.3 Coupled Photocatalysts

Coupling or co-doping was also briefly studied using tungsten oxide (WO_3) during this study. This method is used to exploit the low band gap of one material to produce a photocatalytic effect in a wide gap material such as TiO_2 by increasing the charge separation and extending the energy range of photoexcitation for the system. Figure 10 shows the valence band and

conduction band positions for TiO_2 and WO_3 prior to contact. If a photon that is not energetic enough to excite TiO_2, but is energetic enough to excite WO_3 is incident, the hole that is created in the WO_3 valence band is excited to the conduction band of TiO_2, while the electron is transferred to the conduction band of TiO_2. It is this electron transfer that increases the charge separation and increases the efficiency of the photocatalytic process. After separation, the electron is free to reduce the adsorbed pollutant and the hole is available to oxidize as described above [6].

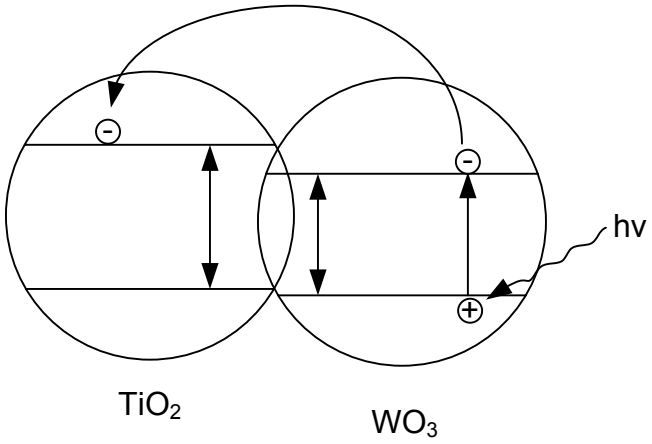

Figure 10 Coupled TiO_2-WO_3

3.9 Degussa P-25 TiO_2

Degussa P-25 powder titanium dioxide was used for this study, and is considered to be the benchmark photocatalytic material for TiO_2 powders. An exhaustive study on TiO_2 was performed by Diebold et al. [10], and it is an excellent manuscript for detailed analysis. P-25 is primarily composed of anatase and rutile phases. Published values for the composition of P-25 typically

range from 20-25% for rutile and 75-80% for anatase. Ohno et al. also report that an amorphous phase also accounts for approximately 1% [17]. The BET surface area for P-25 is approximately 50 m^2/g, which is considerably smaller than some studies that report surface areas as high as 200 m^2/g for TiO_2 prepared by a titania precursor.

Degussa P-25 TiO_2 is produced by an aerosol process using titanium tetrachloride as a precursor. The vapor phase hydrolysis method is used in a hydrogen flame to produce the powder [18]. The sizes of the particles vary from 25 nm to 85 nm in diameter, and grow until their size, or the agglomerate's size, causes them to be removed from the reaction due to their weight.

The morphology and relationship of the anatase and rutile phases was a topic of considerable discussion during this study. The initial hypothesis was that anatase particles were converted to rutile particles at elevated temperatures during either calcination or doping processes, especially at temperatures in excess of 600°C. The review of the literature showed that Bickley et al. performed one of the original studies on the morphology of Degussa P-25 and in fact made a similar conclusion.

Bickley et al. concluded that some of the anatase phase particles were covered with a thin layer of rutile phase TiO_2. They reported that the increased photocatalytic activity was, in part, due to this layered anatase-rutile particle. They speculated that a potential difference across the space charge region of the

two phases, and localized electronic states from the amorphous phase particles were the mechanism for this increase [12].

However, both Datye et al., and later Ohno et al., concluded that anatase phase particles do not have an over-layer of rutile phase on the surface. Instead, anatase phase and rutile phase particles exist completely separate from one another [17, 18].

It has been reported in many places that the combined presence of anatase and rutile phases enhances the photocatalytic effect of Degussa P-25. As noted, the average surface area of P-25 is approximately 50 m^2/g, and anatase particles have a larger surface area than rutile particles. Ohno et al. concluded that the larger surface area of anatase particles "improves the efficiency of decomposition of the pollutant in air and water". Further, that the "presence of both anatase and rutile phases is important for some photocatalytic reactions where oxygen is used as the electron acceptor" [17]. Datye et al. concluded that the "well developed crystallinity" was responsible for the high efficiency. They reasoned that this allowed for a low density of recombination centers [18].

Figure 11 shows the TEM images of P-25 powder from Ohno et al. They concluded that the images clearly indicate that the two phases exist separately. Ohno et al. also concluded that anatase and rutile particles grow on different nuclei, which also was not the original hypothesis of this study. As stated previously, the original hypothesis was that rutile was purely a thermal phase

transformation of anatase [17]. This author concurs with the conclusions of Ohno et al., and has used this model throughout this study.

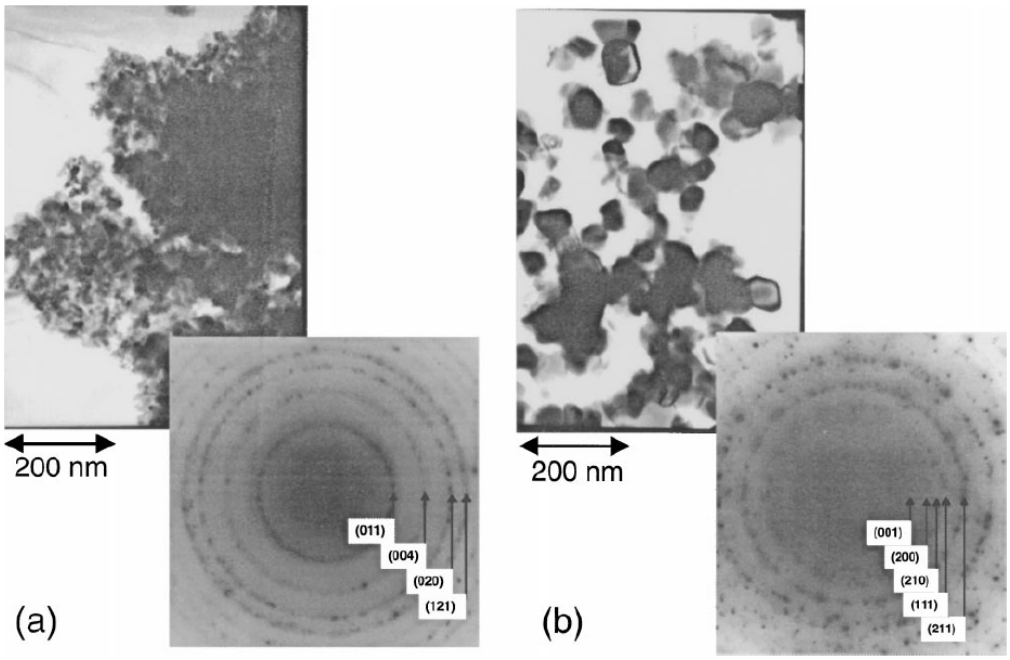

Figure 11 TEM Images of Degussa TiO_2 P-25 Powder, (a) Anatase Particles (b) Rutile Particles

Experiments were conducted for calcinated P-25, which will be detailed below, that show improved photocatalytic efficiency. The improvement in efficiency can be attributed to reduction of TiO_2, which was explained in detail above. This reduction causes a red-shift to wavelengths longer than 400 nm, which is attributed to the reduction of Ti^{4+} to Ti^{3+}. Hence, the rutile particles in the P-25 powder are considered to contain the Ti^{3+} ions that create electron donors. Ohno et al. conclude that a "fairly large band bending is generated in the rutile particles." They attribute the higher efficiency of P-25 to this [17].

CHAPTER 4: METHYL ORANGE AS A MODEL POLLUTANT

4.1 The Real World Problem of Methyl Orange

In this thesis, methyl orange (MO, $C_{14}H_{14}N_3SO_3Na$) was used as the model pollutant. Methyl Orange is a common industrial dye favored for its stability and is categorized as an azo-dye. Azo-compounds, which are synthetic inorganic chemical compounds, account for up to 70% of the dyes in use today. It is estimated that between 10-15% of the dye used in textile processing is lost and released as effluent [19]. The release of this effluent is considered “non-aesthetic pollution” as amounts smaller than 1 ppm is visible in water sources. Although this is the primary motivation for degrading methyl orange, the dye waste water can also produce dangerous by-products during various chemical reactions such as oxidation and hydrolysis [20].

As stated, these azo-compounds are very stable, which is due to the large proportion of aromatics in the dye. Biological treatments may only de-color the dye effluents as opposed to degrading the effluent. A similar de-coloration phenomenon was discovered during this study for thermochemically ammonia treated Degussa P-25 TiO_2, and is discussed in detail below. Common physico-chemical treatments are effective in discoloration, but are also non-destructive.

Instead, these treatments transfer the organic compounds from the water to another phase [20].

Due to the difficulty in degrading pollutants such as MO, a process referred to as an Advanced Oxidation Process was proposed as an alternative to water purification. This process differs from the traditional oxidation by holes, with oxidation by a very reactive species such as hydroxyl radicals $(\bullet OH)$. These reactive species can non-selectively oxidize a broad range of pollutants. It has been determined that heterogeneous photocatalysts, such as TiO_2, are the most destructive with regard to azo-compounds [21]. This destruction can be promoted by both artificial solar sources and sources employing solar technologies. The noted advantage to this method is that it is destructive, and that it can occur under ambient conditions. Further, it has been shown that it may lead to the complete mineralization of organic carbon into CO_2 [20].

4.2 Chemical Composition of Methyl Orange

The chemical formula and molecular composition for methyl orange, depicted in Figures 12 and 13, is $C_{14}H_{14}N_3SO_3Na$. It is the presence of the benzene rings which keeps this pollutant from decomposing easily by chemical or biological methods [22].

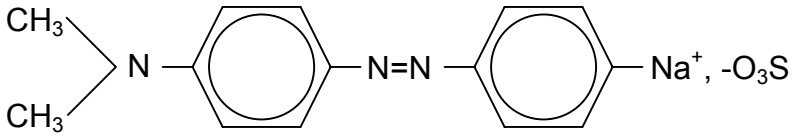

Figure 12 Chemical Composition of Methyl Orange

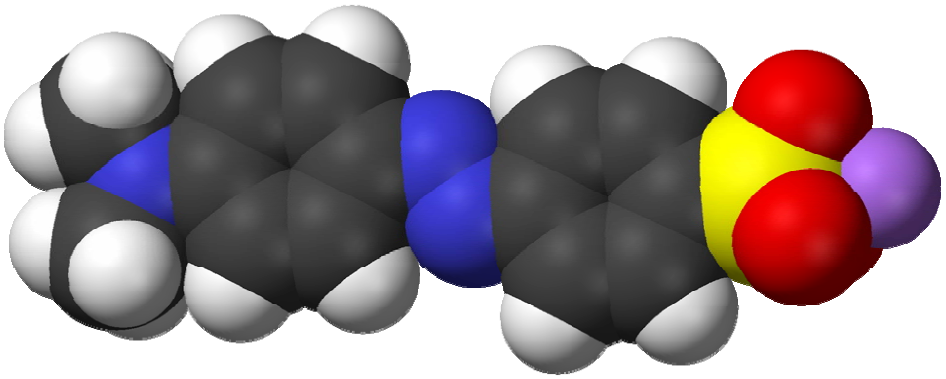

Figure 13 Molecular Structure of Methyl Orange

Initial experiments were conducted using de-ionized water as the solvent, to determine the optical absorption spectra of methyl orange. Figure 14 shows the spectra for a 20 ppm solution of methyl orange. These spectra show two absorption peak maxima, one at approximately 272 nm and a second with a higher absorption magnitude at 451 nm. Consistent with published work in this area, the second maxima peak at 451 nm was used to calculate the concentration changes as a function of time for methyl orange [20, 22]. These peaks and corresponding spectra are in line with published works depicting absorption peaks at 270 nm and 458 nm [20].

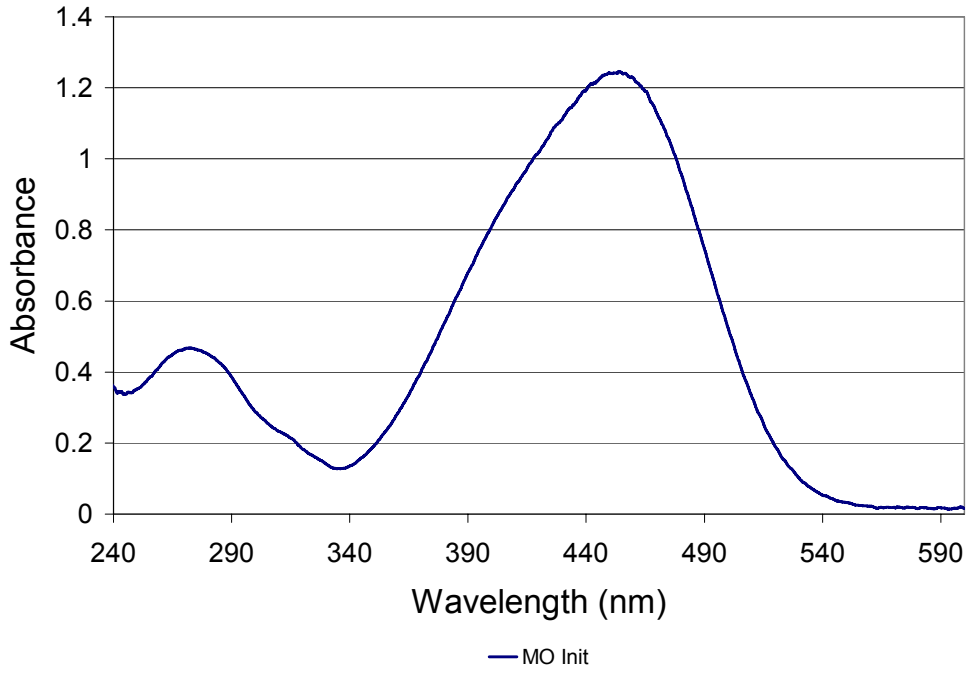

Figure 14 Spectra of a 20 ppm Methyl Orange Solution

4.3 Chemical Stability of Methyl Orange

As noted earlier, methyl orange is considered to be a very stable compound. To test this stability methyl orange was prepared in varying concentrations from 5 ppm to 20 ppm. Samples were syringed into centrifuge tubes and exposed either to ambient light or shielded from all light sources. Figure 15 shows the measured spectra for those samples measured at time zero, after 24 and after 144 hours. As is routinely reported elsewhere, there is a negligible change in concentration for all samples.

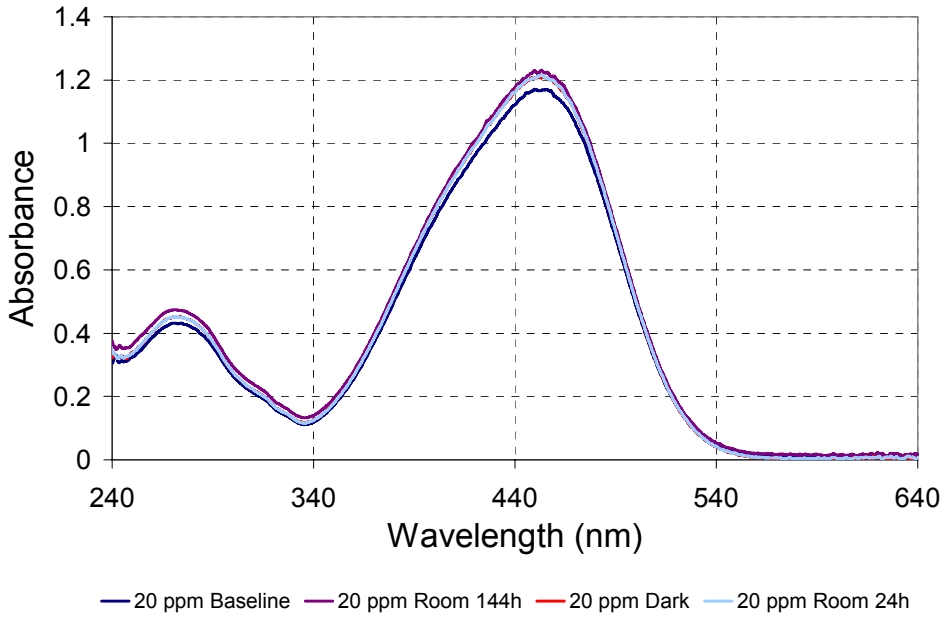

Figure 15 Stability Spectra of Methyl Orange Without Irradiation

To test the stability of MO in the presence of TiO_2, but without a light source, an experiment was conducted. A 20 ppm MO solution prepared in a glass beaker was loaded with 1 g/L of TiO_2 and stirred in the dark with samples taken after 30 minute intervals. The results are depicted in Figure 16. Consistent with the literature, there was no degradation of the MO stirred in the dark, and in the presence of TiO_2 [20, 22]. However, there is an adsorption-desorption process that along with experimental error account for the insignificant changes in concentration. This adsorption process, referred to as the Langmuir equilibrium, will be discussed below.

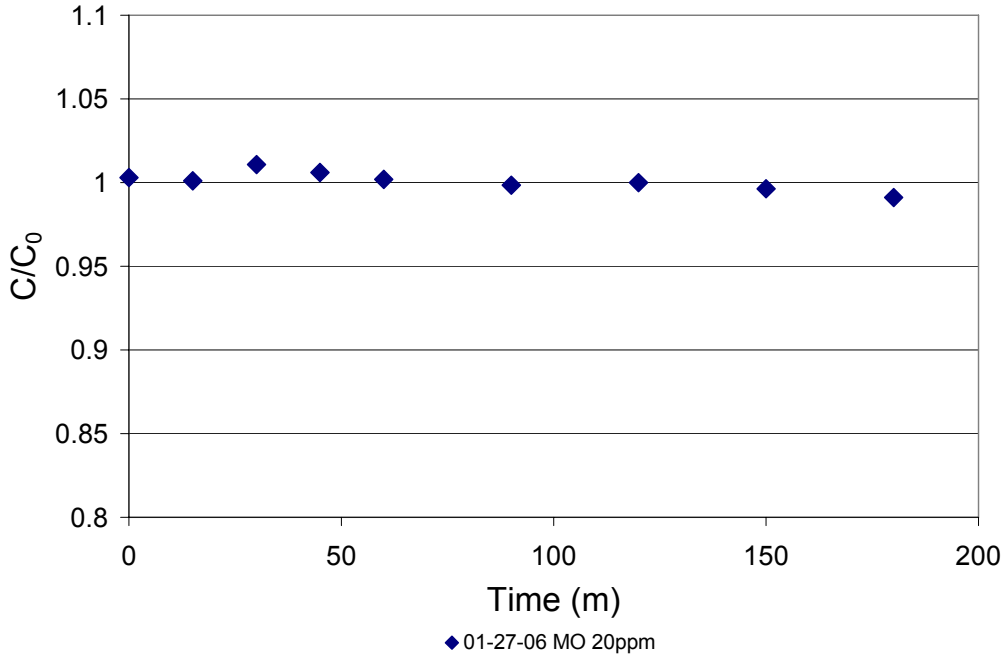

Figure 16 Concentration as a Function of Time for Methyl Orange in the Presence of Degussa P-25 TiO_2 But Without an Irradiation Source

Guettai et al. found that the complete disappearance of the dye could only be observed in the simultaneous presence of TiO_2 and UV-A (320 nm to 400 nm) light. They concluded that the system is therefore "working in a pure photocatalytic regime" [20]. These stability findings are the baseline of the photocatalytic study included in this thesis.

4.4 Calculation of Rate Constants

Consistent with published works regarding the degradation of methyl orange by TiO_2, the peak at 451 nm was used as the evaluation point [20, 22]. Figure 17 shows the spectra for MO as a function of irradiation time for the whole spectrum.

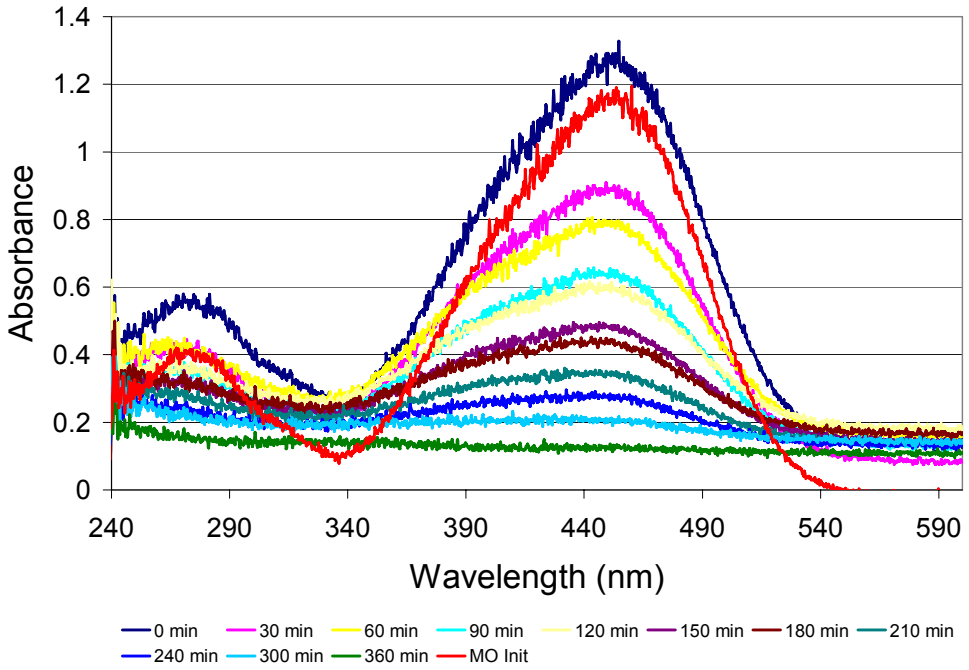

Figure 17 Absorbance Spectra as a Function of Time for Methyl Orange in the Presence of Calcinated TiO_2 and Simulated Solar Spectrum (SSS) Irradiation

The value for 451 nm was derived using a box car smoothing method for the values between 449-453 nm to account for the fluctuations of data points recorded by the optical spectrometer. The ratio of the concentration versus initial concentration for 451 nm was then plotted as a function of time as depicted in Figure 18. Typically, this curve was a good approximation of a first order chemical reaction for simulated solar spectrum (SSS) irradiation as shown in Figure 18. However, for visible-light irradiation the curve more accurately reflected a zeroth order chemical reaction. These results are the first indication of the difficulty in characterizing the photocatalytic chemical kinetics as strictly first order reactions, and therefore the motivation for developing the Langmuir-Hinshelwood equation.

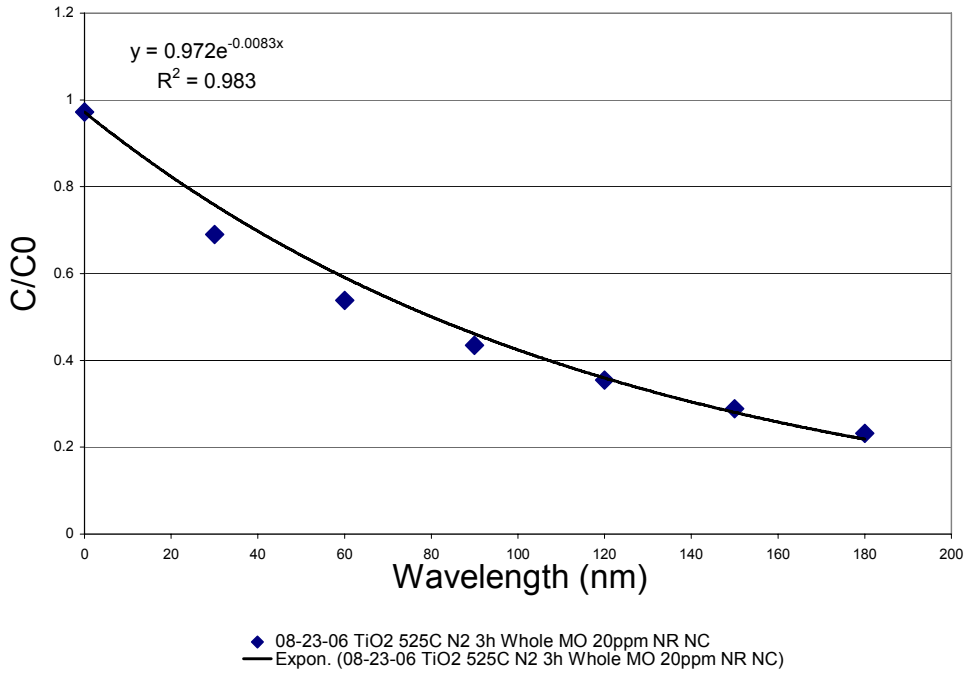

Figure 18 C/C0 Versus Time for Methyl Orange Discoloration in the Presence of Calcinated TiO_2 and SSS Irradiation

From the plot of concentration versus initial concentration a rate constant for first order kinetics was calculated. The method used here mirrors the technique employed by both Guettai et al. and Al-Qaradawi et al. for determining rate constants for first order kinetics. The negative log plot of ratio of concentration to initial concentration (see Figure 19) is plotted and the tangent provides the apparent rate constant for each material.

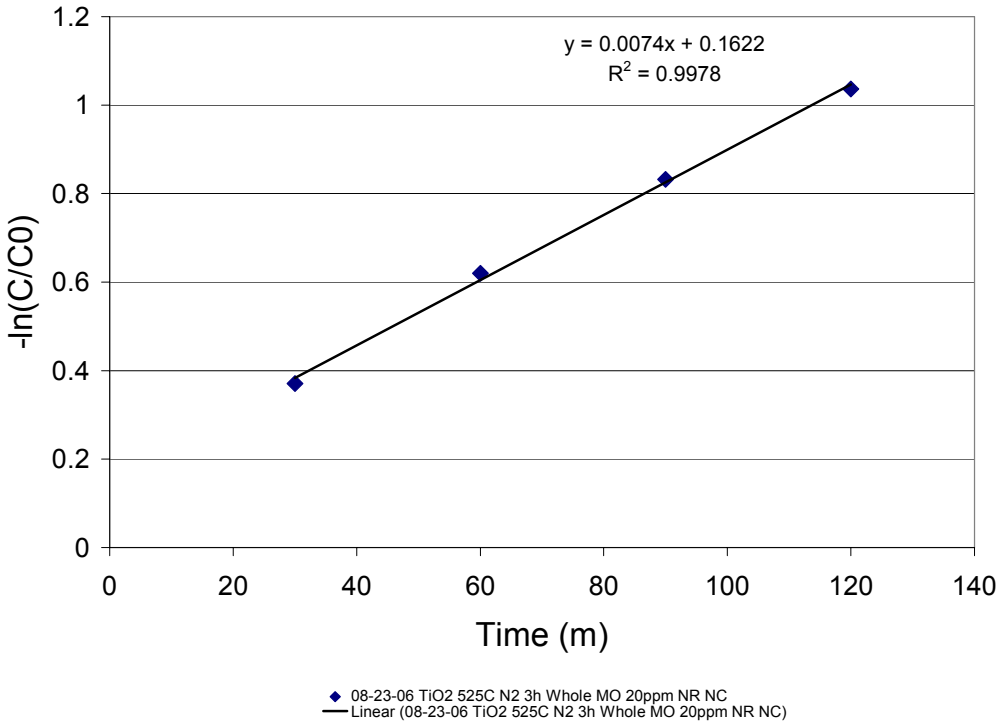

Figure 19 Calculation of Apparent Rate Constant for a First Order Chemical Reaction

Yates et al. implored that “great care” must be used in the design of the experimental setup in order to differentiate between the discoloration of the dye due to photocatalytic activity, and the discoloration of the dye due to reduction as a result of electron transfer reactions [23]. This caution again illustrates the difficulty in properly characterizing the reaction kinetics.

The spectra in Figure 20 show the problem with using the value at 451 nm as the only point for determining MO degradation. As can be seen, the complete degradation of the pollutant has not occurred, but instead intermediates have been formed that show absorption at shorter wavelengths. It is obvious that such a result cannot be used for evaluating a rate constant for the photocatalyst.

Further, it cannot be concluded that the resulting pollutant species will be fully degraded. The spectra only show an increase in absorbance at 350 nm due to the creation of intermediates that corresponds to the decrease at 451 nm of the original pollutant. It is not possible to conclude that the species identified at 350 nm will degrade. Although rare, similar spectra were found for both visible and whole light irradiation experiments during this study. Although not concluded, it is hypothesized that the absorption of ultraviolet light has been retarded by the thermochemical ammonia treatment. The result here and in other experiments shows degradation in species in the visible range, and an increase and no degradation of the intermediates formed in the ultraviolet wavelengths. This result could be of further research interest.

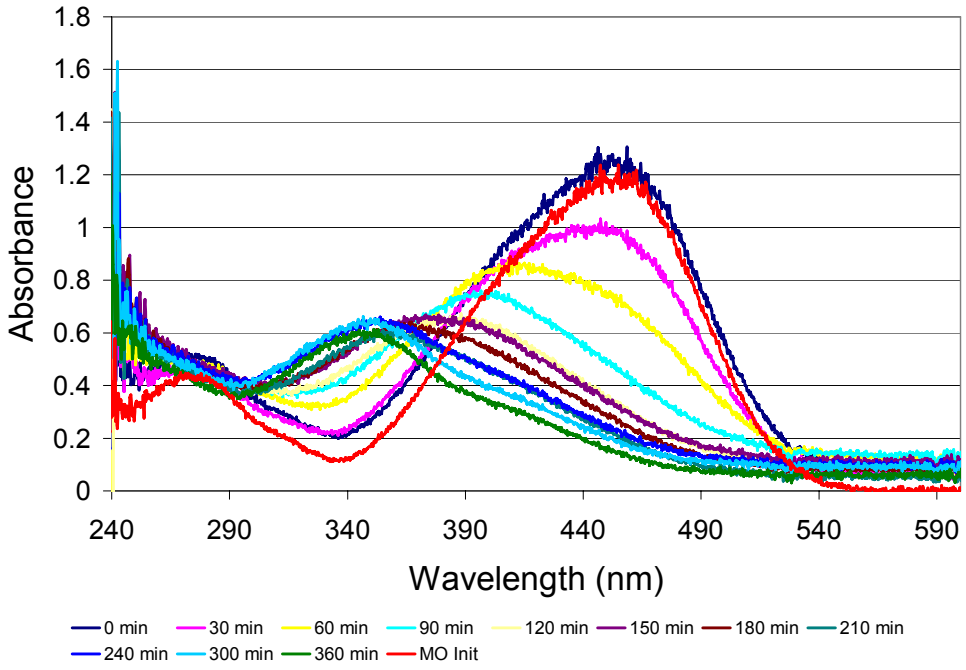

Figure 20 Creation of Intermediate Products During Photocatalytic Reaction of Ammonia Thermochemically Treated TiO_2 Under SSS Irradiation

4.5 Catalyst Loading and Discoloration

The effect of catalyst loading was tested to determine the optimal loading for both the visible simulated solar spectrum (VSSS) and simulated solar spectrum (SSS). The specifics of the light sources are detailed below in the section on the characterization of the light sources.

All of the experiments in this study were conducted in a natural pH solution of TiO_2 (which is commonly reported as pH_{NAT} = 6.3), with differing catalyst loadings. In line with the findings of Al-Qaradawi et al. and Guettai et al., the de-colorization of MO can be approximated as pseudo-first order kinetics for simulated solar spectrum irradiation as shown in Figure 21 [20, 22].

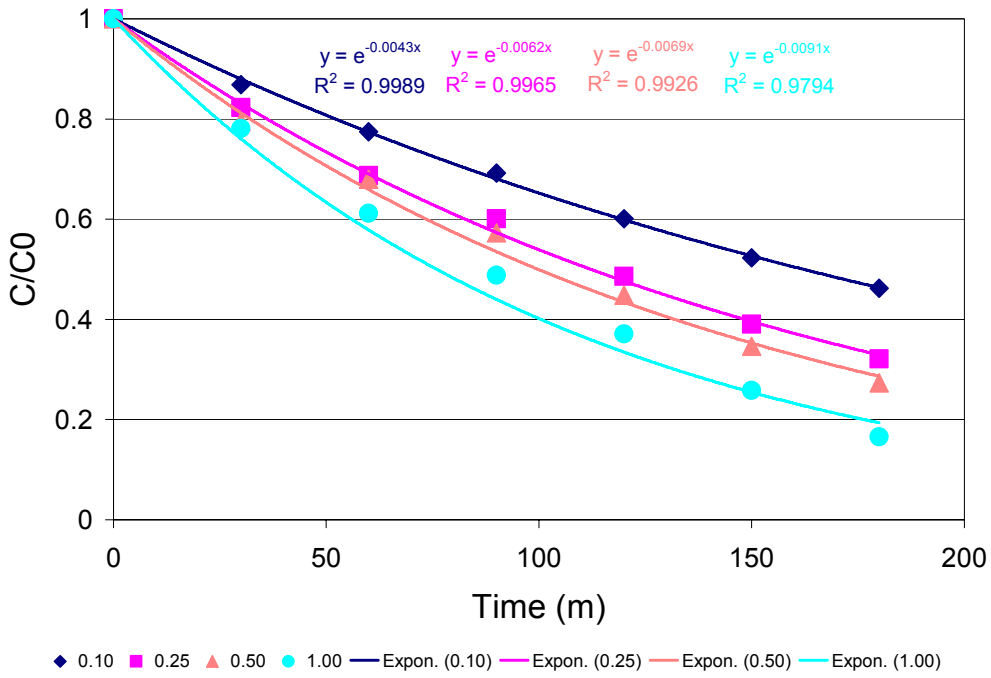

Figure 21 Effects of Catalyst Loading (g/L) on the Rate of Discoloration for Untreated Degussa P-25 TiO_2 Under SSS Irradiation

By considering the kinetics of the reaction to be first order, we can plot – ln(C/C0) to arrive at the rate constant for the reaction, which is shown in Figure 22. It is this rate constant that is used as the point of comparison to Degussa P-25 TiO_2 for simulated solar spectrum experiments.

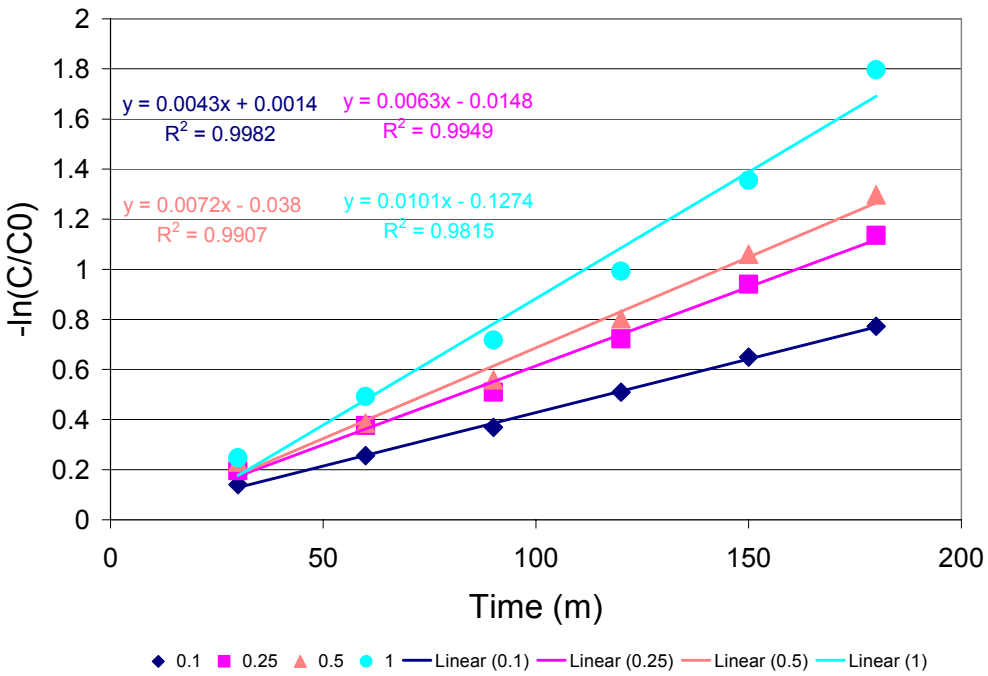

Figure 22 Calculation of Rate Constants for Catalyst Loading (g/L) for Untreated Degussa P-25 TiO_2 Under SSS Irradiation

Figure 23 is a plot for the apparent rate constants for differing catalyst loadings for Degussa P-25 TiO_2 under SSS irradiation.

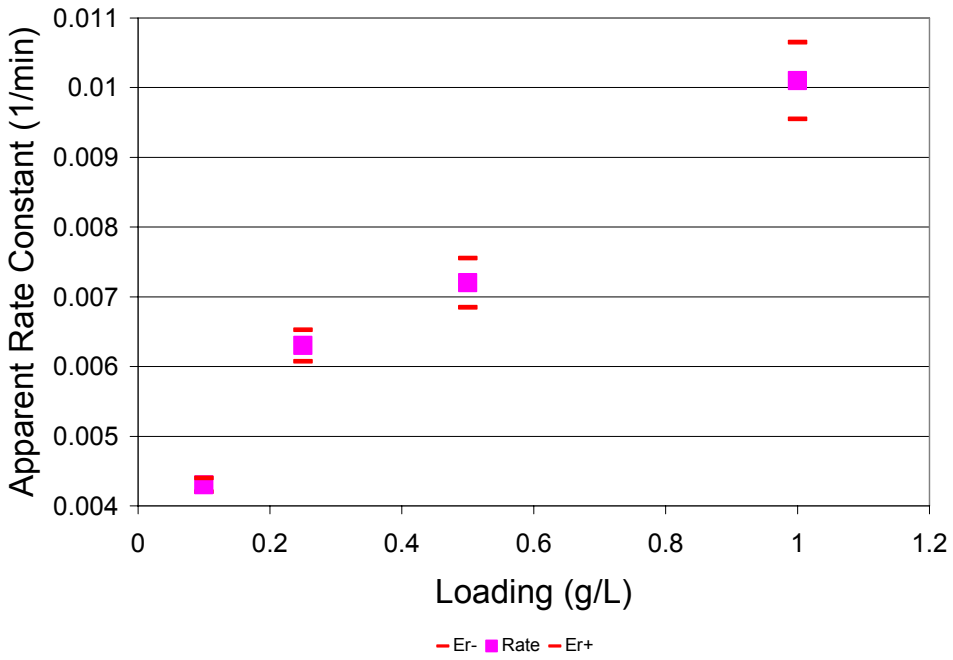

Figure 23 Apparent Rate Constant for Catalyst Loading (g/L) for Untreated Degussa P-25 TiO_2 Under SSS Irradiation

Similar experiments were conducted to find rate constants VSSS irradiation. In Figure 24, the degradation rate for visible-light increases significantly as the catalyst loading increases from 0.5 and1.0 g/L. This is in line with the literature where others reported similar results. Guettai et al. reported that the degradation rate increased rapidly as the catalyst concentration increased from 0.2 to 0.8 g/L. They hypothesized that this was, “probably due to the increase of active sites with the suspension of catalyst loading”. The optimum catalyst loading found in this study was determined to be 1.0 g/L, with no further increase or decrease in the performance due to increased loading. This is in contrast to the findings of Guettai et al., who found that the 0.8 g/L gave the most effective decomposition rate [20].

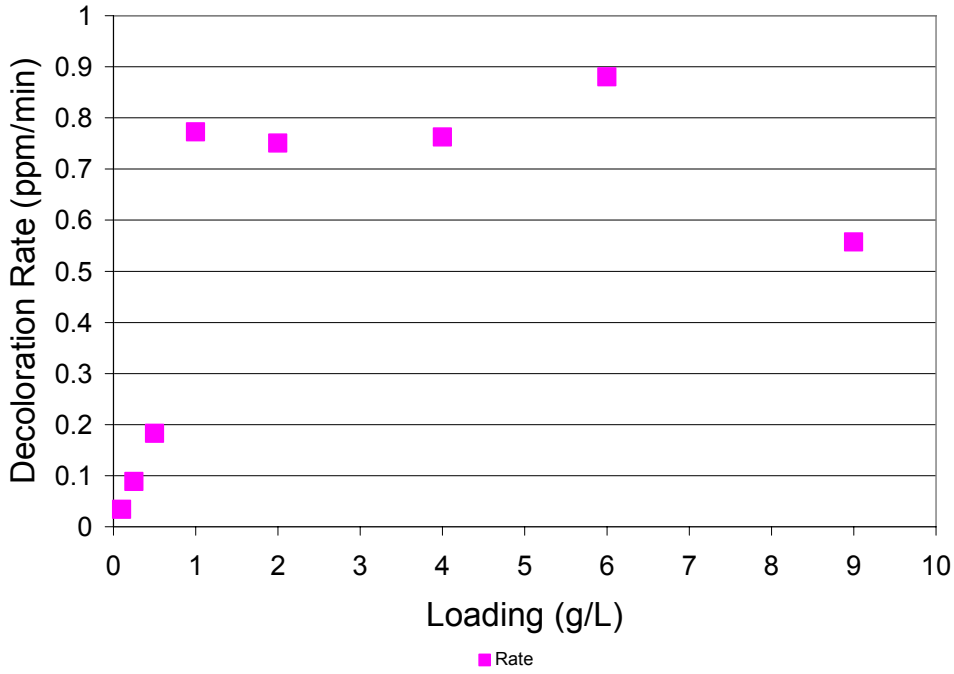

Figure 24 Apparent Rate Constant for Catalyst Loading (g/L) for Untreated Degussa P-25 TiO_2 Under Visible Simulated Solar Spectrum Irradiation

More significantly, they reported a decrease in discoloration with an increase in catalyst loading, which was also found in this study as shown in Figure 24. Guettai et al. speculated that light scattering was the cause of this decrease in efficiency.

Figure 25 shows the light intensity for a given loading. As can be seen, increasing the catalyst loading limits the light penetration through the solution. The result is a smaller volume that can be irradiated and therefore the effects of catalyst loading reach their maximum. These results are similar to the results reported in the literature. It is hypothesized that the higher concentration of suspended catalyst serves as a shield for the catalyst in bulk of the solution. The

result is that part of the catalyst is not able to adsorb photons and participate in the photocatalytic process [20].

Figure 25 shows the light penetration for a catalyst loading of 4 g/L. Contrast this with Figure 26 with a catalyst loading of 1 g/L.

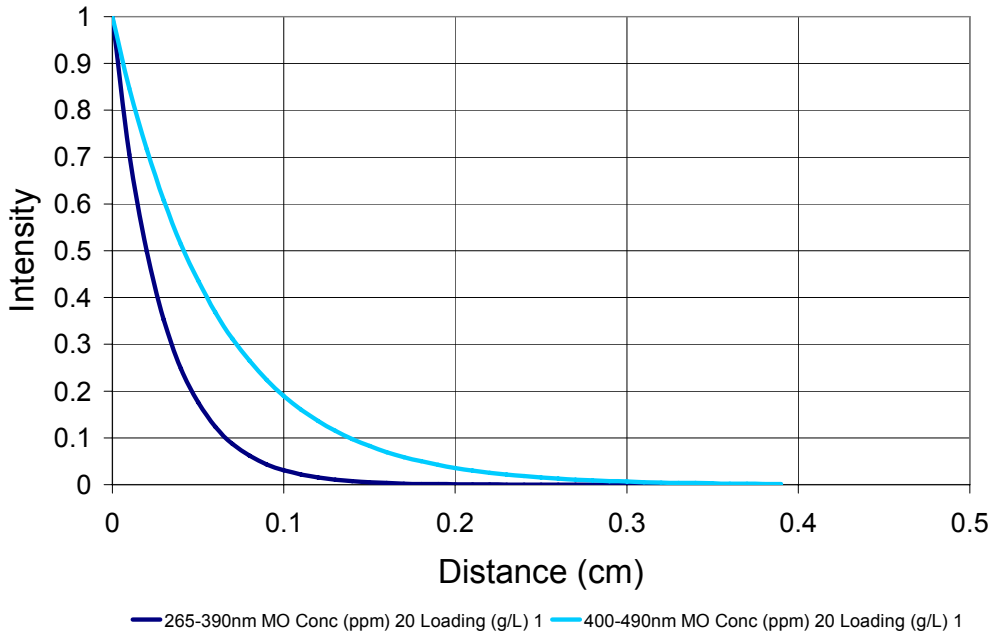

Figure 25 SSS and VSSS Light Intensity as a Function of Distance from the Source for a 20 ppm Methyl Orange Solution and 1 g/L of Untreated Degussa P-25 TiO_2

As can be seen, the fall off in intensity is dramatic. It should be noted here however that experiments for Degussa P-25 TiO_2 in VSSS irradiation showed complete degradation of the pollutant during this study. This too, could be the source of an interesting study.

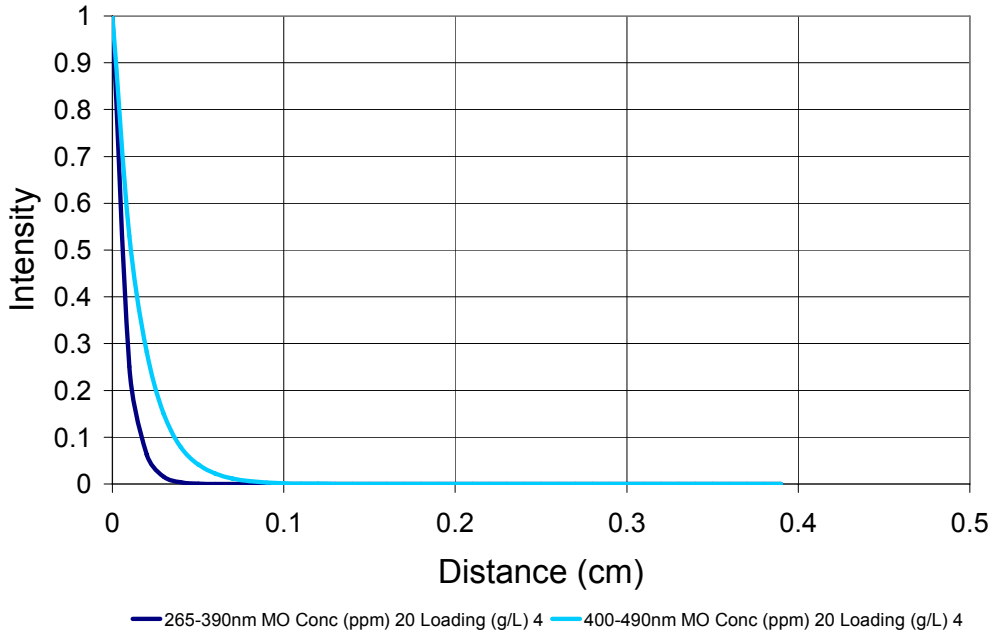

Figure 26 SSS and VSSS Light Intensity as a Function of Distance from the Source for a 20 ppm Methyl Orange Solution and 4 g/L of Untreated Degussa P-25 TiO_2

It also must be noted that the actual catalyst loading concentration required is a function of type of reactor used, its geometry and the incident radiation. As shown in Figures 23 and 24, the optimal loading differed for simulated solar spectrum and visible simulated solar spectrum light sources. The reported values for optimum loading vary from 0.15 g/L to 8.0 g/L for suspension photocatalytic processes [20].

4.6 pH and Discoloration

In this study, no attempt was made to control the pH level of the photocatalytic process although pH values were measured for varying loading

levels for some experiments. However, the pH level is considered to be the major factor influencing the rate of the photocatalytic process [20].

Guettai et al. conducted experiments in a pH range from 2 to 10 using NaOH and H_2SO_4 solutions to control the pH values. They reported that the best discoloration results were produced in an acidic solution; 98.58% (pH = 2), 91.85% (pH = 3) and 56.42% (pH = 5) after 5 hours of irradiation. For a neutral pH, they reported a discoloration of 28.58% (pH = 7.04). For a basic solution, they reported 16.67% (pH = 9.01). Their results show a significant difference in the discoloration of MO in strong acidic solutions (pH = 2–3) and near neutral (pH ≥6) solutions. They concluded that the initial pH has a strong influence on the adsorption of the pollutant, and therefore a significant effect on the discoloration of the pollutant [20].

Al-Qaradawi et al. reported similar results showing the best degradation occurring at a pH of 3 [22]. However, they also reported that a pH of 9 produced the next best result, which is in contrast to the value reported above. Additionally, it was determined that the pH of the solution changes over time to become more acidic, with the exception of a pH of 3, which remained unchanged.

One interesting property of TiO_2 is that it is amphoteric, meaning that it can behave as an acid or base depending on the pH of the solution. It is this property that is used to explain the difference in behavior in relation to differing

pH values. Below are the reactions that Guettai et al. propose for the reactions with pH values around its point of zero charge (pH_{PZC}) [20]:

$$TiOH + H^+ \Leftrightarrow TiOH_2^+ \qquad pH < pH_{PZC}$$

$$TiOH + OH^- \Leftrightarrow TiO^- + H_2O \qquad pH > pH_{PZC}$$

These equations show how the pH changes can thus influence the adsorption of the pollutant on the surface of TiO_2, which is an important step if photooxidation is to take place. The literature shows the measured pH_{PZC} value for Degussa P-25 TiO_2 to be around 5.8 to 6.8. For acidic solutions, pH < 6, MO is strongly adsorbed to the TiO_2 surface. This is a result of the electrostatic attraction between the positively charged TiO_2 particles and the pollutant. In a basic solution, pH > 7, the MO molecules are negatively charged. In this case the adsorption of the pollutant is also affected due to an increase in the density of TiO^- on the catalysts surface. The resulting coulombic repulsion retards the adsorption of the pollutant on the catalyst surface [20]. Further, for basic solutions with high pH values, the scavenging of hydroxyl radicals happens so quickly that there is no reaction with the pollutant. The photocatalytic reactivity of sulphonated dyes, to which MO belongs, are maximum in acidic solutions, and decrease as the pH increases [20].

The literature also shows that interpreting the effects of pH is very difficult due to the differing reaction mechanisms. There are three reaction mechanisms

that can be involved in the photodegradation process. First, hydroxyl radicals may participate:

$Dye + OH^{\bullet} \rightarrow$ degradation product.

Second, holes may directly oxidize the pollutant:

$Dye + h_{VB}^{+} \rightarrow$ oxidation products.

And, third, electrons may reduce the pollutant:

$Dye + e_{CB}^{-} \rightarrow$ reduction products.

The difficulty in interpretation, and a point of debate, is that at a low pH holes are thought to be the major oxidizing species, but at neutral and high pH levels the hydroxyl radicals are believed to be the major oxidizing species [20]. In contrast, Al-Qaradawi et al. concluded that the degradation rate increases with a high pH value. They state that a basic solution will have a higher number of hydroxyl radicals at the catalyst surface where they will trap the photo-induced holes [22].

$$TiO_2 + hv(UV - A) \rightarrow TiO_2\left(e_{CB}^{-}\right) + h_{VB}^{+}$$

$$TiO_2\left(h_{VB}^{+}\right) + H_2O \rightarrow TiO_2 + H^{+} + OH^{\bullet}$$

$$TiO_2\left(h_{VB}^{+}\right) + OH^{-} \rightarrow TiO_2 + OH^{\bullet}$$

The effects of pH on the calculation of photocatalytic rate are seen in Figure 27. A 20 ppm solution of MO was prepared with 1 g/L of Degussa P-25 TiO2. The pH of the solution was adjusted to produce acidic and basic solutions and the spectra were measured. As can be seen in figure 27, the peak at 451 nm is shifted due to the change in pH. This must be considered when considering the photocatalytic rate.

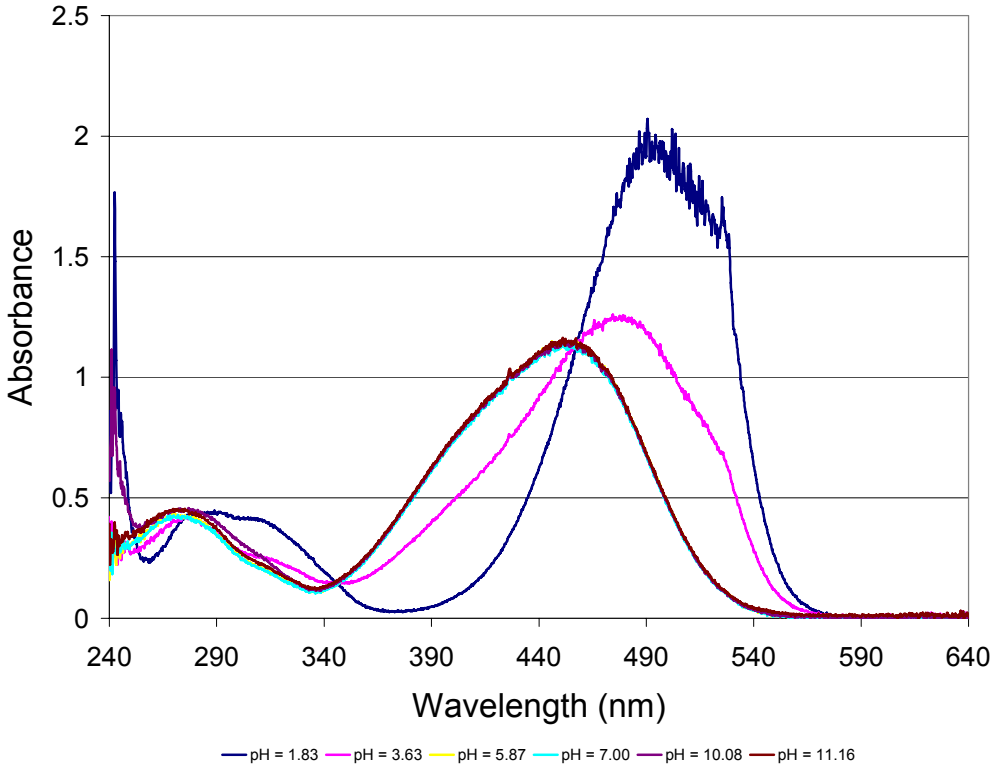

Figure 27 Spectra of 20 ppm Solutions of Methyl Orange and 1 g/L of Degussa P-25 TiO_2 for Varying pH Levels

4.7 Initial Concentration and Discoloration Rates

The initial concentration of MO is also a factor in the discoloration rate. In this study, it was found that significant adsorption of the pollutant occurs during

the first 15 minutes. This was first discovered when seemingly similar experiments resulted in different degradation rates. It was discovered that a sonication step meant to de-agglomerate the catalyst produced differing results. Subsequent study of the cause showed that the time used for sonication, not the sonication itself, was responsible for the adsorption of the pollutant on the catalyst surface. This initial adsorption changed the initial concentration, and therefore seemingly the order of the reaction from first order to zeroth order. Figure 28 shows the change in MO concentration due to adsorption of the pollutant on the catalyst over 30 minutes. This adsorption-desorption process is known as the Langmuir equilibrium.

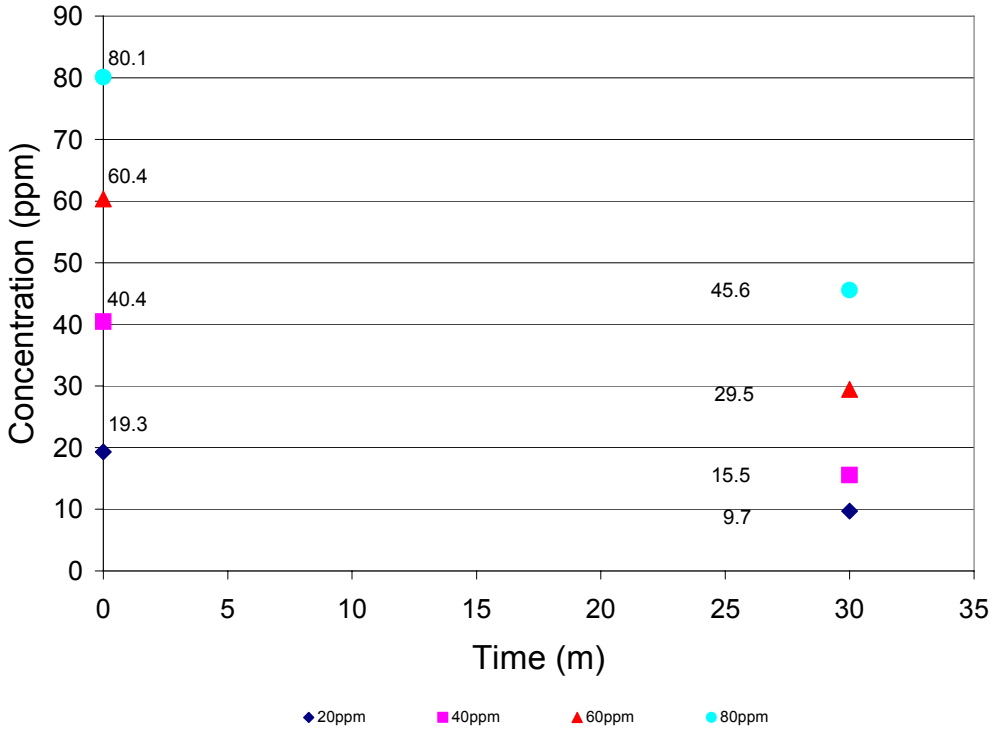

Figure 28 Change in Concentration as a Function of Time Due only to the Adsorption of Methyl Orange to Untreated Degussa P-25 TiO_2 (3 g/L)

The effect of initial MO concentration on the photocatalytic effectiveness of the process was studied by Guettai et al. The study was conducted for initial MO concentrations from 5 to 75 mg/L for a pH=3, and a catalyst loading of 0.8 g/L. They made two conclusions from their study. First, that the degradation of MO satisfactorily follows the Langmuir-Hinshelwood model. Second, the percentage of degradation ultimately decreases with an increasing initial concentration of the pollutant. For levels above 75 mg/L, the degradation rate becomes very slow [20].

Initially, an increase in the concentration of MO increases the probability of a reaction between the pollutant and the oxidizing species. This in turn results in

an increase in the discoloration rate. As the concentration of MO increases, the active sites on the catalyst surface are more fully covered reducing the photogeneration of holes or hydroxyl radicals [20]. It has also been speculated in the literature that “UV screening” (the adsorption of incident photons by MO molecules) is another possibility regarding the decrease in rate [22]. The general conclusion is that the optimum catalyst loading is a function of active surface area and the pollutant concentration, and therefore is not necessarily static [20]. Similarly, Al-Qaradawi et al. also found that an increase in initial catalyst concentration ultimately decreases the overall degradation efficiency overall [22].

4.8 Photocatalytic Intermediates of MO

Methyl orange has an orange color in a basic medium and a red color in an acidic medium. Its color is a result of absorbing certain wavelengths of visible-light and either transmitting or reflecting other wavelengths. As an azo-compound, MO derives its color from the azo-bonds $\left(-N=N-\right)$ and their associated chromophores and auxochromes.

A chromophore is a region in a molecule where the energy difference between two different molecular orbitals falls within the range of the visible spectrum. Visible-light that hits the chromophore can be absorbed by exciting an electron from its ground state into an excited state.

An auxochrome is a group of atoms attached to a chromophore which modifies the ability of that chromophore to absorb light. If these groups are in

direct conjugation with the pi-system of chromophore, they may increase the wavelength at which the light is absorbed and as a result intensify the absorption.

As stated previously, there are two peaks with maxima at 272 nm and 451 nm. The peak at 451 nm has the highest absorbance magnitude, and was used as the reference point for calculating the discoloration of the methyl orange. The discoloration of the MO – catalyst solution indicates that MO has been degraded. Figure 29 shows the change in spectra over time, and depicts the degradation of the pollutant. Note that the band at 272 nm is increasing with time, and that a new band appears at 334 nm, which can be attributed to the formation of intermediates. This is similar to the findings of Al-Qaradawi et al. [22] and Guettai et al. who state that intermediates are formed during photocatalytic degradation, and they, too, absorb light. It is also clear that these intermediates also degrade over time [20]. Al-Qaradawi et al. concluded that the aromatic rings are responsible for this absorption and that this is responsible for the increase in the intensity and new band which forms at 330 nm. Ultimately, the magnitude of these bands decreases, which indicates the degradation of MO to CO_2 and H_2O [22].

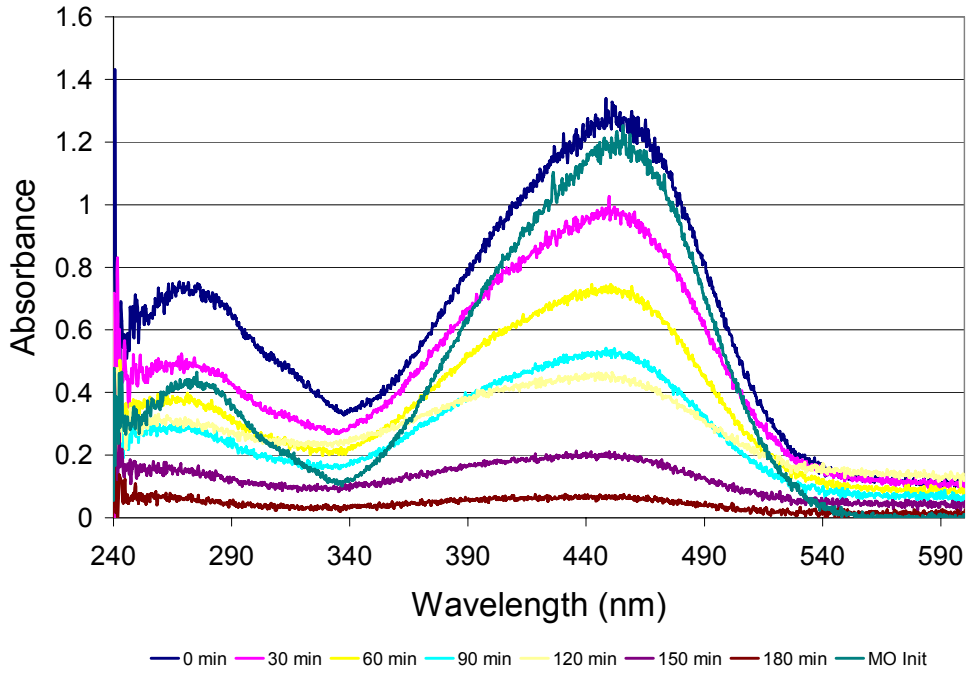

Figure 29 Absorbance Spectra as a Function of Time for Methyl Orange in the Presence of Untreated Degussa P-25 TiO_2 and Simulated Solar Spectrum Irradiation

Further, it was concluded that the two aromatic rings in MO start to degrade thereby creating mono substituted aromatic molecules. Similar to the results of this study, the absorption maxima for both MO and the intermediate products disappear with the exceptions that were previously noted. As a result, the photocatalytic degradation destroys both the conjugate system, which includes $-N=N-$, and either partially or completely destroys the intermediate product(s) converting them to CO_2 and H_2O [20].

4.9 Adsorption of Methyl Orange on Titanium Dioxide

It is widely agreed that the photocatalytic degradation of a pollutant can be modeled using the Langmuir-Hinshelwood model. The Langmuir-Hinshelwood

model describes the mechanism that allows for a reaction to take place at the surface of a catalyst and the adsorbed pollutant in an aqueous solution. In doing so a number of assumptions must be made:

1. The surface of the catalyst has a limited number of adsorptions sites.
2. The surface of the catalyst is covered only by a monolayer, and the adsorption site can only adsorb one molecule.
3. The molecule can both adsorb and desorb from the surface.
4. The surface of the catalyst is homogeneous.
5. There is no interaction between the adsorbed molecules on the catalyst surface.

The Langmuir adsorption model can be given for compounds in an aqueous suspension according to the following equation [24]:

$$\theta = \frac{Q_{ads}}{Q_{\max}} = \frac{K_{ads}C}{1+K_{ads}C} \text{ with, } Q_{ads} = \frac{V}{m}(C_0 - C_t),$$

where θ is the ratio of the TiO_2 surface covered by the adsorbed pollutant, Q_{ads} is the actual quantity adsorbed on the surface, and Q_{max} is the maximum quantity that can be adsorbed on the surface. K_{ads} is the Langmuir adsorption constant, and C is the concentration of the pollutant. The quantity of the pollutant adsorbed on the surface, Q_{ads}, is the ratio of the reaction volume, V, and the

mass of the catalyst, m, multiplied by the difference of the initial dye concentration, C_0, and the dye concentration at time t, C_t.

The adsorbed equilibrium quantity (Q_{eq}) can be measured at equilibrium using the following equation:

$$Q_{eq} = Q_{\max} \frac{K_{ads} C_{eq}}{1 + K_{ads} C_{eq}},$$

where C_{eq} is the adsorption equilibrium concentration.

Although adsorption of an organic pollutant is not required due to the ability of OH radicals diffusing into the bulk of the solution and oxidizing the pollutant, it was concluded in the study by Guettai et al. that no photodegradation took place without the adsorption of MO on the catalyst surface. It is likewise conjectured here to be the same [24].

4.10 Photocatalytic Degradation of Methyl Orange

It has been concluded that the hydroxyl radical is responsible for most heterogeneous photocatalytic oxidations. The hydroxyl radical is formed by the reduction reactions of holes with either water or hydroxide ions [22].

There are many factors that affect the photocatalytic activity of TiO_2. These include the lattice structure and phase of the material, specific surface area, adsorption of the pollutant, electron-hole generation and recombination, carrier lifetime and trapping, solution pH, method of synthesis, catalyst loading, and initial pollutant concentration, among many others. The research for this

study also showed the profound difference that the design and materials of the reactor itself can have on the photocatalytic effect or rate. Although outside of the scope of this work, it was evident by this study that metals ions would be an interesting area of further research as it relates to carrier scavenging [22].

The degradation decay for this study agrees with the literature and follows first order kinetics for simulated solar spectrum irradiation. Figure 30 is representative of the general results obtained showing this first order decay [22].

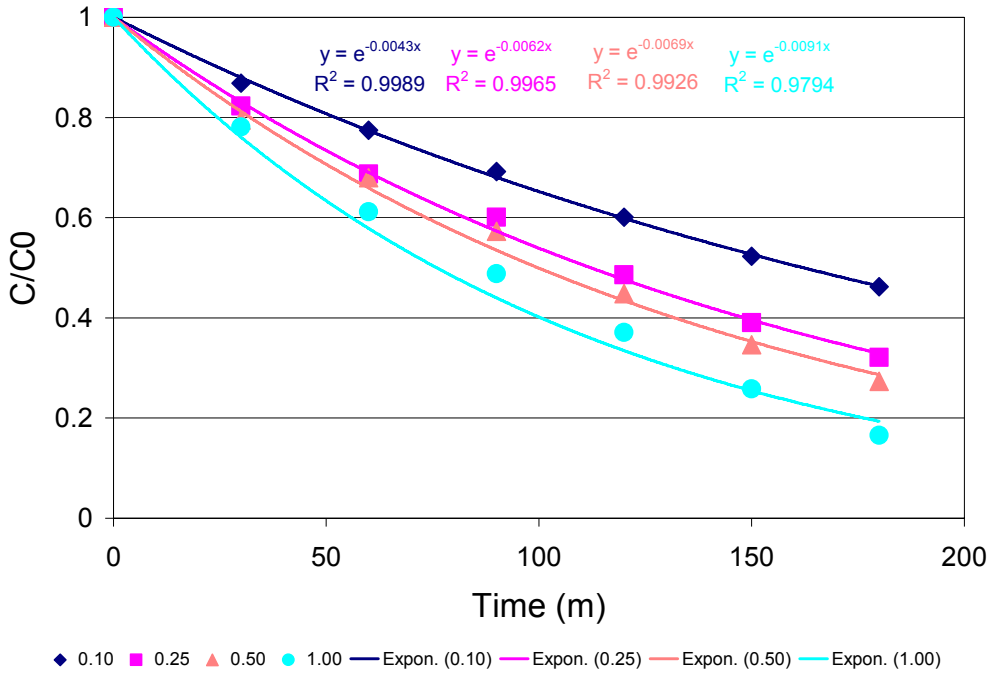

Figure 30 Effects of Catalyst Loading (g/L) on the Rate of Discoloration for Untreated Degussa P-25 TiO_2 Under SSS Irradiation

The first order rate constant is then calculated from the slope of the log plot of the ratio of the measured concentration and original concentration with respect to time. An example of the first order rate constant is illustrated in Figure 31.

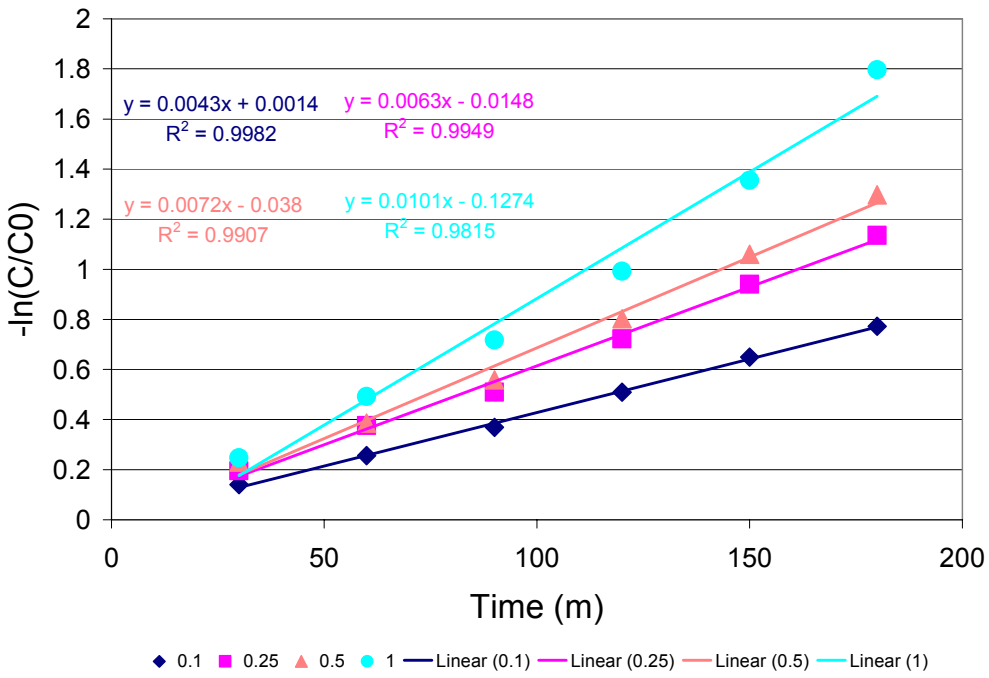

Figure 31 Calculation of Rate Constants for Catalyst Loading (g/L) for Untreated Degussa P-25 TiO_2 Under SSS Irradiation

As stated previously, the results of the photocatalytic degradation for this study fits the Langmuir-Hinshelwood model, which is in line with published work in this area. Simply stated, the oxidation rate, r, can be expressed as:

$$r = \frac{-dC}{dt},$$

where C is the concentration of the pollutant, and t is time. However, the Langmuir-Hinshelwood model must be modified to account for the fact that the catalyst particles are in solution. In solution, both hydroxyl radicals and water molecules have the ability to be adsorbed on the catalyst surface, which means that the active sites of the catalyst could be covered by either, which will impact

the reaction rate [24]. The result is that the expression must account for the adsorption of the pollutant. The expression therefore must be re-written as:

$$r = \frac{-dC}{dt} = k_r\theta = \frac{k_r K_{LH} C}{1 + K_{LH} C + K_S C_W},$$

where k_r the reaction rate constant, θ is the ratio of the TiO_2 surface covered by the adsorbed pollutant, K_{LH} is the pollutant adsorption constant, K_S is the adsorption constant of the solvent (water), and C_w is the concentration of the its solvent. Guettai et al. concluded that given that the concentration of the solvent was much greater than the concentration of the pollutant, the concentration of the solvent remains constant and the coverage of the catalyst by water molecules also remains constant. Holding all experimental conditions constant, the concentration of the pollutant is the only variable and the expression can now be re-written as [24]:

$$r = \frac{-dC}{dt} = \frac{k_r K_{LH} C}{1 + K_{LH} C},$$

Intermediates formed during the photocatalytic process make it particularly difficult to determine the actual photocatalytic degradation rate. Figure 32 shows another example of this phenomenon. The traditional absorption peak at 451 nm continuously shifts to lower wavelengths indicating that intermediate products are forming and degrading. Further, the absorbance spectra, Figure 32, differ significantly from Figure 29 above for wavelengths below 440 nm. The classical

cleavage, described above, into two mono substituted aromatic molecules, cannot be seen in this spectrum.

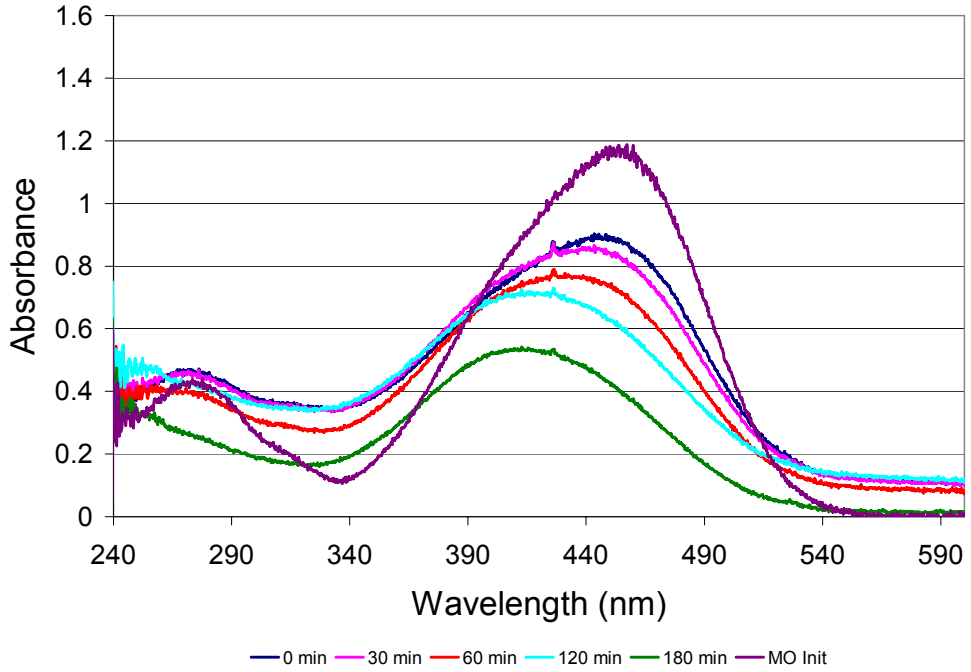

Figure 32 Shift in Spectra Due to Intermediates for 20 ppm Methyl Orange Solution in the Presence of 3 g/L of Degussa P-25 TiO_2 With No Oxygen Source and Under VSSS Irradiation

These intermediates will ultimately compete in the adsorption-desorption process and will complicate the determination of the actual photocatalytic rate. Guettai et al. chose to make calculations at the beginning "illuminated conversion." The rationale was that any changes could be negated. From this, they could re-write the photocatalytic degradation rate only as a function of initial concentration and adsorption constant of the pollutant, as shown in the expression below [24]:

$$r_0 = k_{LH}\theta = k_{LH} = \left(\frac{K_{LH}C_0}{1+K_{LH}C_0}\right),$$

where r_0 is the initial rate of photocatalytic degradation of MO, θ is the ratio of the TiO_2 surface covered by the adsorbed pollutant, and C_0 the initial concentration of the pollutant, which is said to be "equal as possible to the concentration at the adsorption equilibrium, C_{eq}" [24]. Assuming a small value for C_0, this equation is simplified to the first order equation shown below:

$$Ln\left(\frac{C_0}{C}\right) = k_r K t = k_{app} \qquad \text{or} \qquad C_t = C_0 e^{-k_{app} t},$$

where $k_r K = k_{app}$. From this equation for the apparent first order rate constant, k_{app}, the initial degradation, r_0, rate is given by the equation:

$$r_0 = k_{app} \cdot C_0,$$

Consistent with the literature, this study found that the plot of Ln(Ce/C) versus time produces a straight line. The literature concluded that the k_{app} is given by the slope of the linear regression of this plot [24].

Guettai et al. concluded that the degradation rate is a function of the initial concentration of the pollutant. The initial concentration causes the rate to increase until a concentration threshold is reached, and that beyond this point, the degradation rate is independent of the concentration [24]. Using the reciprocal of the initial rate, $\frac{1}{r_0} = \frac{1}{k_r} = \frac{1}{kK_r} \cdot \frac{1}{C_0}$ Guettai et al. also concluded that the plot of the reciprocal confirms the Langmuir-Hinshelwood model. This again

points to the photocatalytic process beginning with the adsorption of the pollutant.

Further, they concluded that given that the reaction does follow the Langmuir-Hinshelwood model, and K_{HL} is the actual adsorption affinity of the pollutant on the surface of the catalyst, then K_{ads} and K_{LH} should be identical. From this relationship, they concluded that the “photocatalytic degradation of MO under optimized working conditions follows satisfactory the Langmuir-Hinshelwood model” [24].

CHAPTER 5: FUNDAMENTALS OF NITROGEN-DOPING

5.1 Decreasing the Band Gap of TiO_2

Untreated TiO_2 can utilize less than 4% of the available solar energy for photocatalysis. Given the exceptional photocatalytic properties of TiO_2, a great deal of study has gone into decreasing the band gap to allow visible-light activated photocatalysis. Doping TiO_2 by metals or transition metals, and anion doping have dominated this area of research. Research has shown that the substitution of oxygen by nitrogen in metal oxides can cause a red-shift of the absorption edge and facilitate the absorption of visible-light [25]. One of the primary goals of this research was to investigate a relatively inexpensive way to lower the band gap of Degussa P-25 TiO_2 by doping it with nitrogen.

Anion doping is a method that has received a great deal of attention and is the focus of this study. Numerous studies using carbon, sulfur, iodine, and nitrogen have been conducted showing that the band gap of TiO_2 can be reduced [3, 8, 9, 19, 22-49]. Doping TiO_2 with anions alters the conductivity and optical properties by creating new surface states that are believed to lie near the conduction band or valence band of TiO_2 [9]. It was found that these materials had high photocatalytic efficiencies in the visible region. As a result, the improvement was attributed to a shift in the absorption edge and narrowing of the

band gap of the material. Subsequent studies show that the actual mechanism for the improvement is of great debate.

The doping of oxides such as TiO_2 creates a set of problems of its own, such as the creation of recombination centers in the created electronic states. It has been shown that the electrical properties are strongly influenced by defects and dopants [10]. Therefore a great deal of research has focused on delaying the recombination of photogenerated electron-hole pairs by adjusting microstructure, processing routes and composition of TiO_2 [3].

Previous work in this area has shown that substitutionally doping TiO_2 with nitrogen to produce $TiO_{2-x}N_y$ is an effective method of creating a visible-light active photocatalyst [26-30]. By calcinating TiO_2 in an ammonia atmosphere, or by a wet chemical method, TiO_2 can be easily modified for utilization of the visible spectrum [31]. This study accomplishes substitutional nitrogen-doping of the catalyst using a gas phase impregnation method using anhydrous ammonia as a nitrogen source.

5.2 Mechanism of Visible-Light Absorption and Photocatalytic Activity

There appear to be as many conclusions as there are studies regarding the result of nitrogen-doping. In general, it is agreed that doping TiO_2 with nitrogen creates new surface states that result in new energy levels in the band gap. These new levels provide pathways for electron transfer between the

catalyst and the acceptor species in the solution [9]. However, there is no consensus on where these new states are, or how this is accomplished. In general, the results of nitrogen-doping can be categorized as follows:

1. Nitrogen-doping decreases the band gap by the overlap of nitrogen 2p orbital (N2p) and the oxygen 2p orbital (O2p) [32].
2. Nitrogen-doping does not decrease the band gap, but instead creates new electronic state(s) above the valence band [33].
3. Nitrogen-doping does not decrease the band gap, but instead creates new electronic state(s) below the conduction band [34].
4. Oxygen vacancies, which are a result of the thermal effect of the nitrogen-doping process, are responsible for photocatalytic improvement [35, 36].

5.2.1 Decrease in Band Gap Due to the Overlap of N2p and O2p Orbitals

A number of studies regarding the density of states for nitrogen-doped TiO_2 concluded that the N2p states and the O2p states overlap due to the substitutional doping of oxygen with nitrogen. Liu et al., Irie et al., and Miyauchi et al., all performed calculations of the densities of states for anion doping in anatase TiO_2. They concluded that nitrogen-doping was the most effective method of achieving visible-light photocatalytic activity [25, 33, 37].

Irie et al. concluded, along with a number of authors, that the band gap decreases due to the creation of an isolated nitrogen 2p (N2p) band above the oxygen 2p (O2p) valance band by substitutionally doping nitrogen atoms in place of oxygen atoms in the lattice of TiO_2. Further, they concluded that this N2p band is responsible for the visible-light photocatalytic activity [33]. In contrast, Diwald et al. concluded that the "co-doping effect" of nitrogen and hydrogen is the cause for the visible-light photocatalytic activity [38].

Although Pan et al. agreed that band gap narrowing is a result of the mixing of N2p and O2p states; they draw a different conclusion regarding visible-light absorption. They concluded that visible-light absorption is due to the formation of Ti^{3+} from the reduction by H_2 of Ti^{4+} during the decomposition of ammonia during treatment at 600°C. They found that the higher the temperature of ammonia treatment, the greater the red-shift was [39]. This study has found similar results.

In the study by Madhsudan et al., they proposed how nitrogen-doping reduces the band gap of TiO_2. Figure 33, from their study, depicts the effect of nitrogen-doping on the creation of new surface states. The band bending illustrates the initiation of redox charge transfer reactions [9]. Diagrams a, b, and c represent the band pinning at the semiconductor–electrolyte interface. Figure (a) shows the accumulation of charge at the interface when the pH of the solution is 2. Figure (b) depicts the flat band where the Fermi level (E_F) is in equilibrium. Figure (c) shows the depletion layer for a solution of pH of 10. The

band diagram (d) illustrates intermediate levels that are produced in TiO_2 after nitrogen-doping. Figure (e) shows the band bending at the nitrogen-doped TiO_2–electrolyte interface.

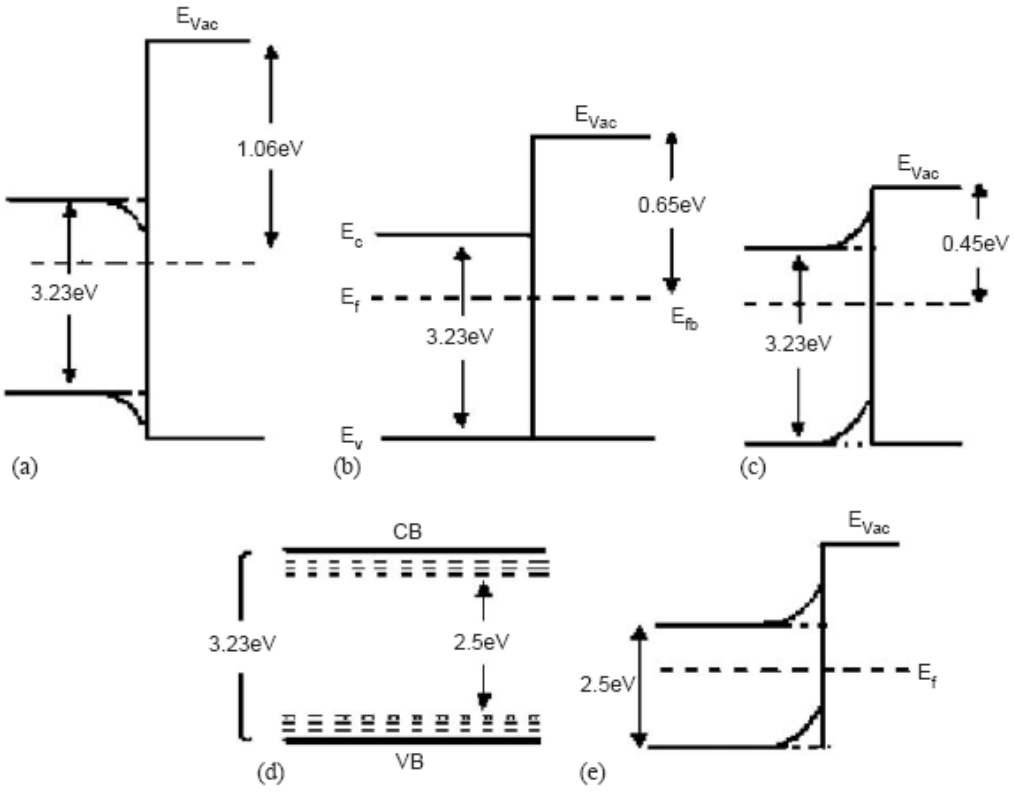

Figure 33 Hypothetical Band Gap of Nitrogen-Doped TiO_2 Proposed by Madhsudan et al. [9]

5.2.2 Creation of New Electronic States Above the Valence Band [9]

Asahi et al. concluded that the narrowing of the band gap by nitrogen-doping results in visible-light photocatalytic activity [32]. Whereas Irie et al. concluded that it was not the narrowing of the band gap, but instead a narrow band above the valence band that is responsible for the visible-light activity [33].

In the study by Irie et al., $TiO_{2-x}N_y$ irradiated with ultraviolet light produced a higher photocatalytic rate than $TiO_{2-x}N_y$ irradiated with visible-light. They claim that nitrogen was substitutionally doped into the TiO_2 oxygen lattice sites, and this resulted in an isolated narrow band above the valence band. Ultraviolet radiation excites the electrons from both the valance band and the narrow band. However, if visible-light is used to irradiate the catalyst, only electrons in the narrowband are excited to higher energy levels. From this difference an important conclusion is drawn. If the band gap of TiO_2 is narrowed by substitutional nitrogen-doping, then the photocatalytic rate should be the same for both ultraviolet and visible-light, which of course it is not. Therefore, Irie et al. concluded that the band gap of TiO_2 is not narrowed, but instead the isolated narrow band above the valence band which is created by nitrogen-doping is responsible for the visible-light photocatalytic activity [33].

5.2.3 Creation of New Electronic States Below the Conduction Band

Torres et al. concluded that nitrogen-doping created a new set of electron trap states just below the conduction band positioned energetically in a broad range of 1.3 eV [34]. These states, which they calculated to have a similar density of states as nitrogen atoms also acted as electron-hole recombination centers. The new states responded to ultraviolet, visible and infrared light at wavelengths greater than 700 nm and worked as long-lived electron traps [34].

5.3 Creation of Oxygen Vacancies Due to Thermal Effects

What also must be considered is the thermal effect of the treatments on oxygen deficiencies in the lattice of TiO_2, as oxygen vacancies alone can cause TiO_2 to respond to visible-light. This leaves open a debate whether the oxygen vacancies are created by thermal effects associated with doping methods, or doped nitrogen atoms are responsible for visible-light activity.

Thermal treatments alone have been found to create sub band gap levels in their electron structures. These electron structures are believed to allow low energy excitation pathways. Further, oxygen deficient sites on the catalyst surface are highly reactive sites that react with oxygen molecules. Ihara et al. determined that 400°C is the "transition temperature" for the creation of the maximum number of oxygen vacancies [35]. While calcination alone increases oxygen vacancies, it also has the negative impact of reducing the adsorption affinity of the catalyst as a result of a decrease in specific surface as seen in BET surface area measurements [35].

From two separate studies, Nakamura et al. concluded that the photocatalytic activity of nitrogen-doped TiO_2 is caused by surface intermediates of oxygen reduction, or by H_2O oxidation and not by direct reaction with the holes trapped at nitrogen induced mid-gap levels [13], and, that the oxygen vacancies that are formed during the nitriding process act as electron traps that improve the visible-light reactivity [40]. Yates et al. concluded that this occurs "when an electron is excited to the oxygen vacancy state from the valance band (even

under visible-light). “These electrons (or the holes formed) react with atmospheric oxygen (or an oxygen related species) producing reactive species (O^- or atomic oxygen), which participate in the oxidation of surface species” [23]. Prokes et al. however, believe that this same phenomenon actually reduces the photocatalytic activity since trapped photoelectrons cannot easily reach the reactive surface sites of the catalyst [41].

5.4 Nitrogen Concentration and Phases Changes Due to Thermal Effects

Similar to the results of Pan et al. reported above, Wei et al. also observed an increase in the absorption of visible-light with increasing nitrification temperature up to 550°C. However, raising the temperature to 600°C resulted in a decrease in the visible-light absorption. They attributed the observed phenomena to a change in the crystal structure caused by the high doping concentration of nitrogen in the TiO_2. As was found and reported in this study, another explanation may be transition from anatase to rutile phase that takes place at higher temperatures, which is also the conclusion by Mozia et al. They reasoned that if the crystallographic structure of TiO_2 changes, that this could change the doping mechanism. The result is change in the ultraviolet and visible-light absorption of the catalyst [42].

The conclusion of this study is that there is no significant change in anatase to rutile ratio for nitrogen-doped TiO_2 for temperatures below 625°C. Silveyra et al. made a similar conclusion for nitrogen-doped TiO_2 at temperatures

below 600°C. Both studies found that significant differences in anatase to rutile ratio between untreated Degussa P-25 and nitrogen-doped Degussa P-25 begin treatment temperatures over 700°C [43].

The study by Wang et al. concluded that the transition from the anatase to rutile phase during nitrogen-doping is restrained by the doping of nitrogen into the TiO_2 lattice during the preparation of $TiO_{2-x}N_y$. This is the basis of their conclusion that $TiO_{2-x}N_y$ has a higher photocatalytic activity than pure TiO_2. They reason that since the anatase phase has a higher band gap than the rutile phase, the photocatalytic activity must be attributed to visible-light absorption of $TiO_{2-x}N_y$, and not to an increase in rutile phase [11].

Similarly, surface area measurements show the same relationship for nitrogen-doped materials. The results of this study (see Figure 34) also coincide with the findings of Silveyra et al., which find that the change is surface area is negligible for nitrogen-doped TiO_2 treated at 600°C and 625°C [43]. Both studies found that the surface area remains moderately constant until treatment temperatures greater than 700°C where a reduction of surface area increases rapidly with increasing temperature. Silveyra et al. refer to Degussa P-25 TiO_2 as a “nonporous material which consists of spherical particles with a mean diameter of 30 nm”. They concluded that sintering is responsible for the loss of surface area. This study found a reduction of approximately 40% in surface area for nitrogen-doped Degussa P-25 at 675°C, whereas Silveyra et al. found no

significant difference between treated Degussa P-25 and nitrogen-doped Degussa P-25 at 600°C. [43].

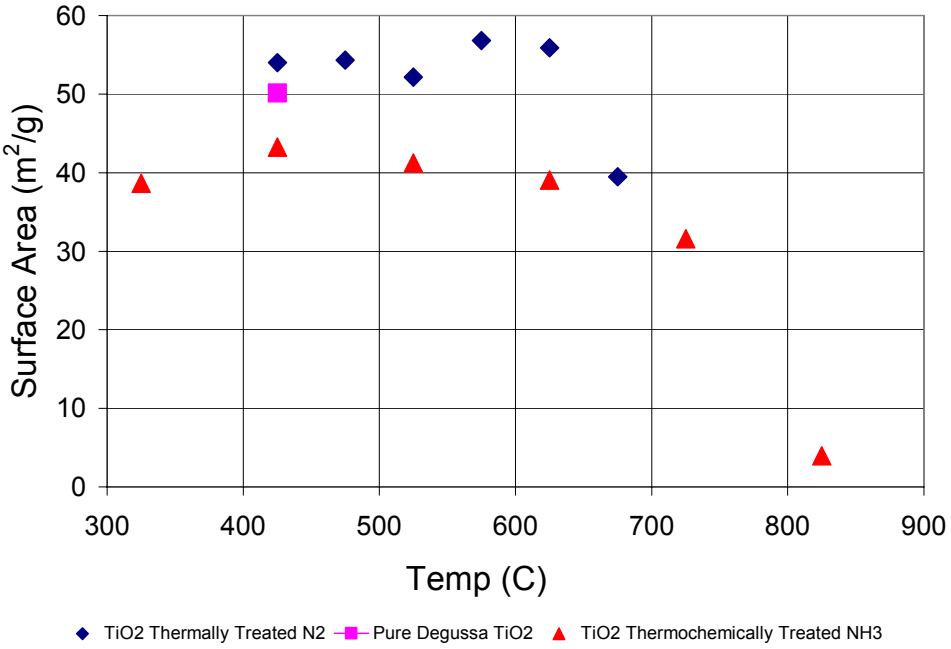

Figure 34 BET Surface Area Measurements for Pure, Calcinated and Thermochemically Ammonia Treated Degussa P-25 TiO_2

The accepted view of this study is that substitutionally doped nitrogen is responsible for the visible-light absorption. A number of studies have used XPS to make conclusions regarding the composition of $TiO_{2-x}N_y$. Yuan et al. concluded that molecularly chemisorbed nitrogen is removed during high temperature doping processes such as annealing [44]. Although some chemisorbed nitrogen does remain and does contribute to visible-light absorption, it was determined that the photocatalytic activity is primarily promoted by substitutionally doped nitrogen [44]. However, it must be again noted that

calcinated Degussa P-25 TiO_2 also has higher photocatalytic activity which might result from the slight phase transformation of TiO_2 from anatase to rutile [44].

5.5 Effect on Photocatalytic Activity

Similar to the effects of nitrogen-doping on the electronic states of TiO_2, there is also debate whether or not nitrogen-doping improves photocatalytic activity. Generally speaking, there are three schools of thought regarding the effect of nitrogen-doping:

1. Positive Effect on Photocatalytic Activity [32, 45]
2. No Effect on Photocatalytic Activity [35, 36, 46, 47]
3. Negative Effect on Photocatalytic Activity [19, 29, 55]

What must be noted is that photocatalytic effect is application specific, and that mistakes may be made in casting overreaching conclusions. It is also apparent that the methods used to synthesize and test the catalyst have a significant effect on the results as similar studies offer conflicting conclusions as even the authors themselves note.

5.5.1 Positive Effect on Photocatalytic Activity

It was concluded in some studies that the visible-light photocatalytic efficiency of nitrogen-doped TiO_2 is a function of doping level. These studies found that the photocatalytic effect increases with increasing nitrogen concentration [22, 58]. This continues until a threshold concentration is

exceeded at which point the photocatalytic efficiency decreases. Further, the concentration level was determined to be doping method specific [45]. The study by Asahi et al. concluded that visible-light photocatalytic activity is a result of the reduction in the band gap due to nitrogen-doping [32].

5.5.2 No Effect on Photocatalytic Activity

In contrast, Ihara et al. and Martyanov et al. concluded that the oxygen vacancies created by thermal effects are responsible for the photocatalytic activity of $TiO_{2-x}N_y$ [28, 52]. Ihara et al. concluded that oxygen-deficient sites formed in the grain-boundaries are important to visible-light photocatalytic activity, and that nitrogen-doped in oxygen-deficient sites in TiO_2 is important as a blocker for reoxidation [35].

The commonly held assertion that nitrogen-doping causes the overlap of the N2p and O2p states, and therefore, is responsible for the visible-light photocatalytic activity is challenged by Xu et al. who concluded that impurity states are localized and lie slightly above the top of the O2p valence band. Their conclusion implies that the mixing of N2p with O2p states is small even for high concentrations of nitrogen [46].

Huang et al. concluded that nitrogen-doping only improves the absorption in the visible region, and that quantum yield, or photocatalytic rate, is still very low and not necessarily useful for practical applications [47].

5.5.3 Negative Effect on Photocatalytic Activity

Yates et al. concluded that photogenerated holes are trapped at the mid-gap states that are created by doping and as a result decrease their oxidation power and reduce the photocatalytic activity of the catalyst. It is also speculated that doping may induce structural instabilities in TiO_2. This is due to lattice distortions and bond weakening that result from doping [23].

It is also believed that increasing the nitrogen concentration actually lowers the photocatalytic activity. There are two conclusions regarding this. First, that doping sites could also serve as recombination sites [33]. Second, that photocatalytic activity is actually reduced since trapped photoelectrons cannot easily reach the reactive surface sites of the catalyst as a result of oxygen vacancies that are created in the doping process [41].

Diwald et al. also concluded that the reduction in photocatalytic activity of substitutionally doped nitrogen is from “induction of ionic charge compensation” [48]. What takes place is that the nitrogen acceptors are compensated by donor levels that are related to additional oxygen vacancies. This results in an increase in electronically reduced Ti^{3+} states. Their conclusion is that a blue shift is caused as a result of substitutional nitrogen-doping due to the partial filling of electrons in the conduction band [48]. Yates et al. alluded to other studies which also draw conclusions based on the reduction of photocatalytic activity of nitrogen-doped TiO_2 [23].

Regarding the reduction of TiO_2, Irie et al. determined that the photocatalytic activity reduces with increasing nitrogen concentration. They found that $TiO_{2-x}N_y$ powders formed using a NH_3 atmosphere not only has oxygen replaced with nitrogen, but that TiO_2 is simultaneously reduced. The result is an increase in oxygen vacancies and the amount of Ti^{3+}. If correct, this conclusion has a dramatic effect on the photocatalytic rate as this suggests that the oxygen vacancies act as a recombination center for holes and electrons. They further concluded that an increase in the NH_3 annealing temperature resulted in an increase in TiO_2 reduction, and a higher number of oxygen vacancies. This is the basis of their conclusion regarding the reduction in photocatalytic activity for increasing nitrogen concentration [33].

5.6 Reducing the Recombination Rate of Electron-Hole Pairs

Lindgren et al. also found a larger density of Ti^{3+} states in nitrogen-doped TiO_2 compared with undoped TiO_2. They concluded that those states, together with slow hole transport in the nitrogen induced band, are the reasons for the high rate of recombination in $TiO_{2-x}N_y$ [49].

It is believed that doping creates new band structures that contribute to the recombination of photogenerated electron–hole pairs. However, it is also believed that by using specific dopants that it is possible to improve the efficiency of the photocatalytic activity by creating new band structures or by suppressing the effects of existing band structures to improve quantum efficiency. Coupling two semiconductors is also seen as a technique to enhance charge separation

given that the semiconductors have conduction and valence band potentials that would enhance the separation [23].

Transition metals such as zinc, iron, and tungsten have been doped to substitute Ti^{4+}. Transition metals enable the separation of photogenerated electron–hole pairs and increase the light absorption [3]. This study did introductory work regarding the coupling, or co-doping of TiO_2 with tungsten but found no evidence of improvement and no motivation for continuing that work.

5.7 Current Methods for Producing Nitrogen-Doped TiO_2

As an initial remark regarding the selection of anhydrous ammonia as the nitrogen source for this study, urea would be more environmentally friendly nitrogen source than anhydrous ammonia. This has been studied by Yuan et al. and should be considered for future work [44].

There are numerous other methods that are being utilized to synthesize nitrogen-doped TiO_2. Those methods include oxidation of titanium nitride [50], calcination of hydrolysis products of $Ti(SO_4)_2$ previously treated with an aqueous NH_3 solution [35], calcination of TiO_2 under an ammonia atmosphere [51], substitutional doping of metal ions [52], DC magnetron sputtering the TiO_2 target in N_2(40%)/argon gas atmosphere [32], ion implantation [53], organic dye sensitization [54], metal organic chemical vapor deposition (MOCVD) method using titanium-tetra-isopropoxide as a precursor and ammonia as the nitrogen source [28], hydrogen plasma reduction of TiO_2 [13], pulsed laser deposition

method [55], hydroxide or surface coordination [56], and high temperature treatment of single-crystal TiO_2 in an argon atmosphere (870K) and nitrogen-doped when argon is replaced by NH_3 [38]. Yates et al. categorized them into three broad areas [23]:

1. Modification of existing TiO_2 in the forms of powder, films and single crystal, or TiN via gas phase chemical impregnation.
2. Modification of existing TiO_2 via ion bombardment.
3. Growth of TiN_xO_y from liquid or gaseous precursors.

5.8 Formation of Titanium Nitride as a Result of Nitrogen-Doping

The visible-light absorption affinity of $TiO_{2-x}N_y$ is understood to be in direct proportion with the nitrogen concentration of the catalyst [31]. In their study, Li et al. concluded that nitrogen exists only as an impurity due to its low concentration. This low concentration is too low to form a new phase that would shift the fundamental absorption edge of TiO_2 [31]. The black and brown materials in this study however, clearly suggest movement of the fundamental absorption edge as noted in Figure 70.

For colored nitride compounds such as the black and brown materials, this shift was attributed to the substitutional doping of nitrogen atoms [57]. Although studies suggest that increasing concentrations of nitrogen are proportional to color, Liu et al. found that visible-light activity was not directly proportional to the red-shift of the second absorption edge [25]. Diwald et al. supposed it is due to a

form of nitrogen that is likely to be interstitial and chemically bound to hydrogen in the first few hundred angstroms below the TiO_2 surface [51].

Miyauchi et al. found that the creation of TiN crystal phases by high temperature TiO_2 annealing in ammonia had a detrimental effect on catalyst activity, which is the conclusion of this study [37].

5.9 Decreasing the Band Gap

The optical absorption data was deduced from the Kubelka–Munk function calculated for untreated Degussa P-25 TiO_2 and the thermochemically ammonia treated Degussa P-25 TiO_2 samples.

The Kubelka-Munk method is a diffuse reflectance technique that uses a salt, NaCl in this case, mixed with the powder being measured. This technique accounts for the difference in transmission and reflectance measurements due to absorption of certain wavelengths by powders. The material was diluted to about 1% by weight in NaCl and ground using a mortar and pestle. Transmission measurements were made of the powders, which were lightly packed into small sample holders, using an optical spectrometer. A Kubelka-Munk conversion was applied to a diffuse reflectance spectrum to compensate for differences. The Kubelka-Munk equation is:

$$f(R) = \frac{(1-R)^2}{2R} = \frac{k}{s},$$

where: R is the absolute diffuse reflectance of the sampled layer, k is the molar absorption coefficient, and s is the scattering coefficient.

A linear relationship is created between the spectral intensity relative to the sample concentration. This equation assumes that the diluting salt is non-absorbing, that the scattering coefficient of the salt is constant, and that the sample thickness is infinite. These assumptions can be made for samples greater than1 mm of highly diluted small particles. Given that we used nanoparticles and had a sample thickness of 3mm, our packing technique was the only variable that could affect the scattering coefficient. This technique was perfected over time by a fellow CERC student, Ms. Paula Algarin.

The UV-Vis diffuse reflectance spectra for thermochemically ammonia treated Degussa P-25 TiO_2 are shown in Figure 35. These materials were thermochemically treated with anhydrous ammonia at a flow rate of 87.3 mL/min. as a nitrogen source at 675°C for six hours. This was followed by annealing in a nitrogen atmosphere at a rate of 41.7 mL/min. for six hours. Finally, the material was oxidized at 400°C for 15 minutes in an oxygen atmosphere.

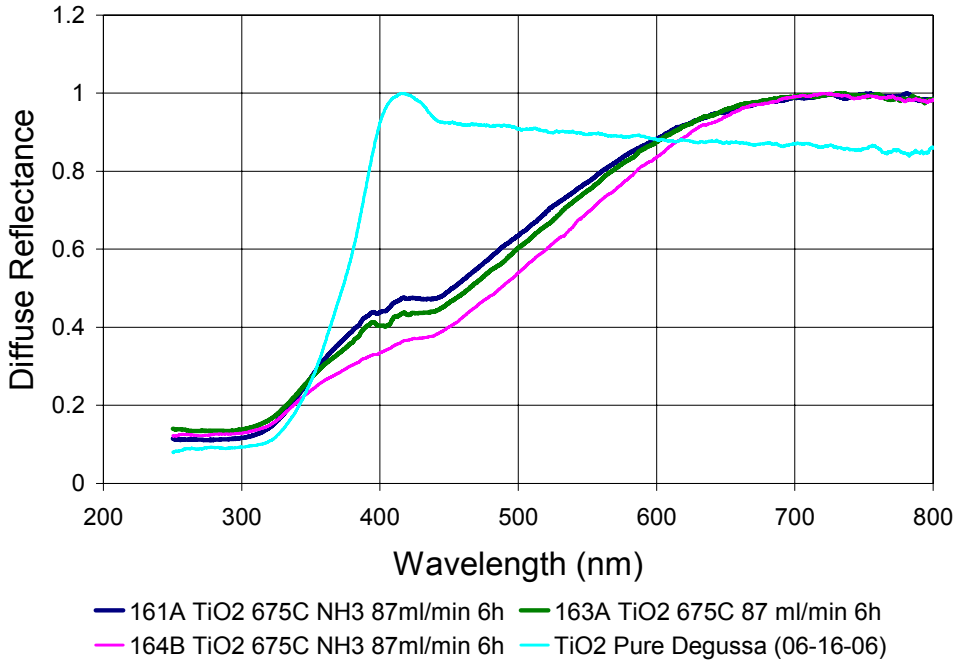

Figure 35 Diffuse Reflectance of Pure, Thermochemically Ammonia Treated Degussa P-25 TiO_2

The absorption edge of the samples is determined by the following equation:

$$E_g = \frac{1239.8}{\lambda},$$

where E_g is the band gap, measured in electron volts, of the sample, and λ is the wavelength of the onset of the spectra measured in nanometers [58]. For TiO_2 to produce active photocatalytic species, it must absorb photons with energy that is equal to or greater than the band gap. For visible-light photocatalysis this requires band gaps of less than 3.1 eV. However, for practical considerations, band gaps around 2.5 eV, which corresponds to wavelengths of 500 nm, have been the goal of this study.

Anatase TiO_2 shows a single sharp edge, while $TiO_{2-x}N_y$ shows a second band edge as can be seen in Figure 36. The first band edge is attributed to the oxide at 390 nm and the weaker shoulder due to nitrogen-doping is at 450 nm. The absorption is probably due to the $O^{2+} \rightarrow Ti^{4+}$ charge transfer. This is a result of the excitation of electrons from the valence band $O2p_{\pi}$ to the conduction band $Ti(d_{xy})$ [8,15]. Jang et al. concluded that this second peak is responsible for the visible-light catalytic activity [26]. The presence of the second absorption edge could be due to the substitutional N-doping. Asahi et al. concluded this edge is due to the excitation of electrons from the valence band of $N2p_{\pi}$ to the conduction band $Ti(d_{xy})$ instead of from $O2p_{\pi}$ as in TiO_2 [32].

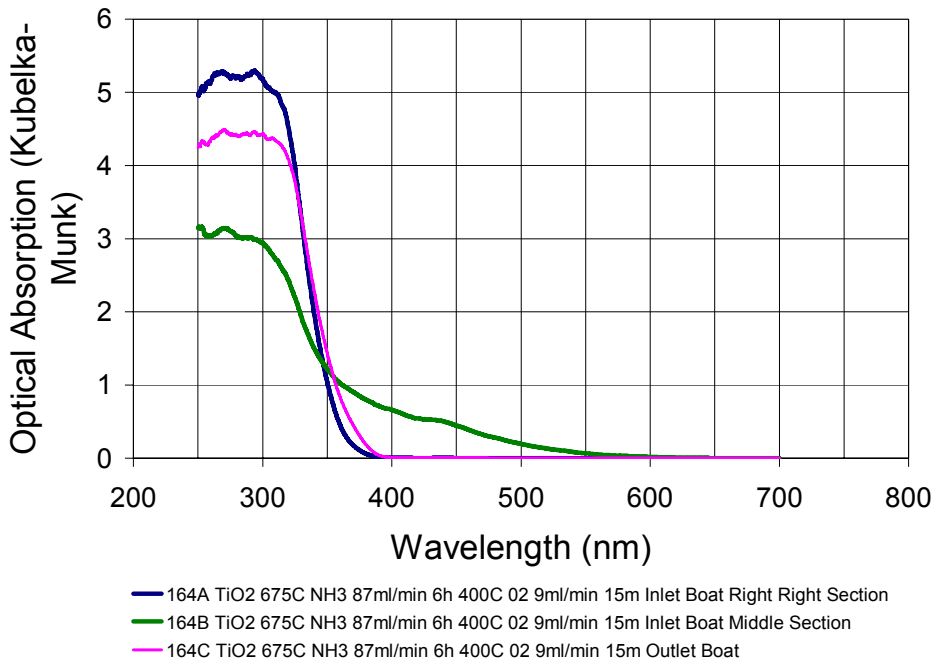

Figure 36 Optical Absorption (Kubelka-Munk) of Thermochemically Ammonia Treated Degussa P-25 TiO_2

The displacement of the first absorption edge is probably caused by the transformation of anatase to rutile due to high temperature heating. From the presence of the additional edge in the visible-light range it can be supposed that the modified catalysts should be active under visible-light illumination [51].

Li et al. concluded that the second absorption band is due to doped nitrogen atoms. They reasoned that:

1. The band does not exist in untreated TiO_2.
2. The yellow color of the catalyst is due to position of the absorption edge in the visible spectrum [31].

The color of untreated Degussa P-25 is brilliant white. The color of the catalysts synthesized in this study varied, and was dependent on temperature and ranged from a very pale yellow to vivid yellow, and to brown and black materials. Materials treated at temperatures below 600°C remained white, and materials were colored as noted. According to Mozia et al., one can conclude that the higher treatment temperatures facilitate nitrogen bonding to the TiO_2 matrix [42]. For temperatures below 600°C the increase in performance, if any, is attributable only to thermal effects.

The shift in the absorption edge in Figure 36 was attributed to Ti^{3+} by Irie et al. This reduction of TiO_2 is accomplished by H_2. During thermal ammonia treatments, NH_3 is decomposed into N_2 and H_2, which is the reducing gas [33]. This second absorption edge indicates the formation of a new N2p band located above the O2p valence band according to Yin et al. [30].

CHAPTER 6: EXPERIMENTAL SYSTEMS

6.1 Thermal and Thermochemical Treatment System

Like most of the systems used during this study, the system used for the thermal and thermochemical treatments were continually upgraded and grew in complexity as greater and greater control was sought. The block diagram in Figure 37 shows that the final thermochemical treatment system consisted of two subsystems, a gas control subsystem, and a furnace reactor subsystem.

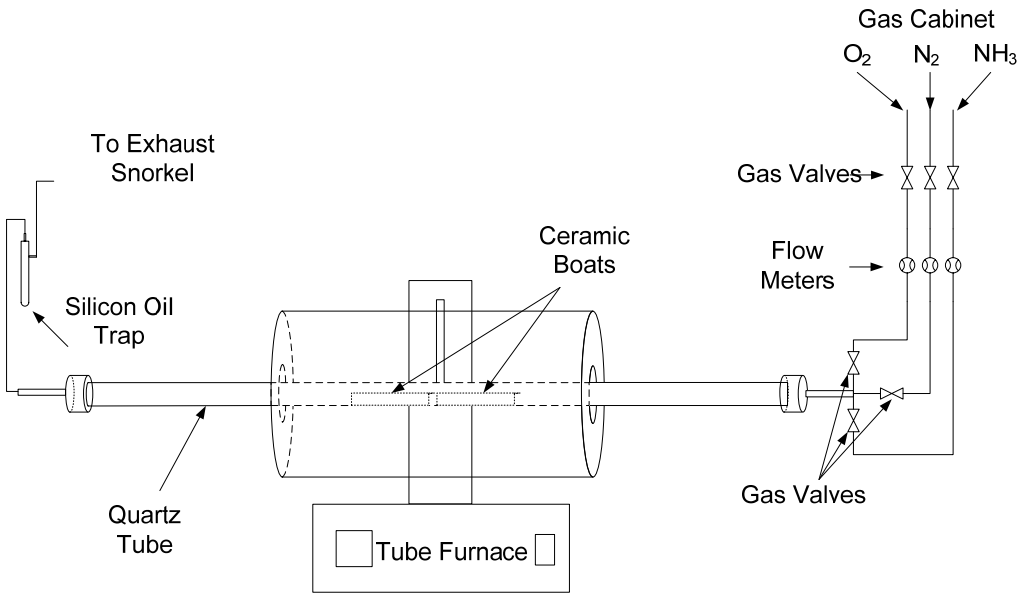

Figure 37 Block Diagram of Tube Furnace Reactor System

The gas control subsystem used ultra-high purity (UHP) nitrogen (N_2), product grade anhydrous ammonia (NH_3) and ultra pure (UP) carrier oxygen

(O_2). Nitrogen was used as a dry inert gas for system purging, calcination, sintering and annealing. Nitrogen-doping was accomplished using a gas phase impregnation process utilizing anhydrous ammonia (NH_3) as a nitrogen source Oxygen or a mixture of nitrogen and oxygen was used for oxidation of the thermochemically treated catalyst. A system of valves and gas specific flow meters were configured to meter specific rates of gas into a quartz reaction tube (Corning 77481). The exhausted gasses were first bubbled through silicone oil, acting as a check valve, to an exhaust snorkel. Although the positive pressure of the gasses made the silicone oil trap unnecessary, it was kept as a visual safety measure due to the use of anhydrous ammonia.

The tube furnace reactor system designed and implemented by the author consisted of a Barnstead Thermolyne 21100 (model F21135) Tubular Furnace and a notebook computer running a custom-made Proportional-Integral-Differential (PID) control program developed in National Instruments, LabVIEW 8.0. The computer and tube furnace were interfaced using a National Instruments Model USB6210 data acquisition device.

The original end-cap insulation of the tube furnace was replaced and the temperature profile of the furnace was studied to insure a uniform working reaction area to be used during the study. Figure 38 is the profile of the temperature gradient along the horizontal axis of the tube furnace. A minimum treatment area of four inches from center was required for this study. This profile was obtained to ensure that a working reaction area could be defined within the

quartz tube, and as can be seen, it extended more than five inches from the center. Coors glazed porcelain boats (L x W x H: 4 x 3/4 x 1/2 in.; Coors #60036) were used as TiO_2 treatment receptacles.

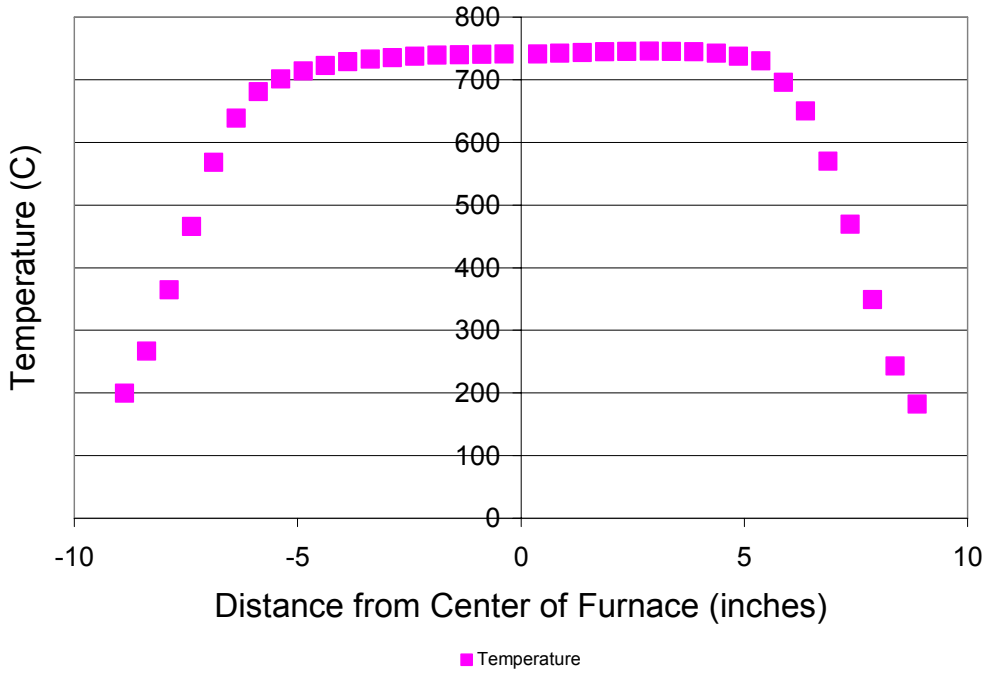

Figure 38 Temperature Profile for Tube Furnace Reactor

6.2 Photocatalytic Reactor

The photocatalytic experiments were performed using a set of three glass suspension batch reactors that was fabricated by Mr. Chuck Garretson, who is the CERC's lab technician. Figure 39 shows the general configuration of the system. A one liter Pyrex beaker was used for the housing of the batch reactor and a plastic mounting plate, as seen in Figure 40, was used for attaching the necessary connections. A cooling coil, using tap water for heat transfer, was made of ¼ inch stainless steel tubing, which fit loosely around the interior

circumference of the beaker. An aerating stone was used to diffuse either compressed air or oxygen into the suspension. Experiments were conducted using breathing quality compressed air and ultra pure carrier oxygen, which were metered through gas specific flow meters.

Four Pyrex (9820) culture tubes housed 150 watt halogen light sources that were mounted through holes in the mounting plate (Figure 40). Simulated solar spectrum (SSS) experiments were conducted using this setup. For visible simulated solar spectrum (VSSS) experiments, four Pyrex (9820 – 18) culture tubes were inserted inside of the larger tubes using stainless steel wire as a spacer for the ultraviolet filter solution. A five molar solution of $NaNO_2$ was used as a filter for ultraviolet (UV) light thereby allowing only the transmission of wavelengths in the visible spectrum. A thermocouple, also mounted through the top plate, monitored the temperature of the solution. A magnetic stirrer and stirring rod were used to suspend the particles throughout the solution.

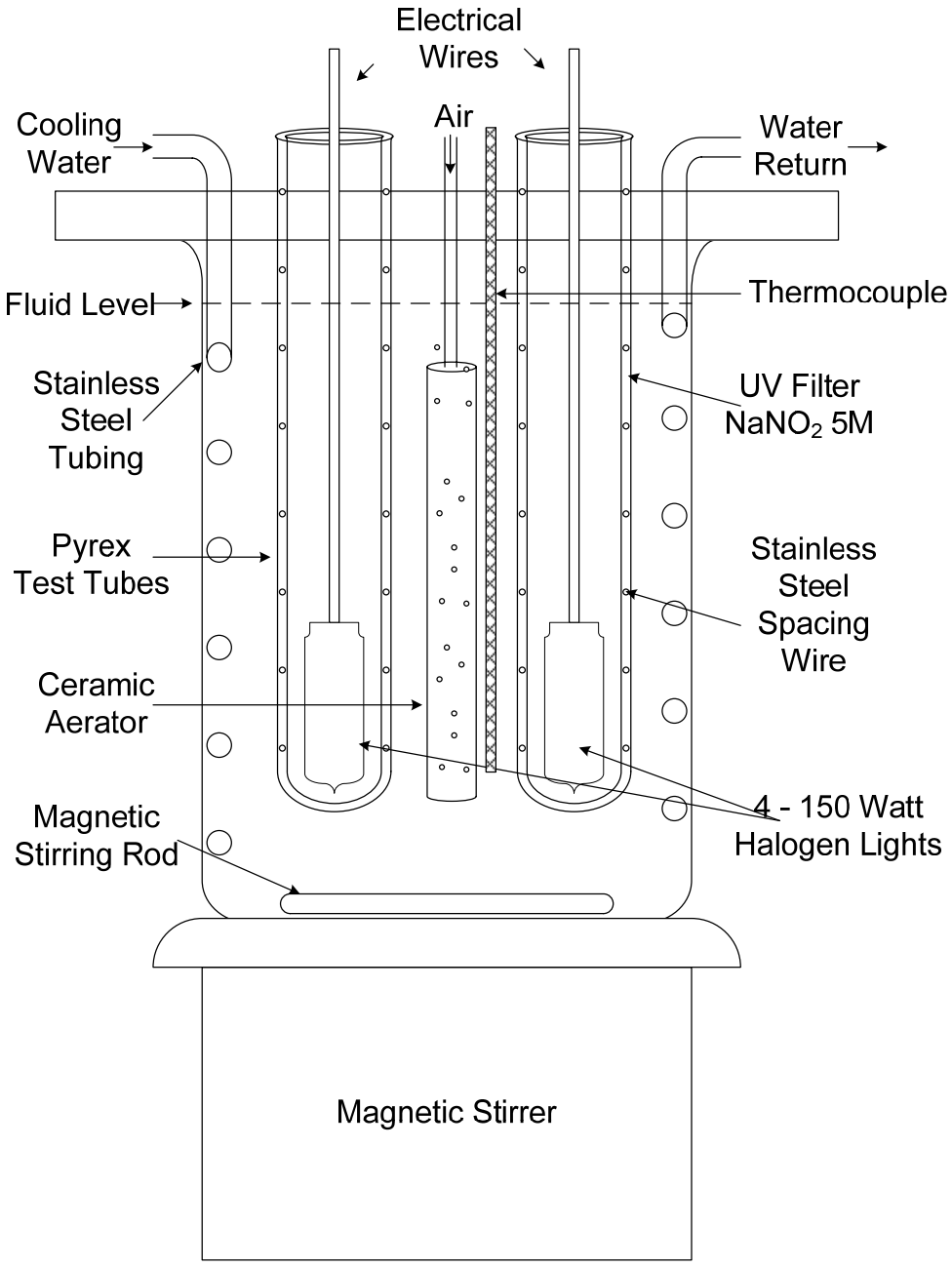

Figure 39 Batch Reactor for Photocatalytic Experiments

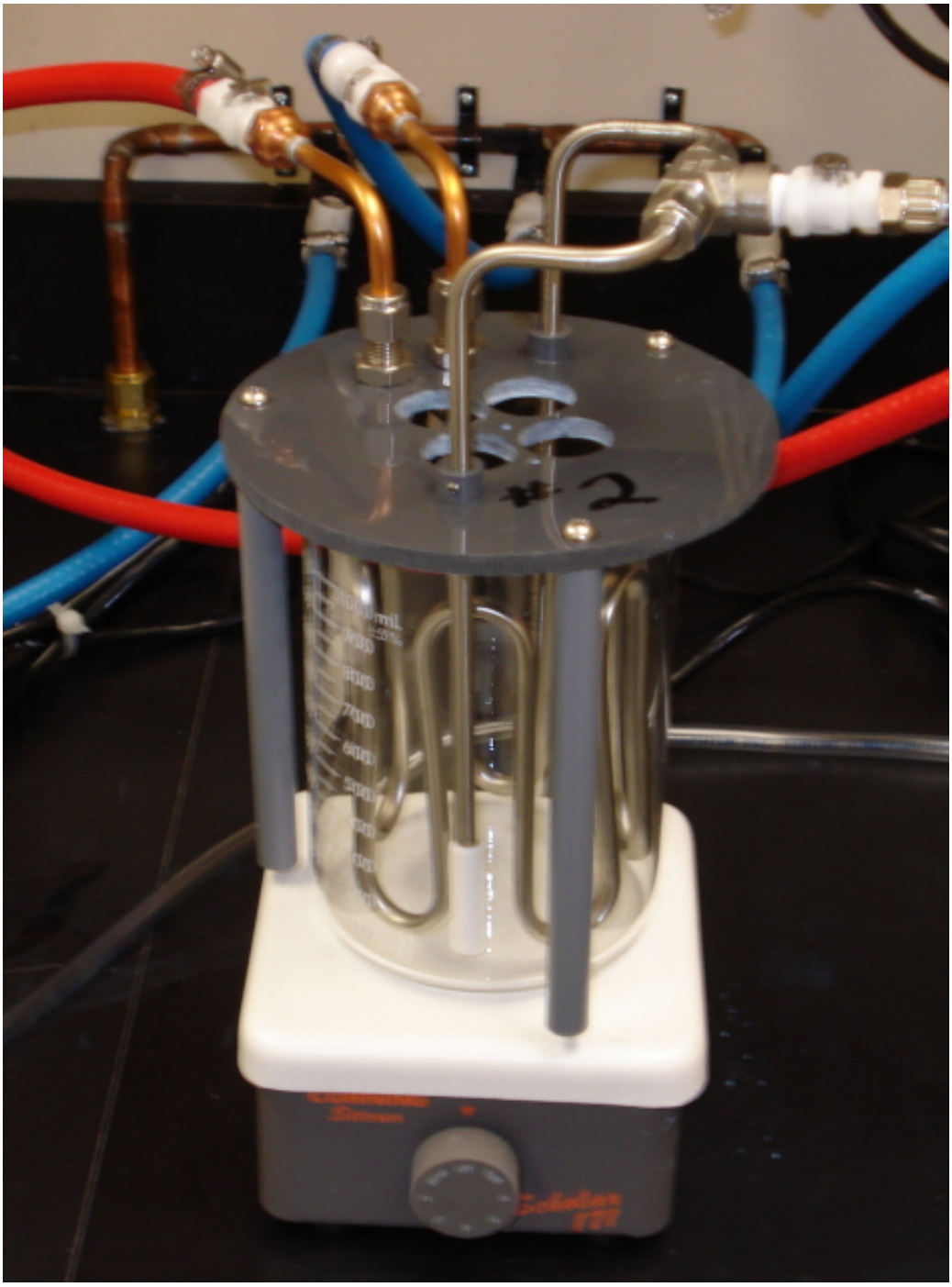

Figure 40 One Liter Photocatalytic Batch Reactor with Stainless Steel Cooling Coils

6.3 Characterization of Light Source

The type of light source used by other researchers in this area varies considerably. Typically, the use of xenon lamps, LED's, halogen lamps and fluorescent lamps appear in most studies. Many of the studies focus on one particular application, and select their light source in accordance. This study considered both the effects of ultraviolet and visible-light radiation.

The experiments conducted were categorized as either simulated solar spectrum (SSS) or visible simulated solar spectrum (VSSS), and informally as whole light or visible-light. The light sources were four 150 watt, 120 volt, halogen lamps (Bright Effects Model #LBPQ150T4/JCD). The lamps' irradiance profile was characterized using an Ocean Optics Spectrometer fitted with an Ocean Optics UV-CC3 filter to attenuate the signals' intensity and Spectra Suite software. This process was then repeated for the total solar irradiance incident on the filter measured here in Tampa, Florida on April 26, 2007 at 1:30PM. Figure 41 shows the spectra for wavelengths in the ultraviolet range are similar in intensity for both the lamps and solar radiation. Although the lamps create spectra similar to a black body radiation of approximately 3000 K, the wavelength intensity in the visible spectrum is considerably greater than the solar irradiation measured.

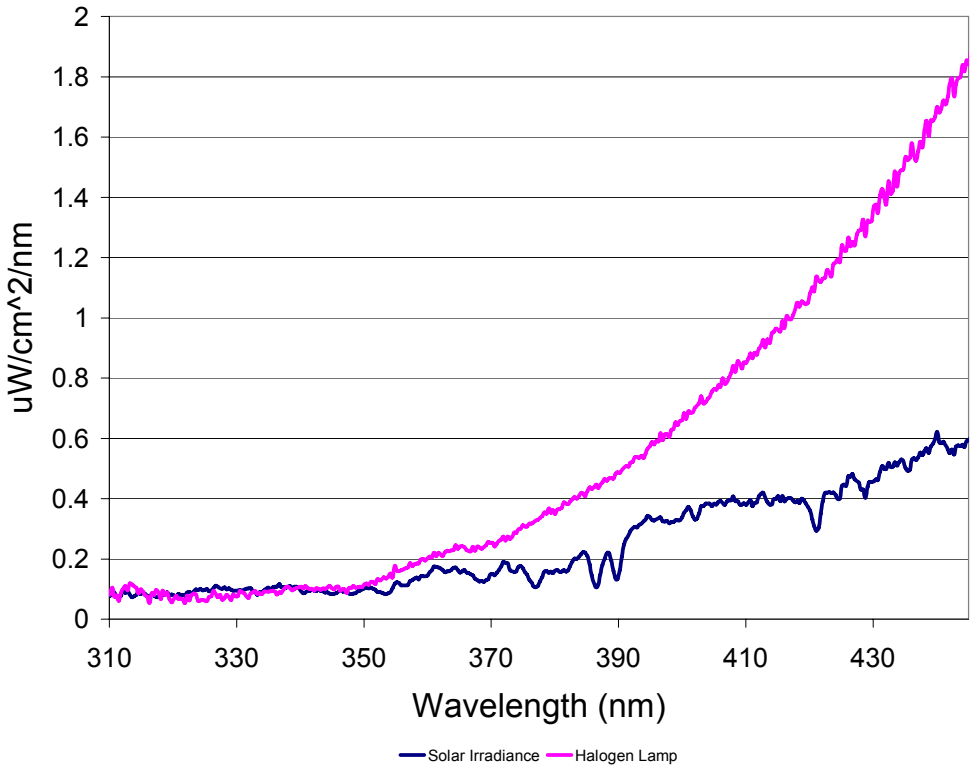

Figure 41 Spectra for Solar and Simulated Solar Spectrum Irradiation

To limit the halogen lamps' radiation to the visible spectrum, a five mole solution of sodium nitrate was prepared by heating the solution at low temperature while magnetically stirring until a clear solution was formed. The solution was syringed in between the culture tubes as described above. Figure 42 shows the spectra for the lamps with and without the UV filter. This figure shows that the filter solution begins attenuating the radiation at approximately 410 nm and completely absorbs the radiation at wavelengths below 390 nm. It is on this basis that experiments that are considered VSSS (visible) are said to have no contribution from the ultraviolet radiation. At the same time, it can also be seen that the filtering solution does not attenuate the wavelengths in the

visible spectrum therefore allowing for direct comparison between SSS (whole) and VSSS (visible) experiments.

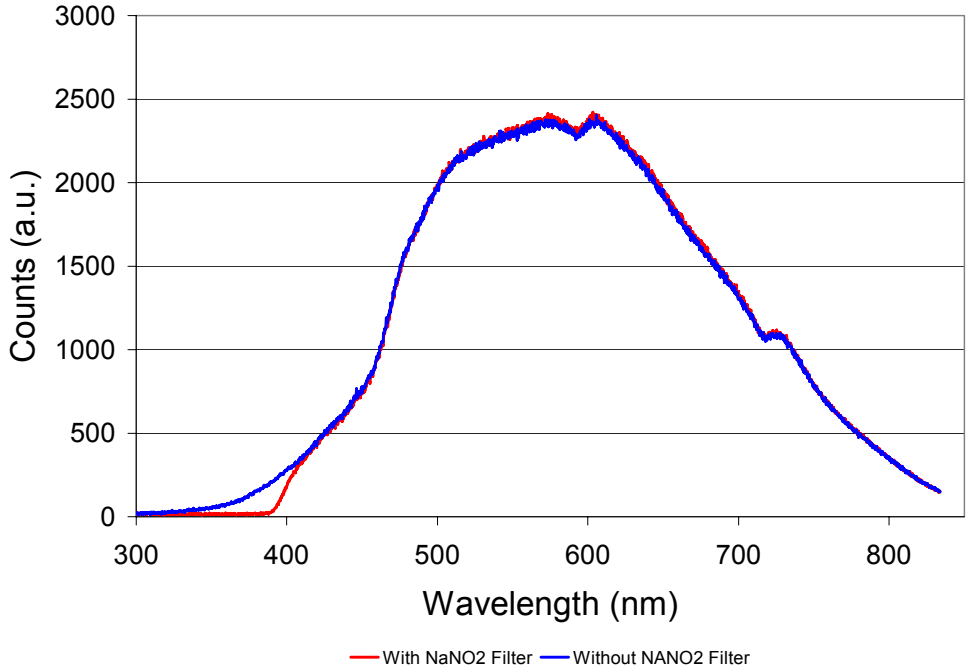

Figure 42 Spectra for Halogen Lamps With and Without Ultraviolet $NaNO_2$ Solution Filtering

CHAPTER 7: EXPERIMENTAL PROCEDURES

7.1 Preparation of Thermally Treated Photocatalytic Materials

Two Coors glazed porcelain boats were weighed, then filled with Degussa P-25 TiO_2, then weighed again to record the initial catalyst weight. Figure 43 shows the configuration of the calcination system. A Barnstead Thermolyne 21100 Tube Furnace was fitted with a 36 inch long, 1 inch in diameter Corning quartz tube that served as a treatment chamber. The boats containing the catalyst were centered inside of the reactor.

Figure 43 Original Calcination System

Nitrogen was used as a dry inert gas for the calcination environment. The temperature was raised 100°C per five minutes until the calcination temperature was reached. Treatment temperatures ranged from 275°C to 825°C for three hours. At the conclusion of the treatment the material cooled to ambient temperature under nitrogen flow.

7.2 Preparation of Thermochemically Treated Photocatalytic Materials

Two Coors glazed porcelain boats were weighed then filled with Degussa P-25 TiO_2, then weighed again to record the initial catalyst weight. Figure 44 shows the configuration of the thermochemical treatment system. A Barnstead

Thermolyne 21100 Tube Furnace was fitted with a 36 inch long, 1 inch in diameter Corning quartz tube that served as a reaction chamber. The tube was connected by compression fittings to the gas delivery and outlet systems. The boats containing the catalyst were centered inside of the reactor tube.

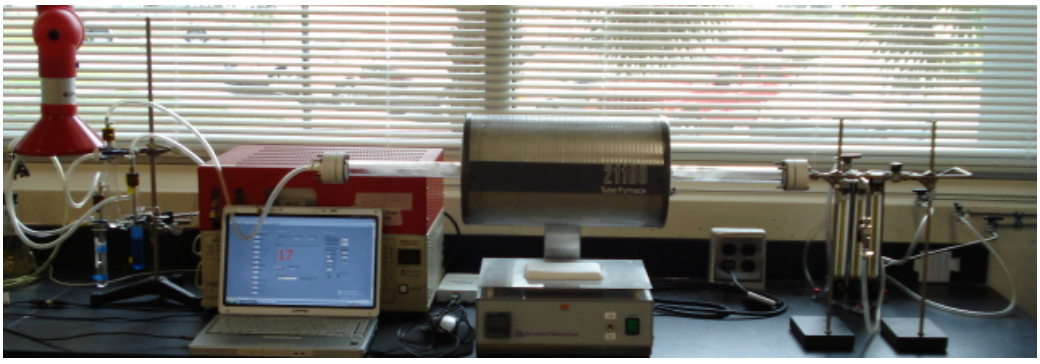

Figure 44 Tube Furnace Reactor System

Nitrogen-doping was done by a gas phase impregnation process using anhydrous ammonia (NH_3) as the nitrogen source. To begin this process, the atmosphere in the reactor was replaced by ultra-high purity (UHP) nitrogen (N_2) to suppress the affects of the ambient atmosphere on the thermochemical process. The reaction tube had a volume of approximately 485 cm^3, and the concentration of nitrogen was calculated by the following equation:

$$C = 1 - e^{\frac{V_T}{V_0}},$$

where C is the concentration of nitrogen, V_T is the volume of nitrogen at time T, and V_0 is the volume of the reaction tube. The time required to replace the atmosphere at a particular flow rate was calculated from this equation. By this

calculation, 46 minutes is required to completely replace the ambient atmosphere with nitrogen at a flow rate of 155 mL/min. However, a time of 15 minutes was used, which resulted in replacement of 99.168% of the ambient atmosphere.

After 15 minutes, the nitrogen flow was stopped and anhydrous ammonia, at a flow rate between 6.6 mL/min. and 87.3 mL/min., was begun. The ammonia flowed into the reactor for six minutes prior to the start of the thermal sequence.

The temperature was raised at a rate of 100°C per five minutes with NH_3 at the required flow rate until the treatment temperature was reached. The 33 minutes required to reach the treatment temperature, combined with the six minutes prior to the warm-up process, provided 39 minutes for NH_3 to flow into the reactor. This allowed for 99.91% of the nitrogen atmosphere to be replaced by NH_3 at the start of the doping process. Once the treatment temperature was reached the thermochemical treatment process continued for three hours. At the completion of the process, nitrogen was used to cool the material to ambient temperature.

7.3 Experimental Procedures for Photocatalytic Experiments

Photocatalytic experiments were performed using a glass batch reactor system, which was described in detail above. A 20 ppm methyl orange solution using de-ionized water was prepared using (A.C.S. Reagent) MO from Sigma-Aldrich. Methyl orange was dissolved into solution using a magnetic stirrer for 15 minutes. Samples were drawn and the initial concentration was measured and

calculated in accordance with Beers Law using an Ocean Optics USB2000 optical spectrometer.

Once the 20 ppm solution was prepared, 150 mL of the MO solution was reserved in a beaker. The prepared catalyst was ground in a crucible with 2 mL of MO solution to de-agglomerate the material. Portions of the reserved MO solutions were added to dilute the catalyst paste that was then poured back into the beaker. This process was repeated with the remaining MO solution until the maximum amount of the catalyst was recovered from the crucible.

To further de-agglomerate the particles and achieve a Langmuir equilibrium, the MO-catalyst solution was then sonicated using a Fisher-Scientific Sonic Dismembrator Model 100. Sonication was performed at 5 watts (RMS) for 15 minutes while being magnetically stirred. It is important to note that during this time, adsorption of the pollutant onto the surface of the catalyst also took place altering the initial concentration of the MO solution. This process and its importance were detailed above. The solution was then moved to the experimental area where it again was placed on a magnetic stirrer. Figure 45 shows the photocatalytic experimental set up.

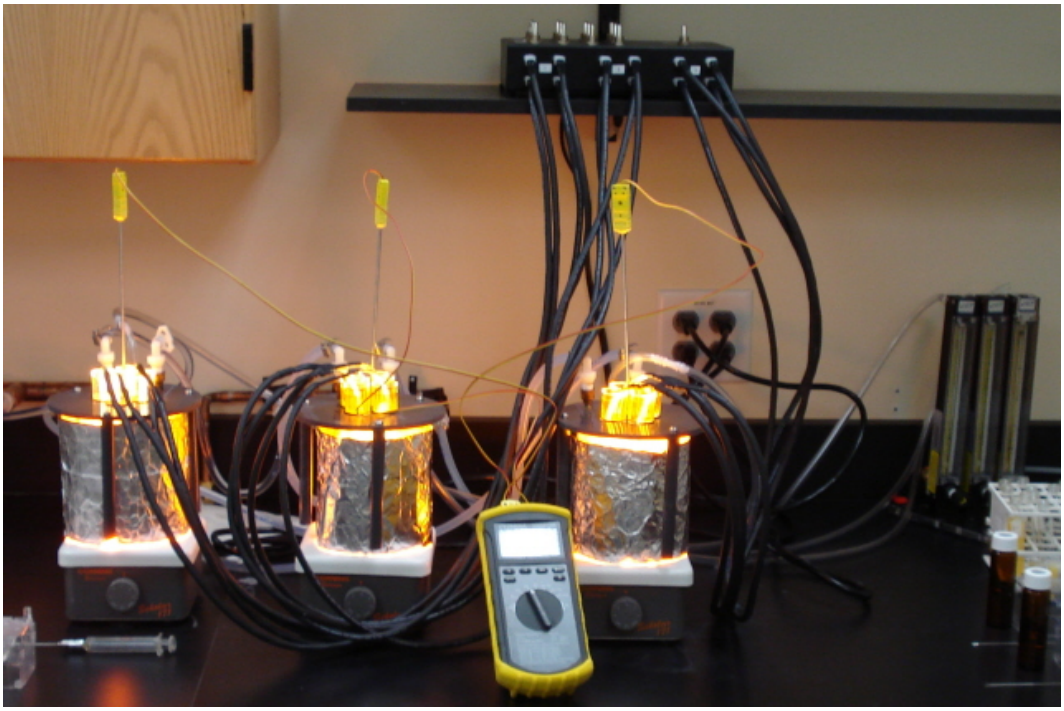

Figure 45 Photocatalytic Batch Reactors for SSS and VSSS Irradiation Experiments

The cooling assembly, which housed the light sources, was then placed into the beakers and connected to tubing for cooling and air flow. Cooling was done by heat transfer using tap water circulating through the stainless steel tubing. A thermocouple was placed in each reactor and used to monitor the solution temperature. As noted in the literature, there is negligible Arrhenius effect, but the temperature was controlled by stirring speed and water flow to create consistency of environment for separate experiments. The photocatalytic experiments were conducted at approximately 40°C. Breathing Quality Air was used as an oxygen source. The flow rate was controlled by flow meters and bubbled into the solution by aerating stones at a rate of 0.5 L/min.

2.0 mL samples, representing zero time, were drawn using Micromate 5cc glass syringes and placed into micro-centrifuge tubes. The solution was then irradiated using the light sources detailed above. Both simulated solar spectrum experiments and visible solar spectrum experiments were conducted for durations of three to six hours. Samples were drawn at 30 minute intervals for the first three hours, followed by one hour intervals if the experiments duration was six hours.

At the completion of the experiment, the samples that were collected were centrifuged using an Eppendorf 5414C centrifuge at 8,000 rpm for 15 minutes. The samples were then syringed to new tubes then centrifuged again at 8000 rpm for 15 minutes.

The concentrations of the samples were then calculated by measuring the absorbance of the samples using a spectrometer. The results were compiled and the rate constant for the material was calculated.

7.4 Control Experiments Using Degussa P-25 TiO_2

Control experiments using Degussa P-25 TiO_2 for both simulated solar spectrum and visible solar spectrum were conducted in the exact manner as the photocatalytic procedures detailed above. The experimental conditions that affect the photocatalytic process have already been addressed. These included the initial concentration of the pollutant, catalyst loading, catalyst particle size, intensity of the light source, initial pH of the solution and the concentration of

oxygen in the solution [59]. The design of these experimental procedures allow for the control or optimization of these parameters. Every effort was made to perform consistent repeatable experiments allowing for the comparison of the results.

CHAPTER 8: EXPERIMENTAL RESULTS

8.1 Untreated Degussa P-25 TiO_2

Baseline experiments using untreated Degussa P-25 TiO_2 were performed under no irradiation, simulated solar spectrum (SSS or whole) for varying times, and visible simulated solar spectrum (VSSS or visible) irradiation for both sonicated and non-sonicated suspensions. Figure 46 shows the normalized change in concentration for each of these conditions.

Consistent with the literature, TiO_2 in the presence of a pollutant, but without an irradiation source (labeled dark below) produced no de-coloration of methyl orange [20]. According to Guettai et al., this shows that the de-coloration of methyl orange is a purely photocatalytic effect.

In Figure 46, the experimental points for VSSS MO degradation can be approximated by a linear dependence from time whereas, for whole spectrum, the experimental points for the initial stage of MO degradation are fitted well with the exponential function from time. Such a big difference in the degradation kinetics can be explained by different limiting stages and types of photocatalytic reactions. Particularly, the linear dependence can be well described by a zero ordered photocatalytic reaction. For a zeroth order reaction, the rate remains constant throughout the reaction and is independent of the concentration of the

reactant(s) [60]. Zeroth order reactions are typically found when the surface of the catalyst is saturated by the reactants. In photocatalytic reactions, it may be the case when the rate of contaminant degradation on the catalytic surface is limited by the intensity of electron-hole excitation.

The plots for simulated solar spectrum (SSS) light can be considered a good first approximation for a first order chemical reaction. A first order reaction is a reaction whose rate depends on the concentration of only one reactant raised to the first power [60]. Other reactants can be present, but each will be zeroth order.

As was shown earlier, the kinetics are more complicated and it is difficult to classify the reaction as purely zeroth and/or first order, although this can be a good approximation. This further explains the need for more sophisticated models such as the Langmuir-Hinshelwood model.

The plots for both sonicated and non-sonicated TiO_2 in visible-light also show a difference in rate. The material used in this study came from large bulk quantities of Degussa P-25 TiO_2. The particle size is commonly reported near 30 nm, with a surface area of 50 m^2/g. However, due to simple settling, the material compacts over time. This explains why the catalyst was ground prior to each experiment and sonicated. The difference in the rates is attributed to the de-agglomeration of the particles, thereby exposing a greater surface area to the pollutant to react at.

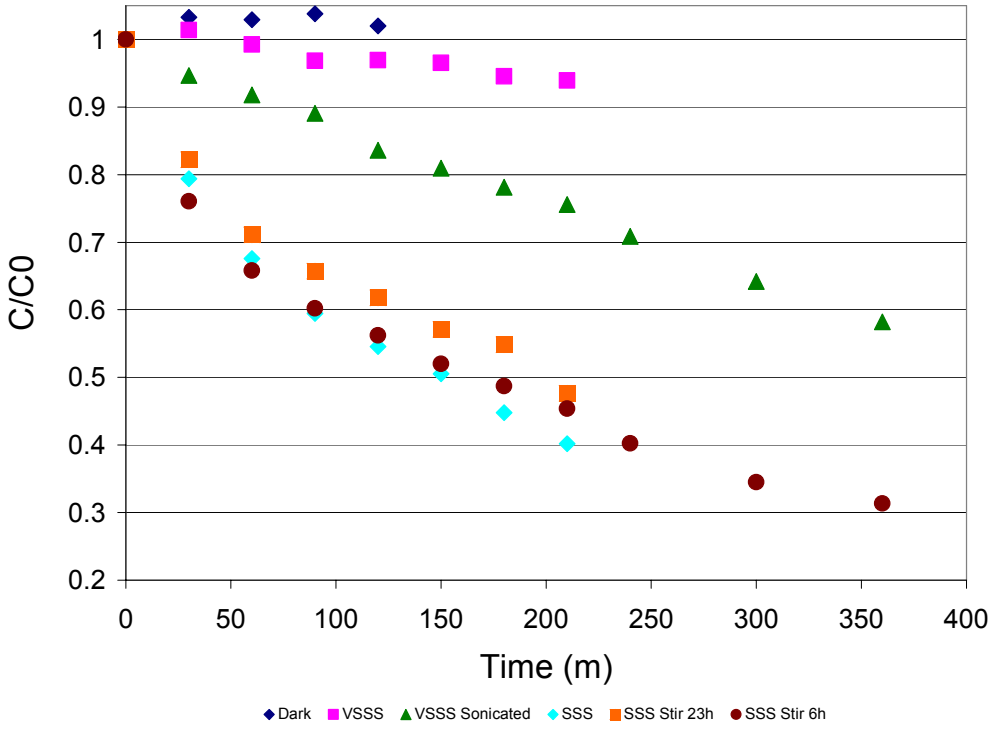

Figure 46 Change in Concentration as a Function of Time for Methyl Orange in the Presence of 1 g/L of Untreated Degussa P-25 TiO_2 Under No, SSS and VSSS Irradiation

By using the integrated rate law, we are able to convert the first order reaction rate using calculus. As shown in Figure 47, the negative natural logarithm of the ratio of the concentration at time (t) to the initial concentration shows what fraction of the original pollutant remains at time (t) [60].

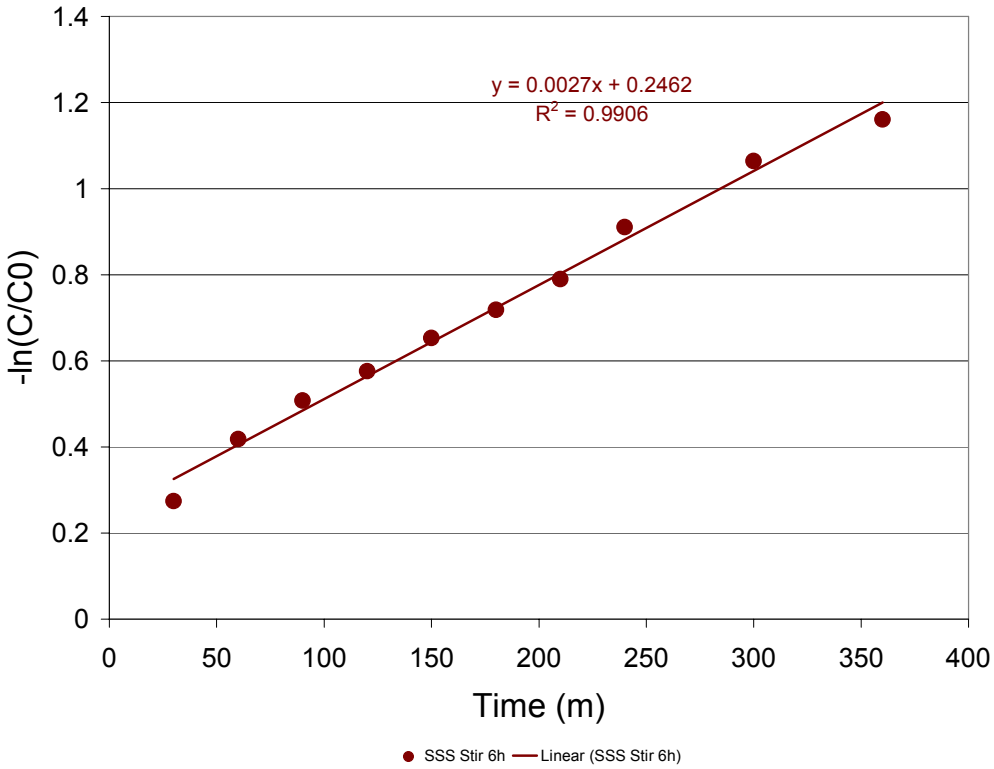

Figure 47 Integrated Rate Law Plot for Untreated Degussa P-25 TiO_2 Under SSS Irradiation

The slope of the integrated rate law plot (Figure 47 above) was then used as the apparent rate constant for the reaction. This rate is given in units of 1/time, which is shown in Figure 48 [20, 22, 60]. It is again important to note that a straight line will only occur for truly first order chemical reactions. Therefore the R-squared value is an important indicator of the validity of categorizing the reaction purely as first order. Again, it is apparent that a good first approximation can be made for the reaction in SSS irradiation to be considered first order. It is also obvious that the complexity of the chemical kinetics cannot be considered purely first order. This further reinforces the need for models such as the Langmuir-Hinshelwood model. The methods used here are identical to the

methods used by Guettai et al. and Al-Qaradawi et al. as both studied the degradation of methyl orange in the presence of TiO_2 [17, 18]. The calculated rate constant for Degussa P-25 TiO_2 under SSS irradiation is given in Figure 48.

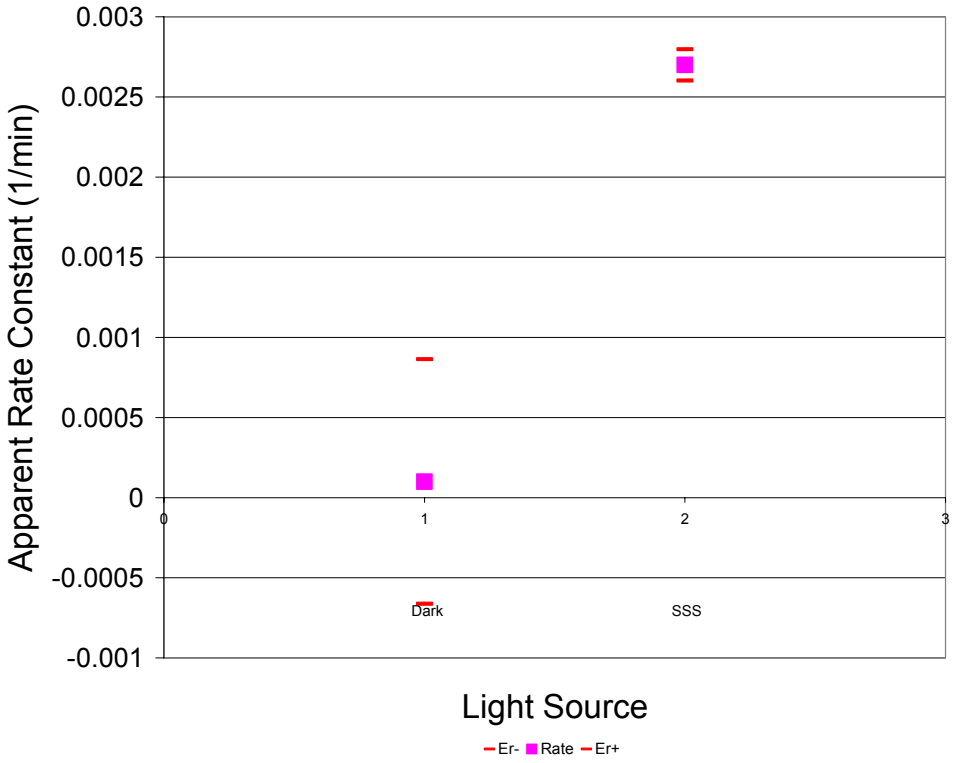

Figure 48 Apparent Rate Constants for Untreated Degussa P-25 TiO_2 Under No and SSS Irradiation

8.2 Effects of Oxygen Concentration on Photocatalytic Rate

One of the established parameters affecting the photocatalytic rate is oxygen concentration in the suspension. Figure 49 shows the affects of using one and two aerating stones. The air flow rate for each reactor was the same (0.5L/min) along with all other conditions for the experiment. Consistent with the

literature, by diffusing a higher concentration of oxygen, more oxygen is available for electron scavenging and therefore a higher photocatalytic effect [6].

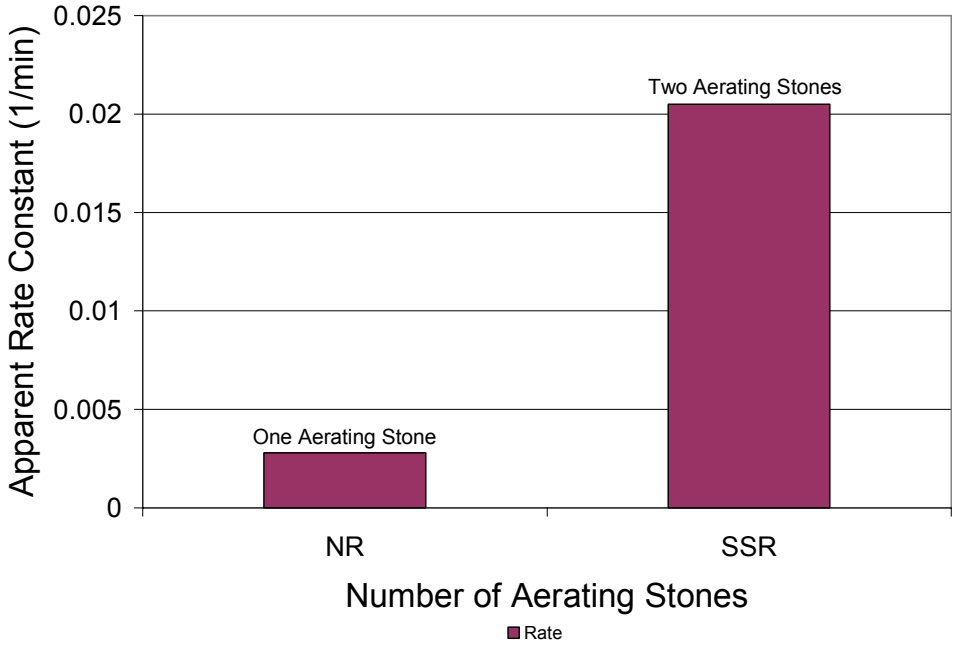

Figure 49 Apparent Rate Constant for Untreated Degussa P-25 TiO_2 Under SSS Irradiating Using One and Two Aerating Stones

In a similar fashion oxygen and air were again bubbled into the suspension at the same rate (0.5 L/min.) and under the same conditions. As seen in Figure 50 the use of pure oxygen increased the photocatalytic activity.

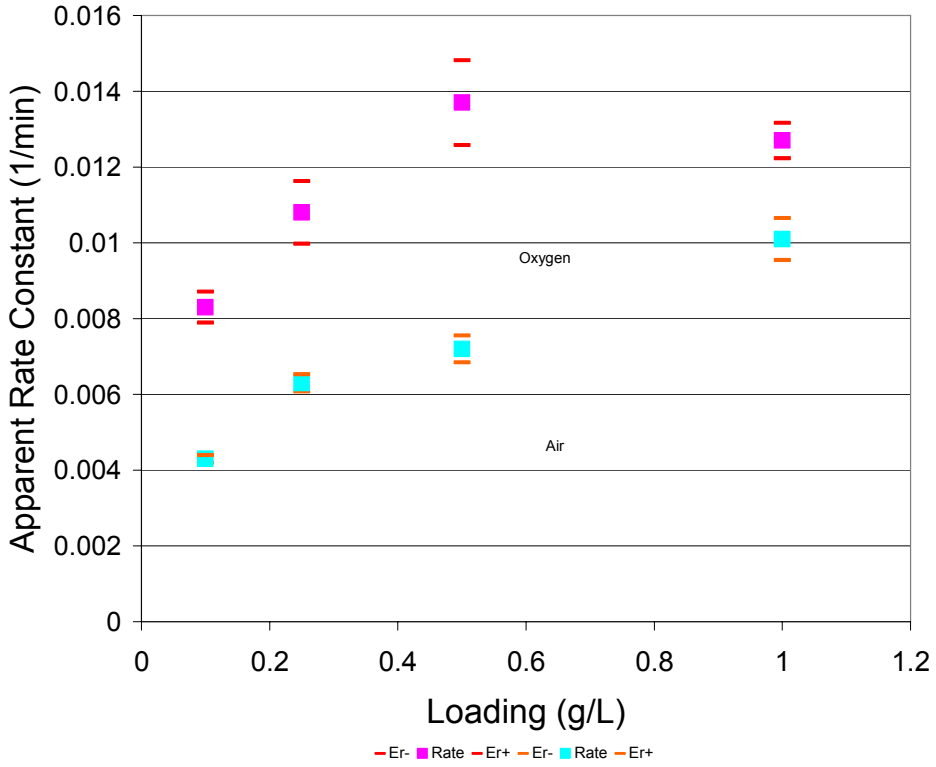

Figure 50 Comparison of Air and Oxygen on the Apparent Rate Constant

Throughout this study we were able to control the parameters that have the greatest influence of over photocatalytic efficiency. While doing so we were also able to show the effects of thermal and thermochemical treatments on the performance of Degussa P-25 TiO_2.

Figure 51 below is a HRTEM image of pure Degussa P-25 TiO_2. This image clearly shows the atomic lines and grain boundaries that are understood to be the location of the oxygen deficiencies.

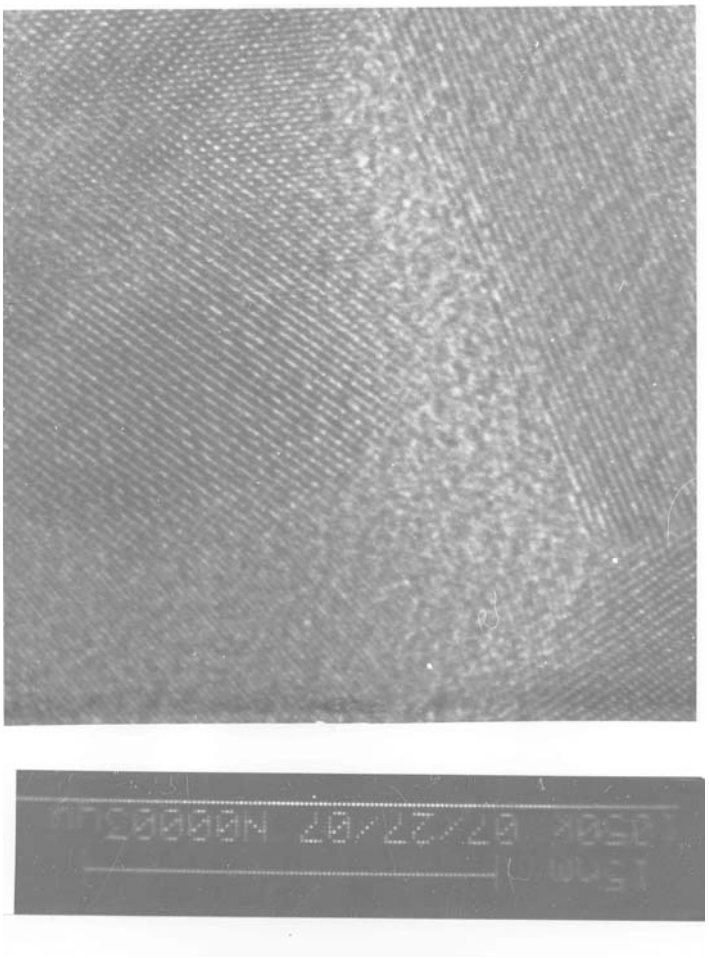

Figure 51 HRTEM Showing the Grain Boundaries of Pure Degussa P-25 TiO_2

8.3 Effect of Thermal Treatment on the Photocatalytic Activity of TiO_2

The established theory is that thermal treatments cause the removal of oxygen ions. This in turn creates oxygen vacancies, which accelerates the anatase to rutile transformation. These oxygen vacancies cause the lattice to contract and the volume to shrink when two of the six Ti–O bonds are broken [58]. Oxygen vacancies are believed to be formed in the grain boundaries [35]. It is these very oxygen vacancies that are believed to increase the photocatalytic effects of TiO_2.

The improvement in efficiency can be attributed to the reduction of TiO_2, which was explained in detail earlier [32]. Asahi et al. further concluded that these oxygen deficient sites are important for the visible response to take place. This reduction causes a red-shift to wavelengths longer than 400 nm, which is attributed to the reduction of Ti^{4+} to Ti^{3+}. Hence, the rutile particles in the P-25 powder are considered to contain the Ti^{3+} ions that create electron donors. Ohno et al. concluded that a "fairly large band bending is generated in the rutile particles." They attribute the higher efficiency of P-25 to this [17].

The curves in Figure 52 show the concentration as a function of time for calcinated TiO_2. As described earlier, the catalyst was calcinated at varying temperatures from 275°C to 625°C for three hours under a dry inert nitrogen atmosphere. The curves below show a good first approximation of first order kinetics.

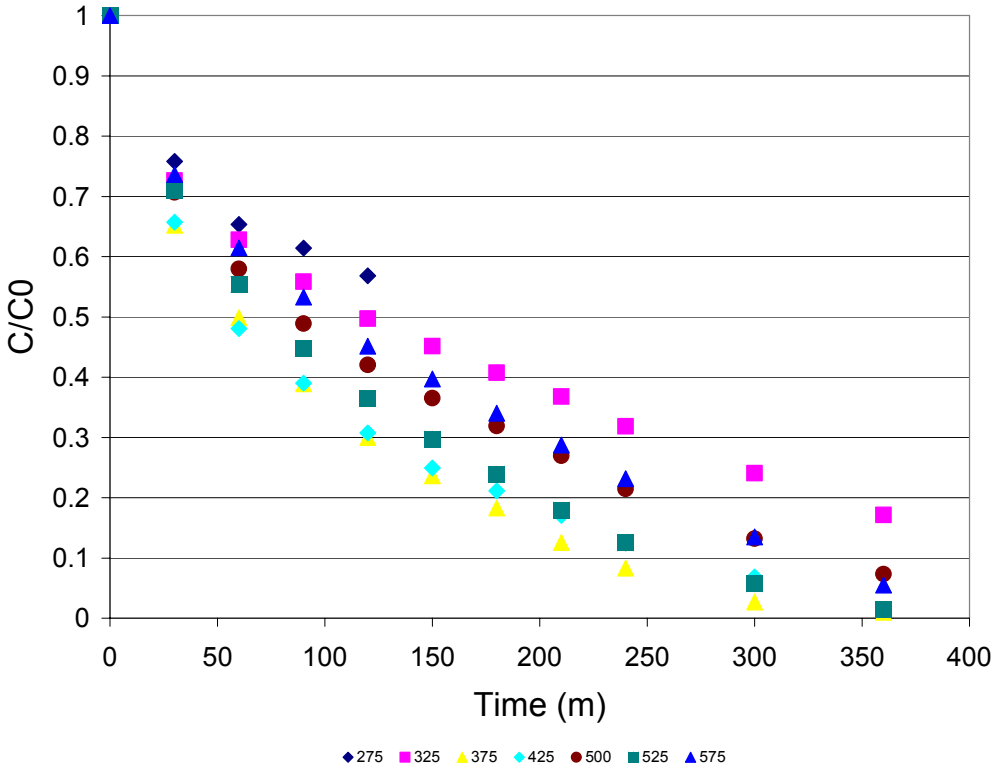

Figure 52 Change in Concentration as a Function of Time for Methyl Orange in the Presence of 1 g/L of Calcinated Degussa P-25 TiO_2 Under SSS Irradiation

As a result of this first order approximation the curves were plotted using the integrated rate law as shown in Figure 53. As can be seen, the slopes of these curves have high R-squared values and give a high level of confidence in their use. What should be further cautioned is that first order reactions must not have a build up of intermediates during the reaction [60]. As illustrated above, there were occasions that intermediates that could not be degraded, and others that could, were produced during some of the photocatalytic experiments. Therefore, these results can be used only as an approximation.

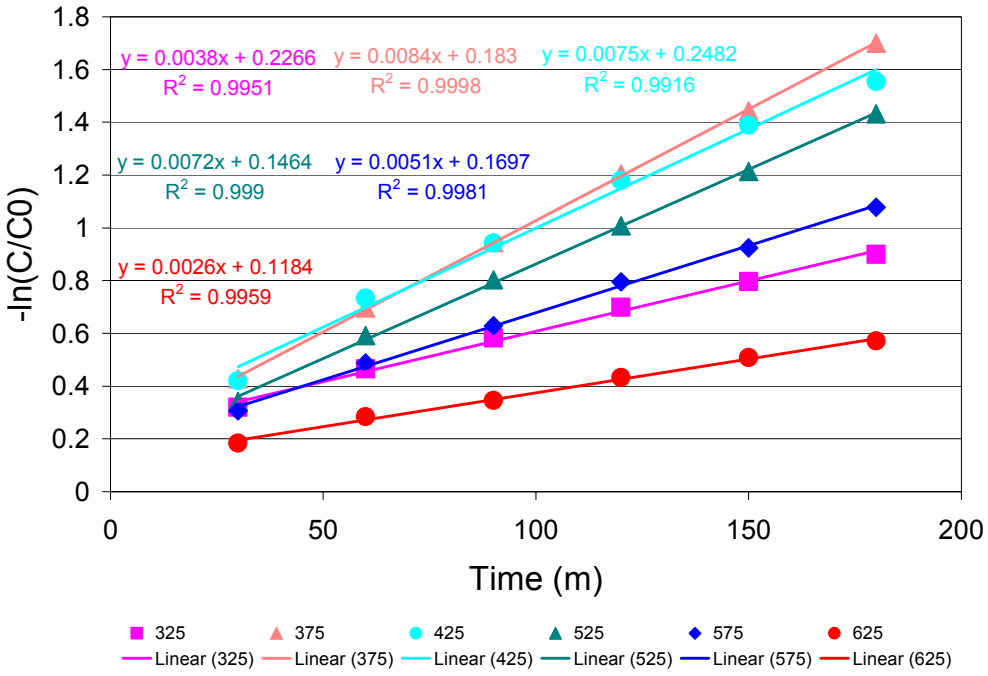

Figure 53 Integrated Rate Law Plot for Calcinated Degussa P-25 TiO_2 Under SSS Irradiation

Plotted in Figure 54 are the apparent rate constants for thermally treated (calcinated) Degussa P-25 TiO_2. This plot shows a broad range of temperatures that produce a positive effect on the photocatalytic rate. This study found that temperatures from 375°C to 575°C had a positive effect on the photocatalytic rate, and that temperatures above 600°C produced a declining effect. The study by Ihara et al. concluded that 400°C is the transition temperature at which oxygen deficiencies are created. They further concluded that this is also the temperature at which the maximum number of deficiencies are created [35]. This decline over 600°C in photocatalytic effect is attributed to the increase in particle size and a shift from anatase to rutile fractions in the catalyst. This was supported by Kosowska et al. who found that materials prepared below 600°C

were mostly anatase, whereas temperatures above 650°C produced a mixture of anatase and rutile phases [51].

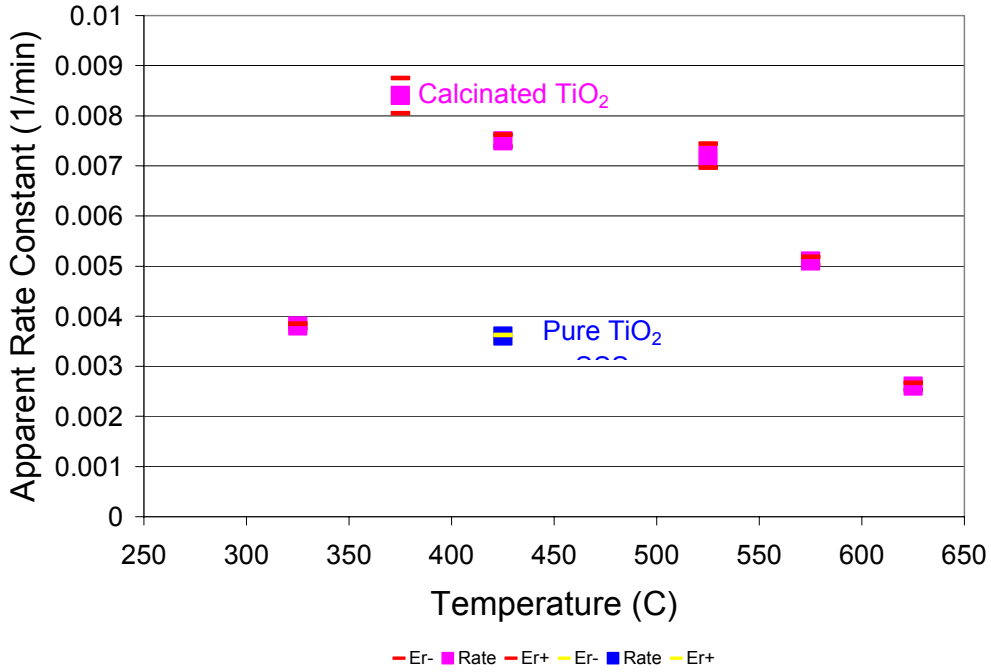

Figure 54 Apparent Rate Constants for Calcinated Degussa P-25 TiO_2 Under SSS Irradiation

8.4 Characterization of Thermally Treated Degussa P-25 TiO_2

Figure 55 shows values for anatase and rutile particle size, number of anatase and rutile particles per volume, photocatalytic efficiency and mass fraction of rutile particles for temperatures in the range of 275°C to 625°C for calcinated Degussa P-25 TiO_2. Rutile particles were found to have an average size of 30 nm and anatase an average size of 10 nm. It can be seen that the size of these particles stays relatively consistent for temperature below 525°C. However, at temperatures above 575°C the average particle size increases rapidly.

The relative photonic efficiency is a plot of the apparent rate constants as shown in Figure 54 above. What can be gleaned from this plot is that the decline in the photonic efficiency (apparent rate constant) coincides with an increase in particle size for anatase and rutile particles. It is the rutile particles however that begin to increase much more rapidly than the anatase particles. This is further indicated by the increase in the mass fraction of rutile particles increasing over 575°C.

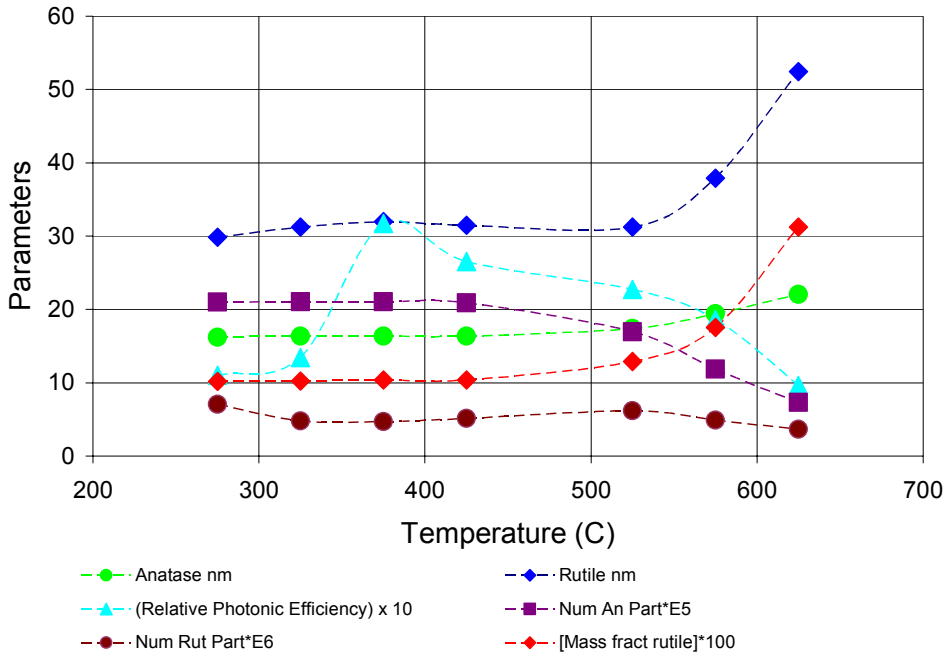

Figure 55 Characterization of Thermally Treated (Calcinated) Degussa P-25 TiO_2 Under SSS Irradiation

8.5 Effect of Thermochemical Ammonia Treatment on the Photocatalytic Activity of Degussa P-25 TiO_2

One of the major objectives of this study was the pursuit of a visible-light activated photocatalyst using Degussa P-25 TiO_2 as the starting material. As

was described in detail earlier, anhydrous ammonia was used as a nitrogen source for the thermochemically treated photocatalyst consistent with the work done by Kosowska et al. [51]. Doping TiO_2 with nitrogen was concluded to improve the visible-light absorption, which increased the number of photons that could take place in the reaction [47]. The overall performance is improved due to this mechanism.

The often cited study by Asahi et al. regarding nitrogen-doping, concluded that the visible-light response is due to the formation of an isolated band, which consisted of N2p orbitals above the O2p orbitals in the valence band [32]. Further, they concluded that the doping could not exceed 1% of the nitrogen. The results below, regarding gas flow rate point to a similar conclusion.

As discussed previously, visible-light experiments produced reactions that could not be considered first order, but could on a first approximation be considered zeroth ordered. Figure 56 shows that photocatalytic effect of thermochemically ammonia treated Degussa P-25 TiO_2 on methyl orange is more accurately modeled as zeroth order reaction.

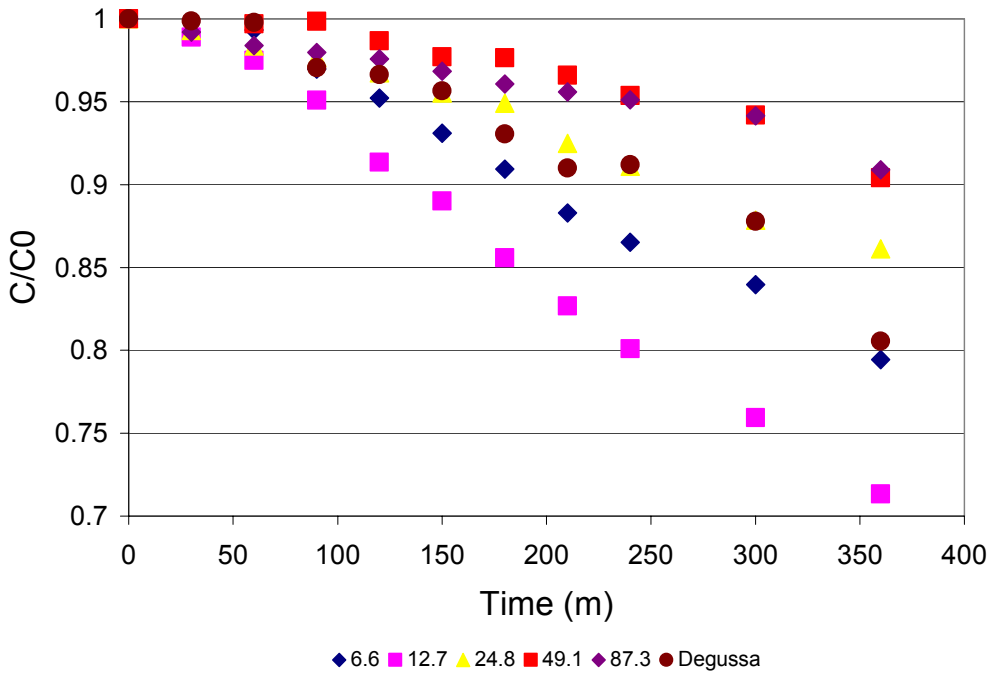

Figure 56 Change in Concentration as a Function of Time for Methyl Orange in the Presence of 1 g/L of Thermochemically Ammonia Treated Degussa P-25 TiO_2 Under VSSS Irradiation

The calculation of the rate is a simple average of the slope over time multiplied times the initial concentration. The result is presented as the de-coloration rate given in units of pollutant ppm decay per minute. Figure 57 shows the De-coloration Decay Rate (which can be thought of as the rate constant) for thermochemically treated (nitrogen-doped) Degussa P-25 TiO_2.

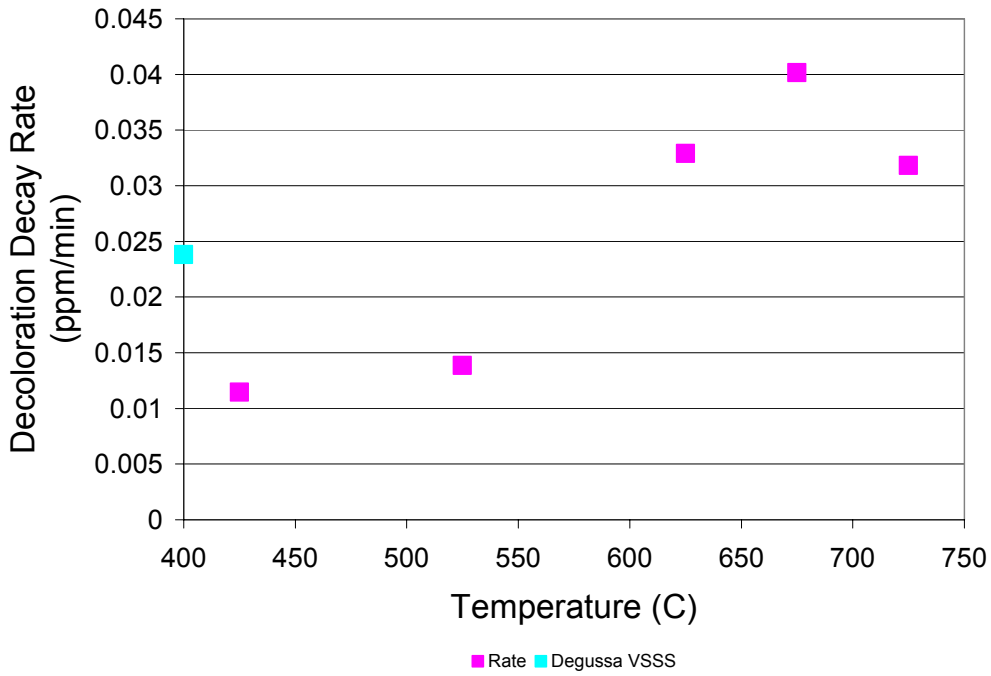

Figure 57 De-coloration Decay Rate as a Function of Treatment Temperature for Thermochemically Ammonia Treated Degussa P-25 TiO_2 Under VSSS Irradiation

Figure 57 above shows that the highest rate of de-coloration occurred at 675°C. Using a similar method but reactive red and phenol as a pollutant, Kosowska et al. found similar results for nitrogen-doped TiO_2 as shown in Figure 58. By comparing Figures 57 and 58 one can conclude that the optimized temperature of the TiO_2 thermochemical treatment is different for different pollutants to be degraded and may also depend of the precursor.

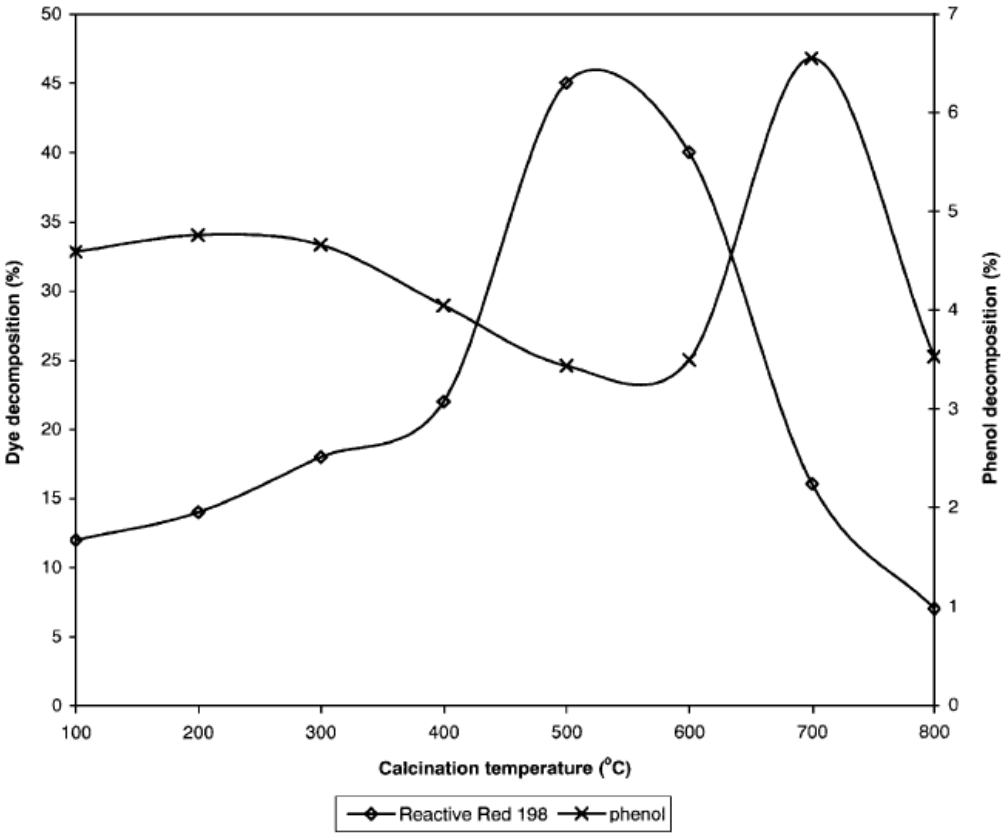

Figure 58 Dye Concentration as a Function of Treatment Temperature for Nitrogen-Doped TiO_2 for Reactive Red and Phenol by Kosowska et al. [51]

8.6 Optimization of Thermochemical Ammonia Treatment Flow Rate

The initial study was expanded into an investigation of ammonia flow rate and its effect on the photocatalytic rate. Having determined an optimum temperature of 675°C for visible-light activated photocatalyst, experiments with flow rates from 6.6 mL/min. to 87.3 mL/min. were conducted.

Figure 59 shows that the highest MO de-coloration rate was obtained for a catalyst thermochemically ammonia treated at a flow rate of 12.7 mL/min.

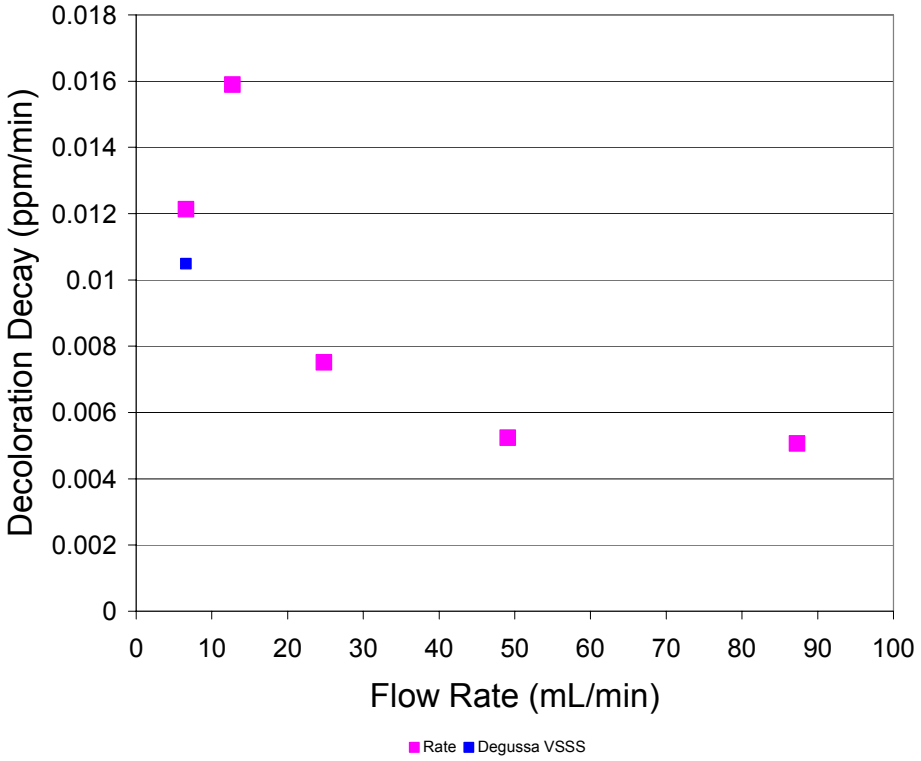

Figure 59 De-coloration Decay Rate as a Function of Ammonia Flow Rate at 675°C for Thermochemically Ammonia Treated Degussa P-25 TiO_2 Under VSSS Irradiation

The color of the catalyst ranged from a very pale yellow at 6.6 mL/min. to a more vivid yellow at 12.7 mL/min., shown in Figure 60. A yellow material is commonly reported in published works for doped materials.

Figure 60 Thermochemically Ammonia Treated Degussa P-25 TiO_2 at 675°C for 3 Hours at 12.7 mL/min.

For flow rates above 12.7 mL/min. the catalyst developed a gradient of color across the boats from the gas inlet side being a green, black or brownish color to a pale yellow on the outlet boat side as shown in Figure 61. Ihara et al. concluded that the reduction reaction that takes place during thermal ammonia treatments are responsible for this change to yellow material [35]. Although not used here in this study, further study found that a small zone existed for maximum deposition of nitrogen that resulted in heavily nitrided black materials.

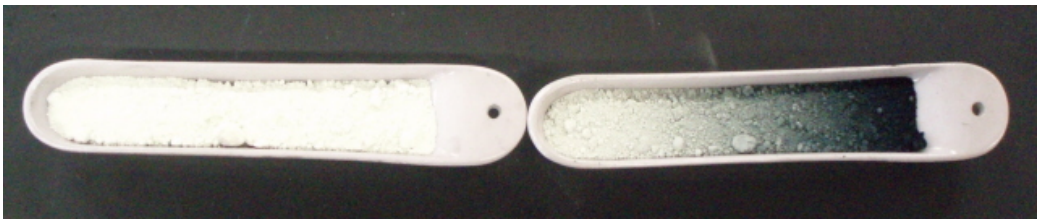

Figure 61 Thermochemically Ammonia Treated Degussa P-25 TiO_2 at 675°C for 3 Hours at 24.8 mL/min.

Figure 62 depicts the area of the color gradient that is typically experienced for flow rates of 24.8 mL/min. The darkened material started from the top far right hand side of the boat on the gas inlet side of the tube furnace reactor and penetrated to the bottom of the boat. From this point, the materials' color gradient followed an angle upward towards the surface of the catalyst. At higher rates, this gradient would extend through the right side boat into the left side boat.

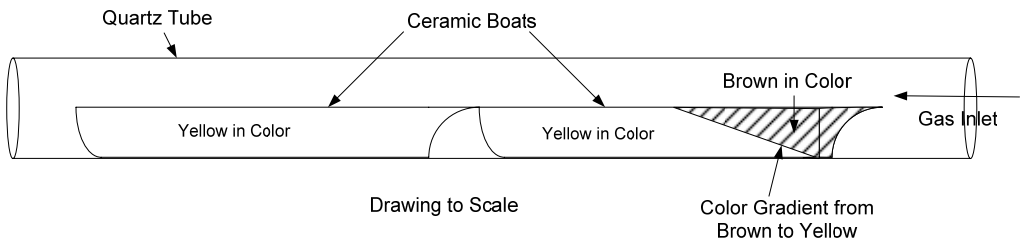

Figure 62 Depiction of Color Gradient After Thermochemically Ammonia Treated At or Above 24.8 mL/min.

Figure 63 shows the color gradient of the material when thermochemically ammonia treated at 675°C at 87.3 mL/min. for 3 hours. Notice the color gradient has now extended across the gas inlet boat and has reached the left hand boat.

Figure 63 Thermochemically Ammonia Treated Degussa P-25 TiO_2 at 675°C at 87.3 mL/min. for 3 Hours

8.7 Effects of Nitrification of Thermochemically Ammonia Treated TiO_2

A short study was done using the same thermochemical treatment procedures for flow rates of 24.8mL/min. This was done to investigate the photocatalytic effect that titanium nitride (found by XRD analysis, see below) had on the rate of MO discoloration.

Figure 64 shows the change in concentration for treatment temperatures from 325°C to 825°C. It can be seen that temperatures below 550°C are

insufficient to dope TiO_2 using anhydrous ammonia as a nitrogen source, which is consistent with the findings of Kosowska et al. [51].

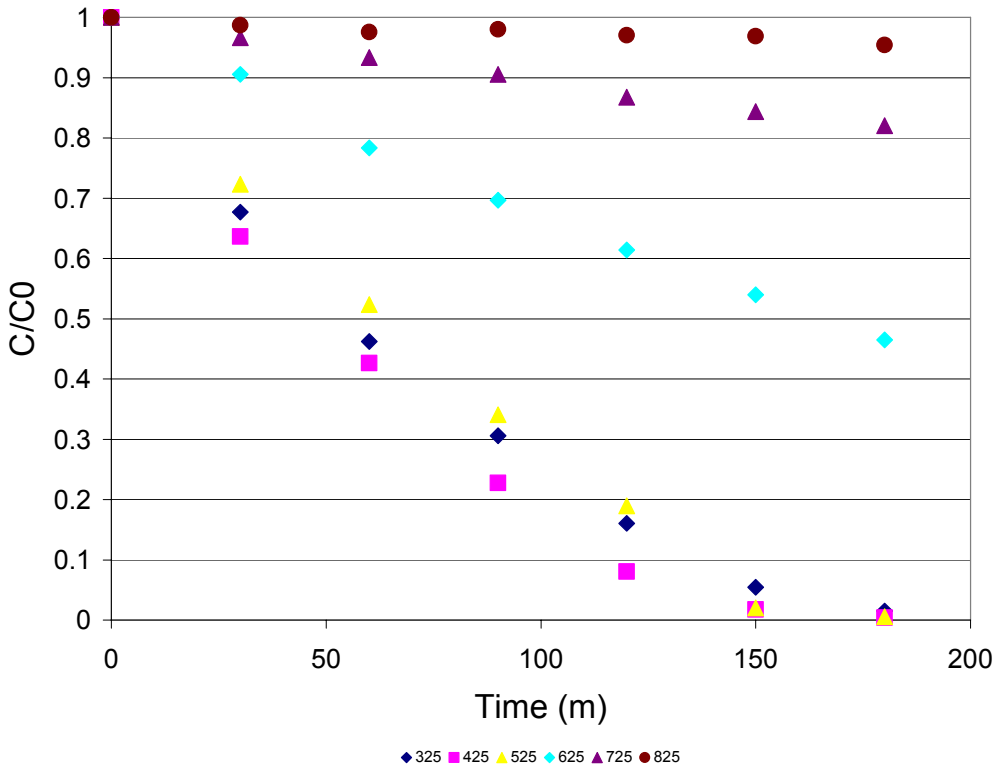

Figure 64 Effects of Nitride on the Photocatalytic Effects of Thermochemically Ammonia Treated Degussa P-25 TiO_2

Figure 65 further illustrates the effect that the thermochemical treatment by ammonia has on the photocatalytic effect of TiO_2. Temperatures below 625°C produced white materials that have essentially been calcinated. The increase in effect can only be attributed to the reduction of TiO_2 similar to the effects seen in thermal treatments using nitrogen.

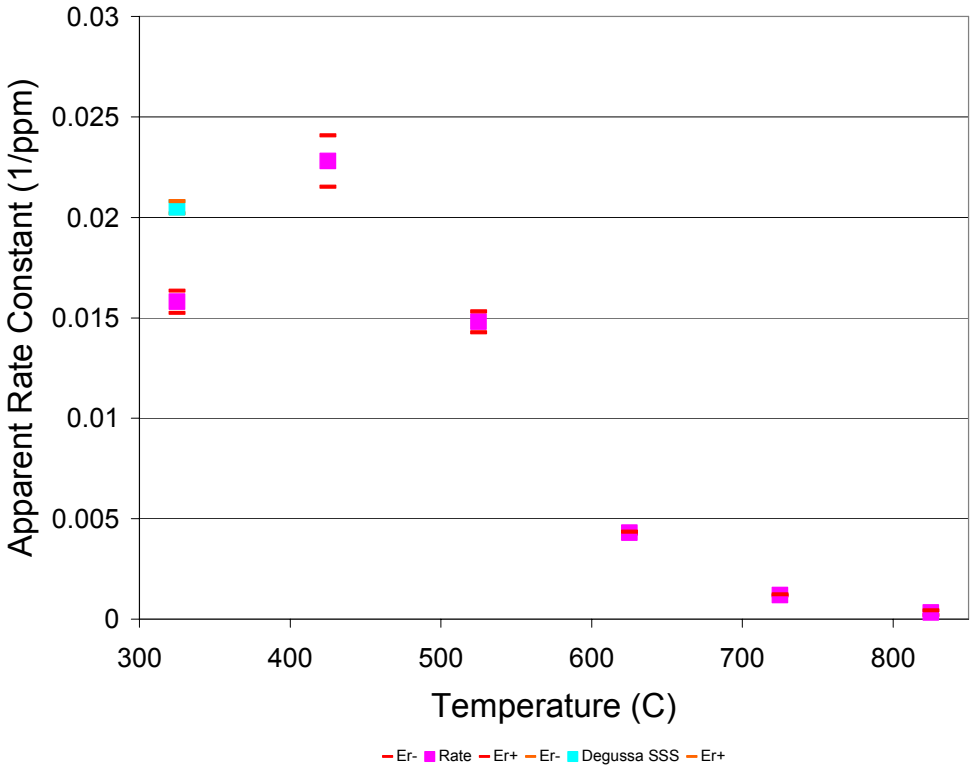

Figure 65 Apparent Rate Constant for Thermochemically Ammonia Treated (24.8 mL/min.) Degussa P-25 TiO_2 Under SSS Irradiation

The phase structure of the untreated Degussa P-25 and the thermochemically ammonia treated Degussa P-25 TiO_2 samples was characterized by x-ray diffraction (XRD). For the quantitative characterization for the phase identification and average grain size has been carried out using Philips X'pert pro PreFix powder x-ray diffractometer with CuKα radiation (λ=1.54060 Å). The incident and diffraction slit width used for all the experiments are 1° and 2° respectively and the incident beam mask used corresponds to 10 mm. The sample preparations for the XRD measurement are strictly followed to obtain maximum signal to noise raise.

The anatase TiO_2 content (C_A) was estimated according to XRD patters based on the following equation:

$$C_A = \frac{A_A}{A_A + A_R} * 100\%,$$

where A_A and A_R are areas for anatase (101) peak and the rutile (110) peak (110) respectively.

The grain size (D) was estimated from the Scherrer equation [35]:

$$D = \frac{\kappa\lambda}{\beta * \cos(\theta)},$$

where κ is the shape constant which was taken as 1.54060 Å, λ is the wavelength of the radiation, θ is the diffraction angle, and β is the half-value width of the anatase diffraction peak.

The XRD plot shown in Figure 66 shows the formation of titanium nitride during the thermochemical process at a temperature of 825°C. Additionally, it also shows the transformation from anatase to rutile phases during this process. These results support the findings of Kobayakawa et al. who found that TiN was formed when high doping ratios of nitrogen were formed in TiO_2 [61]. The samples for heavily treated materials for this study were brownish to black in color, which is similar to the findings of Kobayakawa et al. Further, TiN was not observed for materials that were white or yellow in color.

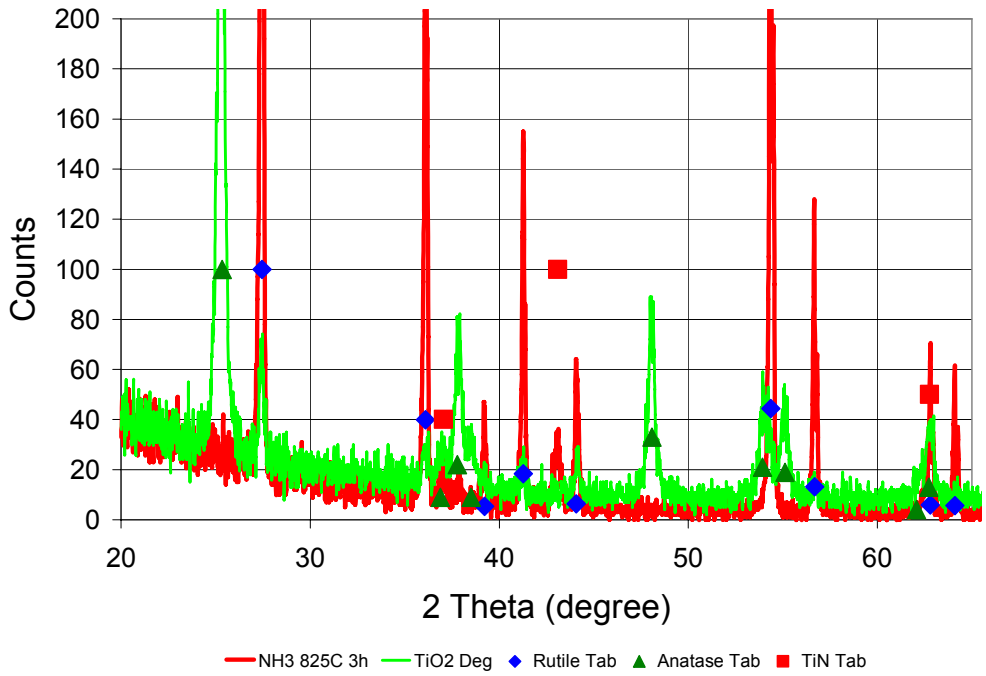

Figure 66 Formation of Titanium Nitride During Thermochemical Ammonia Treatments at 825°C of Degussa P-25 TiO_2

Figure 67 shows the XRD analysis for thermochemically treated Degussa P-25 TiO_2 as it pertains to anatase and rutile phase composition. This plot further identifies 625°C as a critical temperature for the transformation of anatase to rutile phase.

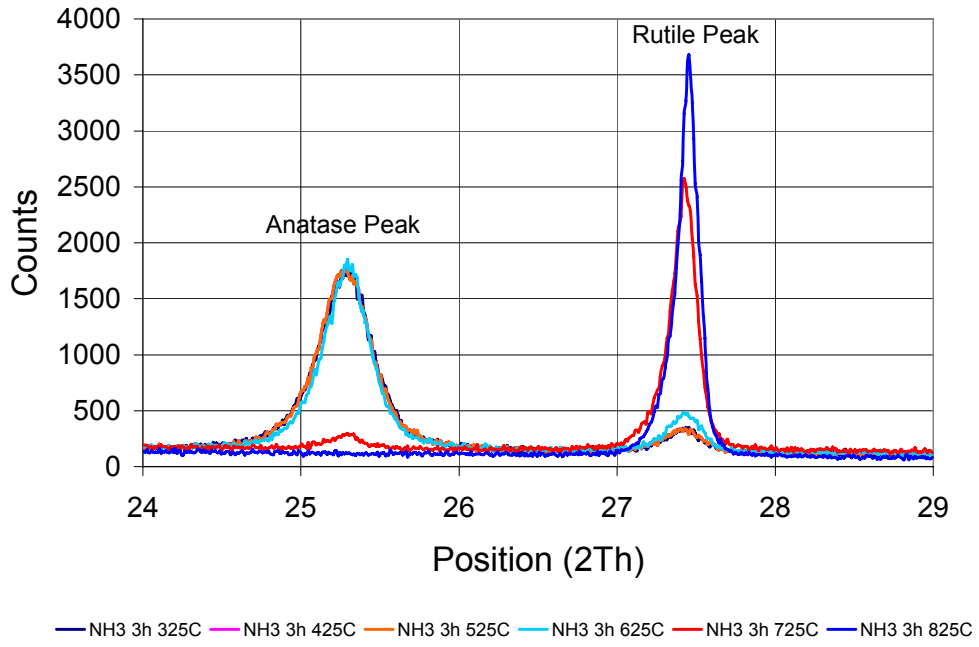

Figure 67 XRD Comparison for Thermochemically Ammonia Treated Degussa P-25 TiO_2

8.8 Characterization of Thermochemically Ammonia Treated TiO_2

Figure 68 shows measured and calculated values as they pertain to thermochemically treated Degussa P-25 TiO_2. Rutile particles were found to have an average size of 30 nm and anatase an average size of 10 nm. It can be seen that the size of these particles stays relatively constant for temperature below 625°C. However, at temperatures above 625°C the average particle size increases rapidly, especially for rutile. It is interesting to note the contrast in temperatures between the calcinated treatment and thermochemical ammonia treatments with regard to their particle size. It can be see that the thermochemical treatment had some influence on the temperature point at which the transition towards a more rutile mass fraction occurred.

The relative photonic efficiency is a plot of the apparent rate constants. What can be gleaned from this plot is that the decline in the photonic efficiency (apparent rate constant) coincides with an increase in particle size for anatase and rutile particles. It is the rutile particles however that begin to increase much more rapidly than the anatase particles. This is further indicated by the increase in the mass fraction of rutile particles increasing over 625°C.

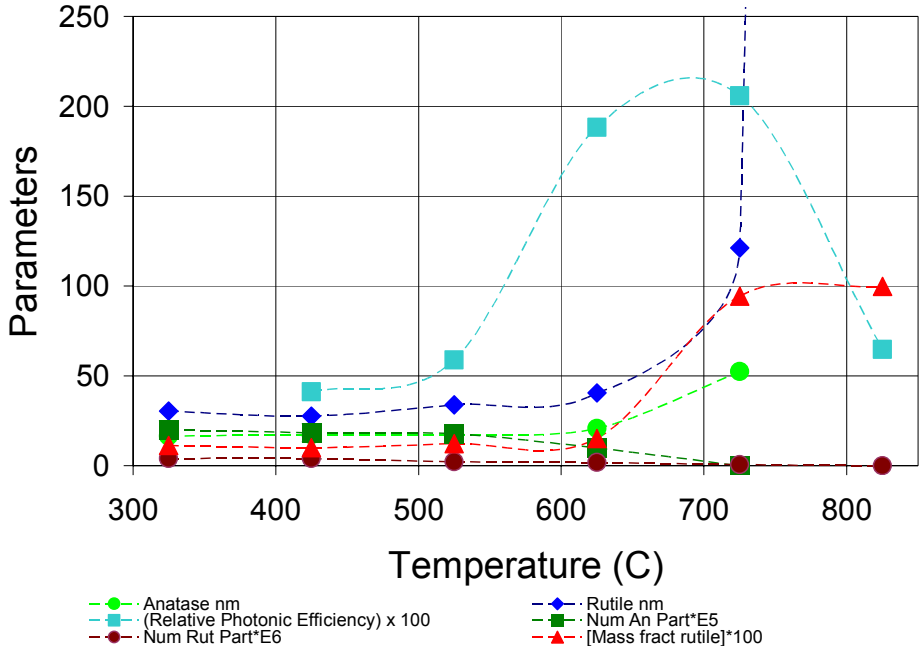

Figure 68 Characterization of Thermochemically Ammonia Treated Degussa P-25 TiO_2 Under SSS Irradiation

Figure 69 is the HRTEM image of thermochemically ammonia treated TiO_2. The results of HRTEM analysis performed by Dr. Yusuf Emirov, indicates that the lattice of ammonia treated TiO_2 is oxygen deficient and can be described as Ti_9O_{17}. No nitrogen compounds were found since their content was probably too low to be detected.

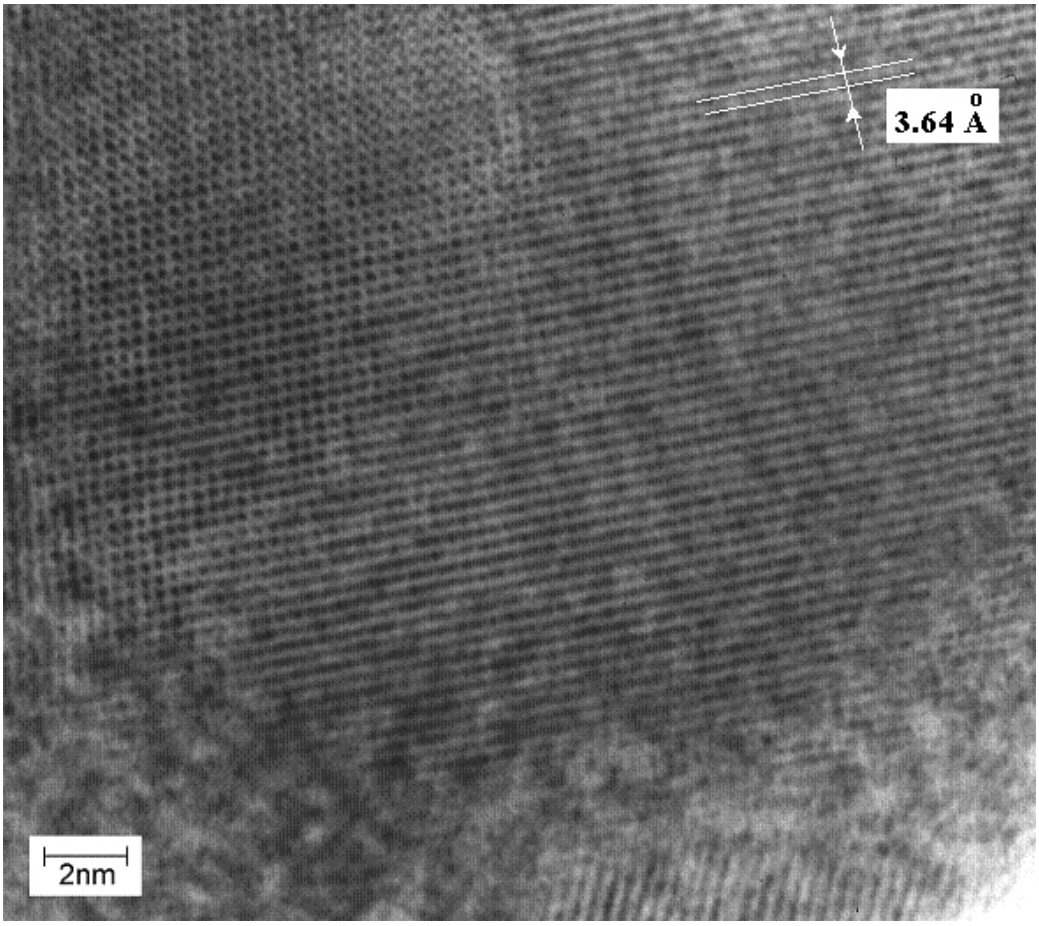

Figure 69 HRTEM of Thermochemically Ammonia Treated Degussa P-25 TiO_2

The optical absorbance was calculated using the Kubelka-Munk technique. As described earlier, an absorption edge is formed during the thermochemical ammonia treatments that allows for absorption of visible length radiation as shown in figure 70.

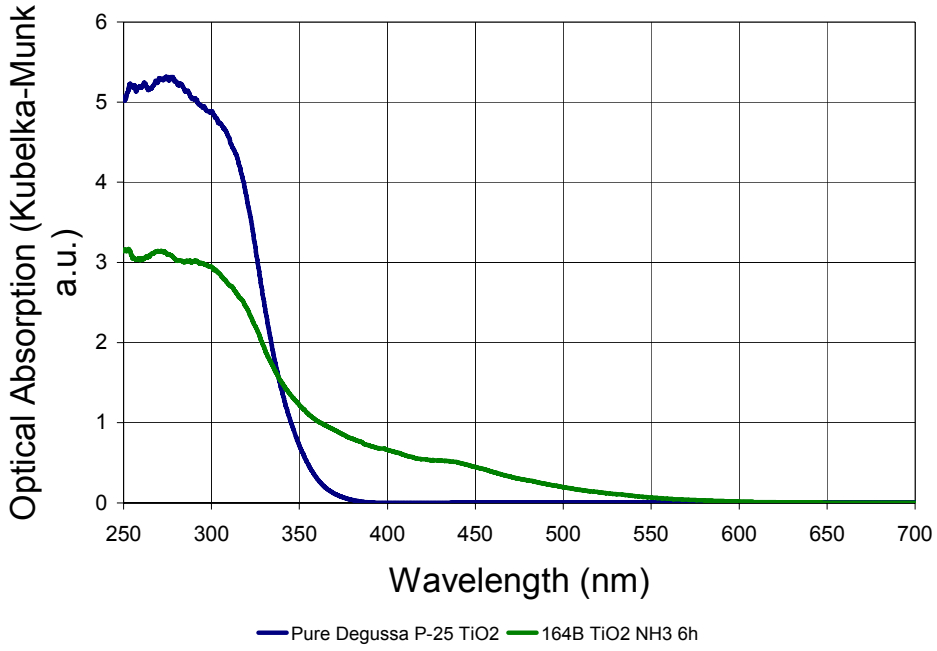

Figure 70 Optical Absorbance (Kubelka-Munk) of Thermochemically Ammonia Treated Degussa P-25 TiO_2

In Figure 71, Jang et al. plotted the absorption for anatase TiO_2 and $TiO_{2-X}N_X$. $TiO_{2-X}N_X$ shows two absorption edges. The first is the edge at 390 nm that is attributed to absorption by the oxide, and a second weaker edge at 451 nm that is attributed to nitrogen-doping. They concluded that this second shoulder peak is responsible for visible-light photocatalytic activity [26].

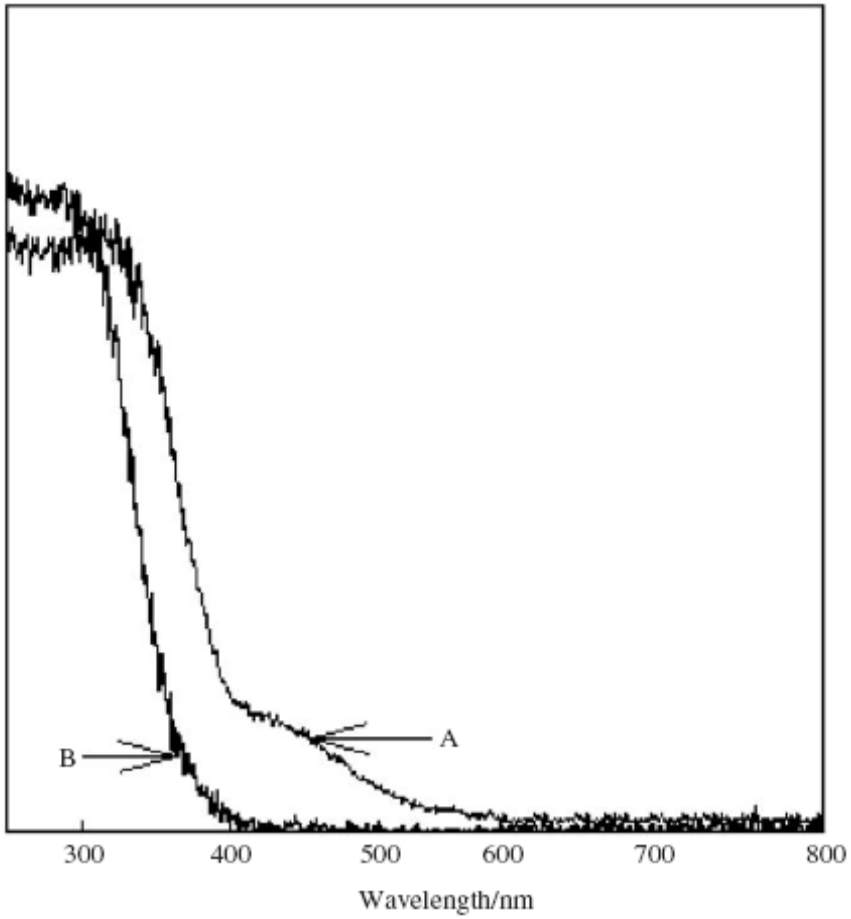

Figure 71 (A) $TiO_{2-X}N_X$ and (B) Pure TiO_2 Calcinated at 400°C [26]

What needs to be stressed here is that while Figure 70 is a good example of the ability to control the absorption edge, the material itself performed very poorly photocatalytically. This is an area of considerable research today, and a topic that was briefly investigated during this study. Further study of this critical component is necessary to draw any further conclusions.

CHAPTER 9: CONCLUSIONS AND RECOMMENDATIONS

The results of this study are as follow:

1. Thermal treatments of Degussa P-25 TiO_2 improve the photocatalytic effect over untreated Degussa P-25 TiO_2 for SSS.

2. The most photoactive catalyst prepared by thermal treatment was at 375°C for SSS. Improvement in photocatalytic efficiency was nearly two times that of untreated Degussa P-25 TiO_2.

3. A simple and inexpensive method of creating VIS-active photocatalyst by modification of Degussa P-25 TiO_2 with nitrogen was accomplished.

4. A thermochemical ammonia treatment process was optimized for temperature, duration and gas flow rate for nitrogen-doping Degussa P-25 TiO_2.

5. The most photoactive catalyst prepared by thermochemical treatment of Degussa P-25 TiO_2 was at 675°C at 12.7 mL/min. for 3 hours under VSSS. Improvement in photocatalytic effect is 1.5 times higher than untreated Degussa P-25 TiO_2.

6. An additional absorption edge in the visible range was observed for thermochemically ammonia treated Degussa P-25 TiO_2 for treatment temperatures above 625°C.

7. Based on XRD results, the temperature of the phase transition from anatase to rutile is 625°C for thermally treated Degussa P-25 TiO_2, and 725°C for thermochemically treated Degussa P-25 TiO_2. This indicates that nitrogen-doping inhibits the phase transition from anatase to rutile.

8. The results of HRTEM analysis indicate that the lattice of thermochemically ammonia treated Degussa P-25 TiO_2 is oxygen deficient and can be described as Ti_9O_{17}. No nitrogen compounds were found and it is believed that their content was probably too low to be detected.

9. The XRD patterns of thermochemically treated Degussa P-25 TiO_2 exhibit diffraction peaks of TiN compound at 825°C.

10. The color of the thermochemically treated Degussa P-25 TiO_2 was dependent upon treatment temperature, duration and gas flow rate.

11. The color ranged from vivid white to grey to pale yellow to vivid yellow to green to brown to black, which may be attributed to TiN content on the surface.

12. The phase composition of the most Vis-active photoactive catalyst was 88% anatase and 12% rutile for thermochemically treated Degussa P-25 TiO_2 at 675°C.

13. A three step thermochemical method was developed for heavy nitrogen-doping of TiO_2 using anhydrous ammonia as a nitrogen source.

14. Thermochemical ammonia treatment of Degussa P-25 TiO_2 is a very promising and inexpensive method for Vis-active photocatalyst preparation on a commercial scale compared with sputtering and ion implantation techniques.

Anhydrous ammonia as a nitrogen source for the doping of Degussa P-25 TiO_2 has the potential to create an efficient and inexpensive visible-light photocatalyst. It has been shown here and in other studies how to create a visible-light photocatalytic effect. As noted, many authors have attributed this to the creation of states capable of utilizing energy from the visible spectrum.

An important question is “how do we get this material to absorb more and more of the available visible-light spectrum without degrading the efficiency of the catalyst in both the visible and ultraviolet spectra?” Initial work in this area was done during this study. While it was shown it is possible to significantly improve the absorption of visible wavelengths, the preliminary results have also shown that this can be done at the expense of photocatalytic efficiency. The improvement in visible-light absorption is not directly related to an improvement in photocatalytic efficiency. Advanced semiconductor theory suggests that materials can become electrically inactive if over doped due to a saturation effect. Could this possibly be the case here?

Future research should include a more rigorous treatment of the photocatalytic rate. The Langmuir-Hinshelwood equation should be used to better model the chemical kinetics that occurs during the photocatalytic process. A focused study should be done on the optimization of treatment temperature, flow rate and duration. Additionally, an in depth characterization of the doped catalyst would be beneficial in identifying optimum doping levels, the role of interstitial and substitutional dopants as well as the effects of TiN. Finally, for practical commercial concerns, further research and development of an improved gas phase impregnation system should be undertaken. All in all, this is an area with a great deal of work to be done.

As a final note, the reader should note that unless otherwise expressly cited, all activities of this study were done under the direction of Dr. Nikolai Kislov. Dr. Kislov should be primarily credited with the design of experiments, experimental systems, procedures and analytical methods.

LIST OF REFERENCES

[1] R. G. Salomon, *Tetrahedron,* vol. 39, p. 485, 1983.

[2] UNICEF, "Water, environment and sanitation," 2007.

[3] J. T. Chang, Y. F. Lai, and J. L. He, "Photocatalytic performance of chromium or nitrogen doped arc ion plated-TiO_2 films," *ICMCTF 2005,* vol. 200, pp. 1640-1644, 2005.

[4] N. A. Serpone and A. V. Emeline, "Suggested terms and definitions in photocatalysis and radiocatalysis," *International Journal of Photoenergy,* vol. 4, pp. 91-131, 2002.

[5] O. Carp, C. L. Huisman, and A. Reller, "Photoinduced reactivity of titanium dioxide," *Progress in Solid State Chemistry,* vol. 32, pp. 33-177, 2004.

[6] A. L. Linsebigler, G. Lu, and J. T. Yates, "Photocatalysis on TiO_2 Surfaces: Principles, Mechanisms, and Selected Results," *Chemical Reviews,* vol. 95, pp. 735-758, 1995.

[7] S. O. Kasap, *Principles of eletronic materials and devices*, 2nd ed. New York, NY: McGraw-Hill, 2000.

[8] D. Beydoun, R. Amal, G. Low, and S. McEvoy, "Role of Nanoparticles in Photocatalysis," *Journal of Nanoparticle Research,* 1999.

[9] K. Madhusudan Reddy, B. Baruwati, M. Jayalakshmi, M. Mohan Rao, and S. V. Manorama, "S-, N- and C-doped titanium dioxide nanoparticles: Synthesis, characterization and redox charge transfer study," *Journal of Solid State Chemistry,* vol. 178, pp. 3352-3358, 2005.

[10] U. Diebold, "The surface science of titanium dioxide," *Surface Science Reports,* vol. 48, pp. 53-229, 2003.

[11] Y. Q. Wang, X. J. Yu, and D. Z. Sun, "Synthesis, characterization, and photocatalytic activity of $TiO_{2-x}N_x$ nanocatalyst," *Journal of Hazardous Materials,* 2006.

[12] R. I. Bickley, T. Gonzalez-Carreno, J. S. Lees, L. Palmisano, and R. J. D. Tilley, "A structural investigation of titanium dioxide photocatalysts," *Journal of Solid State Chemistry,* vol. 92, pp. 178-190, 1991.

[13] I. Nakamura, N. Negishi, S. Kutsuna, T. Ihara, S. Sugihara, and K. Takeuchi, "Role of oxygen vacancy in the plasma-treated TiO_2 photocatalyst with visible light activity for NO removal," *Journal of Molecular Catalysis A: Chemical,* vol. 161, pp. 205-212, 2000.

[14] R. B. Draper and M. A. Fox, "Titanium dioxide photosensitized reactions studied by diffuse reflectance flash photolysis in aqueous suspensions of TiO_2 powder," *Langmuir,* vol. 6, pp. 1396-1402, 1990.

[15] H. Gerischer, "Photoelectrochemical catalysis of the oxidation of organic molecules by oxygen on small semiconductor particles with TiO_2 as an example," *Electrochimica Acta,* vol. 38, pp. 3-9, 1993.

[16] J. Wang, B. Guo, X. Zhang, Z. Zhang, J. Han, and J. Wu, "Sonocatalytic degradation of methyl orange in the presence of TiO_2 catalysts and catalytic activity comparison of rutile and anatase," *Ultrasonics Sonochemistry,* vol. 12, pp. 331-337, 2005.

[17] T. Ohno, K. Sarukawa, K. Tokieda, and M. Matsumura, "Morphology of a TiO_2 Photocatalyst (Degussa, P-25) Consisting of Anatase and Rutile Crystalline Phases," *Journal of Catalysis,* vol. 203, pp. 82-86, 2001.

[18] A. K. Datye, G. Riegel, J. R. Bolton, M. Huang, and M. R. Prairie, "Microstructural Characterization of a Fumed Titanium Dioxide Photocatalyst," *Journal of Solid State Chemistry,* vol. 115, pp. 236-239, 1995.

[19] E. J. Weber and V. C. Stickney, "Hydrolysis Kinetics of Reactive Blue 19-Vinyl Sulfone," *Water Research,* vol. 27, pp. 63-67, 1993.

[20] N. Guettai and H. Ait Amar, "Photocatalytic oxidation of methyl orange in presence of titanium dioxide in aqueous suspension. Part I: Parametric study," *Desalination,* vol. 185, pp. 427-437, 2005.

[21] J. M. Herrmann, "Heterogeneous photocatalysis: fundamentals and applications to the removal of various types of aqueous pollutants," *Catalysis Today,* vol. 53, pp. 115-129, 1999.

[22] S. Al-Qaradawi and S. R. Salman, "Photocatalytic degradation of methyl orange as a model compound," *Journal of Photochemistry and Photobiology A: Chemistry,* vol. 148, pp. 161-168, 2002.

[23] H. M. Yates, M. G. Nolan, D. W. Sheel, and M. E. Pemble, "The role of nitrogen doping on the development of visible light-induced photocatalytic activity in thin TiO_2 films grown on glass by chemical vapour deposition," *Journal of Photochemistry and Photobiology A: Chemistry,* vol. 179, pp. 213-223, 2006.

[24] N. Guettai and H. Ait Amar, "Photocatalytic oxidation of methyl orange in presence of titanium dioxide in aqueous suspension. Part II: Kinetics Study," *Desalination,* vol. 185, pp. 439-448, 2005.

[25] S. Liu, X. Chen, and X. Chen, "Preparation of N-Doped Visible-Light Response Nanosize TiO_2 Photocatalyst Using the Acid-Catalyzed Hydrolysis Method," *Chinese Journal of Catalysis,* vol. 27, pp. 697-702, 2006.

[26] J. S. Jang, H. G. Kim, S. M. Ji, S. W. Bae, J. H. Jung, B. H. Shon, and J. S. Lee, "Formation of crystalline $TiO_{2-x}N_x$ and its photocatalytic activity," *Journal of Solid State Chemistry,* vol. 179, pp. 1067-1075, 2006.

[27] V. Pore, M. Heikkila, M. Ritala, M. Leskela, and S. Areva, "Atomic layer deposition of $TiO_{2-x}N_x$ thin films for photocatalytic applications," *Journal of Photochemistry and Photobiology A: Chemistry,* vol. 177, pp. 68-75, 2006.

[28] S. K. Pradhan and P. J. Reucroft, "A study of growth and morphological features of TiO_xN_y thin films prepared by MOCVD," *Journal of Crystal Growth,* vol. 250, pp. 588-594, 2003.

[29] S. Yin, K. Ihara, M. Komatsu, Q. Zhang, F. Saito, T. Kyotani, and T. Sato, "Low temperature synthesis of $TiO_{2-x}N_y$ powders and films with visible light responsive photocatalytic activity," *Solid State Communications,* vol. 137, pp. 132-137, 2006.

[30] S. Yin, H. Yamaki, M. Komatsu, Q. Zhang, J. Wang, Q. Tang, F. Saito, and T. Sato, "Synthesis of visible-light reactive $TiO_{2-x}N_y$ photocatalyst by mechanochemical doping," *Special issue in honour of C.N.R. Rao,* vol. 7, pp. 1479-1485, 2005.

[31] D. Li, H. Haneda, S. Hishita, and N. Ohashi, "Visible-light-driven nitrogen-doped TiO_2 photocatalysts: effect of nitrogen precursors on their photocatalysis for decomposition of gas-phase organic pollutants," *Materials Science and Engineering B,* vol. 117, pp. 67-75, 2005.

[32] R. Asahi, T. Morikawa, T. Ohwaki, K. Aoki, and Y. Taga, "Visible-Light Photocatalysis in Nitrogen-Doped Titanium Oxides," *Science Magazine,* vol. 293, pp. 269-271, 2001.

[33] H. Irie, Y. Watanabe, and K. Hashimoto, "Nitrogen-Concentration Dependence on Photocatalytic Activity of $TiO_{2-x}N_x$ Powders," *Journal of Physical Chemistry B,* vol. 107, pp. 5483-5486, 2003.

[34] G. R. Torres, T. Lindgren, J. Lu, C. G. Granqvist, and S. E. Lindquist, "Photoelectrochemical Study of Nitrogen-Doped Titanium Dioxide for Water Oxidation," *Journal of Physical Chemistry B,* vol. 108, pp. 5995-6003, 2004.

[35] T. Ihara, M. Miyoshi, Y. Iriyama, O. Matsumoto, and S. Sugihara, "Visible-light-active titanium oxide photocatalyst realized by an oxygen-deficient structure and by nitrogen doping," *Applied Catalysis B: Environmental,* vol. 42, pp. 403-409, 2003.

[36] I. N. Martyanov, S. Uma, S. Rodrigues, and K. J. Klabunde, "Structural Defects Cause TiO_2-based Photocatalysts to be Active in Visible Light," *ChemComm,* vol. 21, pp. 2476-2477, 2004.

[37] M. Miyauchi, A. Ikezawa, H. Tobimatsu, H. Irie, and H. Hashimoto, "Zeta potential and photocatalytic activity of nitrogen doped TiO_2 thin films," *Physical Chemistry Chemical Physics,* vol. 6, pp. 865-870, 2004.

[38] O. Diwald, T. L. Thompson, T. Zubkov, E. G. Goralski, S. D. Walck, and J. T. Yates, "Photochemical Activity of Nitrogen-Doped Rutile TiO_2 (110) in Visible Light," *Journal of Physical Chemistry B,* vol. 108, pp. 6004-6008, 2004.

[39] C. C. Pan and J. C. S. Wu, "Visible-light response Cr-doped $TiO_{2-X}N_X$ photocatalysts," *Materials Chemistry and Physics,* vol. 100, pp. 102-107, 2006.

[40] R. Nakamura, T. Tanaka, and Y. Nakato, "Mechanism for Visible Light Responses in Anodic Photocurrents at N-Doped TiO_2 Film Electrodes," *Journal of Physical Chemistry B,* vol. 108, pp. 10617-10620, 2004.

[41] S. M. Prokes, J. L. Goel, X. Chen, B. Clemmons, and W. E. Carlos, "Defect-Related Optical Behavior in Surface Modified TiO_2 Nanostructures," *Advanced Functional Materials,* vol. 15, pp. 161-167, 2005.

[42] S. Mozia, M. Tomaszewska, B. Kosowska, B. Grzmil, A. W. Morawski, and K. Kalucki, "Decomposition of nonionic surfactant on a nitrogen-doped photocatalyst under visible-light irradiation," *Applied Catalysis B: Environmental,* vol. 55, pp. 195-200, 2005.

[43] R. Silveyra, L. De La Torre Saenz, W. A. Flores, V. C. Martinez, and A. A. Elguezabal, "Doping of TiO_2 with nitrogen to modify the interval of photocatalytic activation towards visible radiation," *Selected Contributions of the XIX Ibero American Catalysis Symposium - Selected Contributions of the XIX Ibero American Catalysis Symposium,* vol. 107-108, pp. 602-605, 2005.

[44] J. Yuan, M. Chen, J. Shi, and W. Shangguan, "Preparations and photocatalytic hydrogen evolution of N-doped TiO_2 from urea and titanium tetrachloride," *International Journal of Hydrogen Energy,* vol. 31, pp. 1326-1331, 2006.

[45] A. Orlov, M. S. Tikhov, and R. M. Lambert, "Application of surface science techniques in the study of environmental photocatalysis: nitrogen-doped TiO_2," *Conversion photochimique et stockage de l'energie solaire - 2e partie,* vol. 9, pp. 794-799, 2006.

[46] P. Xu, L. Mi, and P. N. Wang, "Improved optical response for N-doped anatase TiO_2 films prepared by pulsed laser deposition in $N_2/NH_3/O_2$ mixture," *Journal of Crystal Growth,* vol. 289, pp. 433-439, 2006.

[47] D. G. Huang, S. J. Liao, J. M. Liu, Z. Dang, and L. Petrik, "Preparation of visible-light responsive N-F-codoped TiO_2 photocatalyst by a sol-gel-solvothermal method," *Journal of Photochemistry and Photobiology A: Chemistry,* vol. 184, pp. 282-288, 2006.

[48] O. Diwald, T. L. Thompson, E. G. Goralski, S. D. Walck, and J. T. Yates, "The Effect of Nitrogen Ion Implantation on the Photoactivity of TiO_2 Rutile Single Crystals," *Journal of Physical Chemistry B,* vol. 108, pp. 52-57, 2004.

[49] T. Lindgren, J. Lu, A. Hoel, C. G. Granqvist, G. R. Torres, and S. E. Lindquist, "Photoelectrochemical study of sputtered nitrogen-doped titanium dioxide thin films in aqueous electrolyte," *International Solar Energy Society World Congress 2003,* vol. 84, pp. 145-157, 2004.

[50] A. Glaser, S. Surnev, F. P. Netzer, N. Fateh, G. A. Fontalvo, and C. Mitterer, "Oxidation of vanadium nitride and titanium nitride coatings," *Surface Science,* vol. 601, pp. 1153-1159, 2007.

[51] B. Kosowska, S. Mozia, A. W. Morawski, B. Grzmil, M. Janus, and K. Kalucki, "The preparation of TiO_2-nitrogen doped by calcination of TiO_2*H_2O under ammonia atmosphere for visible light photocatalysis," *Solar Energy Materials and Solar Cells,* vol. 88, pp. 269-280, 2005.

[52] Y. Sakata, T. Yamamoto, T. Okazaki, H. Imamura, and S. Tsuchiya, "Generation of Visible Light Response on the Photocatalyst of a Copper Ion Containing TiO_2," *Chemistry Letters,* vol. 27, pp. 1253-54, 1998.

[53] M. Iwasaki, M. Hara, H. Kawada, H. Tada, and S. Ito, "Cobalt Ion-Doped TiO_2 Photocatalyst Response to Visible Light," *Journal of Colloid and Interface Science,* vol. 224, pp. 202-204, 2000.

[54] B. O'Regan and M. Gratzel, "A low-cost, high-efficiency solar cell based on dye-sensitized colloidal TiO_2 films," *Nature,* vol. 353, pp. 737-740, 1991.

[55] Y. Suda, H. Kawasaki, T. Ueda, and T. Ohshima, "Preparation of high quality nitrogen doped TiO_2 thin film as a photocatalyst using a pulsed laser deposition method," *Thin Solid Films,* vol. 453-454, pp. 162-166, 2004.

[56] M. Anpo and M. Takeuchi, "The design and development of highly reactive titanium oxide photocatalysts operating under visible light irradiation," *Journal of Catalysis,* vol. 216, pp. 505-516, 2003.

[57] R. Marchand, F. Tessier, A. Le Sauze, and N. Diot, "Typical features of nitrogen in nitride-type compounds," *International Journal of Inorganic Materials,* vol. 3, pp. 1143-1146, 2001.

[58] G. Liu, F. Li, Z. Chen, G. Q. Lu, and H. M. Cheng, "The role of NH_3 atmosphere in preparing nitrogen-doped TiO_2 by mechanochemical reaction," *Journal of Solid State Chemistry,* vol. 179, pp. 331-335, 2006.

[59] S. Z. Chen, P. Y. Zhang, D. M. Zhuang, and W. P. Zhu, "Investigation of nitrogen doped TiO_2 photocatalytic films prepared by reactive magnetron sputtering," *Catalysis Communications,* vol. 5, pp. 677-680, 2004.

[60] J. McMurray and R. Fay, *Chemistry, Fourth Edition*, Fourth ed. Upper Saddle River, NJ: Prentice Hall, 2004.

[61] K. Kobayakawa, Y. Murakami, and Y. Sato, "Visible-light active N-doped TiO_2 prepared by heating of titanium hydroxide and urea," *Journal of Photochemistry and Photobiology A: Chemistry,* vol. 170, pp. 177-179, 2005.